THE MECHANISMS DRIVING TITANIZATION OF *CRYPTOCOCCUS NEOFORMANS* AND THEIR IMPACT ON HOST-INTERACTION

by

XIN ZHOU

A thesis submitted to the University of Birmingham for the degree of

DOCTOR OF PHILOSOPHY

Institute of Microbiology and Infection

School of Biosciences

College of Life and Environmental Science

University of Birmingham

July 2021

UNIVERSITY OF
BIRMINGHAM

University of Birmingham Research Archive

e-theses repository

This unpublished thesis/dissertation is copyright of the author and/or third parties. The intellectual property rights of the author or third parties in respect of this work are as defined by The Copyright Designs and Patents Act 1988 or as modified by any successor legislation.

Any use made of information contained in this thesis/dissertation must be in accordance with that legislation and must be properly acknowledged. Further distribution or reproduction in any format is prohibited without the permission of the copyright holder.

Abstract

Cryptococcus neoformans, as a major human fungal pathogen, can cause infection at both lungs and brains of immunocompromised and immunocompetent individuals. During the infection process, a highly heterogeneous population emerges in response to the host environment, and within this population, large yeast (titan) cells are required for survival and proliferation. However, the detailed characterization of different titan sub-populations, as well as their roles in regulating the infection process, has not been fully explored. This thesis (chapter 2) starts with characterizing titan population heterogeneity of typical laboratory strain H99 together with three other clinical strains. This chapter aims to help us to understand the relationship between different titan sub-populations and the changes cells undergo after being exposed to titan induction, in strains with different capabilities to titanize. After that, chapter 3 shows how oxidative and nitrosative stress imposed by host immune response can affect titan cell formation. In this chapter, the fungal endogenous superoxide production is also found to be required for yeast-to-titan transition, which can further lead to DNA damage accumulation in titanized cells. Finally, in chapter 4, we reveal that there is a positive correlation between superoxide production, DNA damage, and titan cell formation. One possible mechanism underlying this correlation is that the cell cycle is arrested by accumulation of DNA damage,

as a result of sustained superoxide activity and delayed DNA repair. In summary, this thesis reveals novel insights on how small cells from titan population impact host interaction, how the host immune response can contribute to titan cell formation by affecting the endogenous stress response, and the regulatory mechanism of this stress response.

Acknowledgments

I would like to express my sincere gratitude to my supervisor Dr. Elizabeth Ballou for her continuous supports of my scientific research and Ph.D. study, encouragement in building my confidence, patience, and motivation. Ever since I started my study in Birmingham, she offered me different kinds of supports so that I can successfully accomplish my Ph.D. study. Most importantly, she taught me how to become a good scientific researcher by teaching me immense knowledge, helping me to develop varied skills, and guiding me in my future career plan.

Besides my primary supervisor, I would like to thank my co-supervisor Prof. Robin May for his supports, suggestions, and encouragement over the last 4 years. As the head of the group, he gave me the warmest welcome since the first day I joined the HAPI lab. I also want to thank Dr. HungJi Tsai for giving me suggestions and guidance for planning my career. A special thanks to Dr. Kerstin Volez for recruiting me into HAPI lab which gave me the chance to get on the research of fungal and host interaction.

I also like to thank all HAPI lab members: Hanna Zafar, Diana Tamayo, Leanne Taylor-Smith, Guillaume Desanti, Fabien Cottier, Farhana Alam, Joao Correia, Harlene Ghuman, Christopher Shave, Chinaemerem Onyishi, Hanqi Li, and Shijie Gong for helping me with both scientific and daily life issues,

keeping me accompanied, and having all funs together. They are not only my teammates but also my friends.

My sincere thanks also go to my entire family: my parents, my brother and his wife, and my baby niece and nephew. They encouraged and supported me to come to a totally new country to carry out my study which I am passionate about. The existence of them gives me the energy and confidence to keep moving forward.

Last but not least, I want to thank Darwin Trust for giving me financial support to make my Ph.D. study possible and Hall Heather who helped with all paper works for my scholarship.

Contents

Abstract....2
Acknowledgments....4
Contents....6
List of abbreviations....9
List of figures and tables....10
Chapter1....13
Introduction....13
1.1 Definition of titan cell....15
1.2 Host immune response to cryptococcal infection....17
1.3 Role in virulence and impact on host interaction....19
1.4 *In vitro* titan cell induction models....21
1.5 The molecular mechanism underlying titanization....23
1.6 The cAMP pathway positively regulates titanization....24
1.7 Uncovering a second regulatory pathway....25
Project Aims....29
Declaration....30
Chapter 2....31
Mini introduction....31
Results....35
2.1 *In vitro* titan inducing conditions trigger a range of cell size and DNA content changes across four clinical isolates....35
2.2 Induced cells exhibit changes in PAMP exposure....40
2.3 Cell density is sufficient to change capsule size and structure during capsule induction....43
2.4 What are titanides?....47
2.5 Modelling fungal-phagocyte interaction *in vitro* reveals strain specific phenotypes....51
2.6 Titan cells enhance the production of TNF....55
2.7 *In vivo* titan inducing conditions match *in vitro* predictions....58
2.8 Clinical isolates show different capacities to produce aneuploid colonies....60

Discussion....64
2.9 Investigating population heterogeneity *in vitro*....65
2.10 Variation in cell size and morphology and impact on host cell interaction....66
2.11 How do titanides contribute to disease progression?....67
2.12 What is the environmental significance of “sub-1C” cells?....69
2.13 Impact of population heterogeneity on drug resistance....70
Declaration....72
Chapter 3....73
Mini introduction....73
3.1 Nitrosative and oxidative stress during host-interaction....73
3.2 Fungal cell oxidative and stress response....74
3.3 Fungal endogenous ROS production....75
Results....77
3.4 Host-derived immune signals induce formation of large titan cells....80
3.5 Exogenous nitrosative stress is sufficient to further potentiate titanization....86
3.6 Exogenous RNS increases mitochondrial potential....87
3.7 Endogenous superoxide levels are dynamic throughout titanization and correlate with the capacity of isolates to form titan cells....93
3.8 Endogenous superoxide is required for titan cell formation yet must be detoxified for the generation of large cells....98
3.9 SOD2 is required for the initial detoxification of superoxide....104
3.10 Titanized cells exhibit high nuclear superoxide and increased DNA damage....110
3.11 Sod1 is localised to the nucleus after titan induction....111
3.12 SOD1 regulates genomic integrity of titan daughters....112
Discussion....116
Chapter 4....124
Mini introduction....124
4.1 ROS can cause damage to DNA, proteins, and lipids....124
4.2 Fungal DNA damage response pathway....125
4.3 Cell cycle of C. neoformans....128
4.4 DNA damage checkpoints control cell cycle arrest....129

Results 132
4.5 Exogenous oxidative stress failed to promote Sod1 nuclear translocation 132
4.6 Accumulation of DNA damage is caused by nuclear oxidative stress 133
4.7 DNA damage response genes control titan cell formation 135
4.8 Cells arrested at G2/M phase are more likely to become titan cells 137
4.9 DNA damage accumulation contributes to titanization by affecting cell cycle transitions 140
4.10 G2/M phase cells have high mitochondrial potential and endogenous superoxide levels 144
Discussion 147
Final discussion and future work 151
Materials and methods 153
Reference 170

List of abbreviations

PAMP	pathogen associated Molecular Pattern
PRRs	recognized by pattern recognition receptors
MPS	mononuclear phagocyte system
GM-CSF	granulocyte-macrophage colony-stimulating factor
CSF-1	macrophage colony-stimulating factor
IFN-γ	interferon gamma
CNS	central nervous system
cAMP	cyclic AMP
HOG	high-osmolarity glycerol
Gpa1	guanine nucleotide-binding protein α subunit
MAPK	mitogen-activated protein kinase
CFW	calcofluor white
iNOS	inducible nitric oxide synthase
ROS/RNS	reactive oxygen and reactive nitrogen species
SOD	superoxide dismutase
CAT	catalase
DSBs	double-strand breaks
DDR	DNA damage response
TFs	transcription factors
ATM	ataxia-telangiectasia mutated
ATR	ATM- and Rad3-related
PI3K	phosphatidylinositide-3-kinase
FHA	forkhead-associated
AT	ataxia-telangiectasia
8-OHdG	8-hydroxy-2′-deoxyguanosine
NOX	NADPH Oxidase

List of figures and tables

Fig 1.1 Large yeast cells were seen from infected patients……...15

Fig 1.2 Heterogeneous populations of titans, yeasts, and titanides……17

Fig 1.3 Schematic graph of three reported *in vitro* titan induction protocols...23

Fig 2.1 Titan cells formation varies among clinical isolates *in vitro*..…….…37

Fig 2.2 Supplemental information for DNA content analysis used Fig 2.1..…39

Fig 2.3. Non-titanising strains also exhibit population heterogeneity…..……41

Fig 2.4 PAMP staining flow cytometry analysis of induced cells from Fig 2.3……..……..42

Fig 2.5 Phenotype characterization of clinical isolates at yeast phase….....45

Fig 2.6 Capsule structure from titan induction……..……...……..…….…...46

Fig 2.7 Titanides from both *in vivo* and *vitro*……..……..…….……....50

Fig 2.8 (A) TEM of Zc8 titanides (B) Mating plates from the indicated isolates crossed with KN99 MATa...……...……..……..……..……..…….……..51

Fig 2.9 *In vitro* titan cells interaction with host immune cells……..……...…54

Fig 2.10 Titan cells enhance the production of TNF…..…….....57

Fig 2.11 Titanizaiton and disease outcomes on mouse model.…...…..……60

Fig 2.12 Clinical isolates produce aneuploid daughter cells with altered dug resistance *in vivo*..……..……..…..……..…..……..…..……..…..…….....63

Fig 3.1 Time-lapse images from co-incubation of pre-induced H99 with macrophages. …..……..…..……..…..……..…..……..…..……..…..…..78

Fig 3.2 Time-lapse movie of interaction between macrophages and *C.neoformans* cells…..……..……..……...…..……..…..……..…..…….....79

Fig 3.3 Fungal cell size increases after co-incubation with BMDMs and is influenced by BMDM activation…...……..…..……..…...……..…..……..83

Fig 3.4 (A) Flow cytometric gating for identification of fungal cells…..…....85

Fig 3.5 Exogenous RNS treatment correlates with increases in both cell size and superoxide level……89
Fig 3.6 JC-1 staining within titanized cells……92
Fig 3.7: Superoxide accumulation is dynamic during titanization……94
Fig 3.8 Superoxide increase with sizes within clinical isolates after co-incubation with monocytes……97
Fig 3.9 Titan cell formation can be inhibited by reducing the accumulation of superoxide. ……99
Fig 3.10 Microscopy images of cells treated with MnTBAP during titanization……100
Figure 3.11 Yap1 regulates ROS detoxification and the degree of titan cell formation……103
Fig 3.12 Superoxide Dismutase (Sod) but not Catalase (Cat) activity is required for titan cell formation……107
Fig 3.13 (A)Microscopy images of catalases mutants after titanization: (B) Microscopy images of *SOD2* and *sod2Δ* titan induced cells at 30°C with or without DPTA NONOate……109
Fig 3.14 Sod1 and superoxide localise to the nucleus of yeast and titan cells under titan inducing conditions. ……111
Fig 3.15 Loss of *SOD1* impacts titan daughter ploidy……113
Fig 3.16 H99 and *sod1Δ* titan daughters re-culture plates……115
Fig 3.17 Summary of interaction between macrophages and *C. neoformans* titan cells……118
Fig 4.1 The models of DNA damage checkpoint and response pathways……126
Fig 4.2 Cell cycle of *C. neoformans*……129

Fig 4.3 (A) Sod1-GFP failed to translocate into the nucleus under different oxidative and nitrosative stresses. (B) Oxidative stress induced DNA damage in titans, yeasts, and titanides...133
Fig 4.4 DDR pathway mutants exhibit increased titan cell formation.....136
Fig 4.5 Cells arrest at G2/M phase are more likely to become titan cells.....139
Fig 4.6 *mec1Δ* showed an abnormal cell cycle which further contributes to titanization.....143
Fig 4.7 G2/M arrest cells showed more active mitochondria and higher endogenous superoxide production.....145
Table 1: Strain list.....153

Chapter1

Introduction

Cryptococcus neoformans is a worldwide opportunistic human fungal pathogen causing life-threatening pneumonia and meningitis in immunocompromised and immunocompetent individuals (Park, Wannemuehler et al. 2009, May, Stone et al. 2016). During cryptococcal infection, the healthy host immune system responds to this infection resulting in *C. neoformans* clearance or containment in granulomas; however, for those immunocompromised or immunocompetent hosts, *C. neoformans* evades the response and disseminates to the brain causing a fatal infection (Heitman, J et al., 2011). It is estimated that each year there are 1 million cryptococcal meningitis incidents globally with 65% mortality, and most occurring in sub-Saharan Africa (Park, Wannemuehler et al. 2009).

Broadly, *C. neoformans* can be classified into three major lineages: VNI, VNII and VNB, with the first two lineages being globally distributed, while VNB appears to be restricted to southern Africa (Chen, Litvintseva et al. 2015). Although most cases of cryptococcal infection were in immunocompromised patients, there are increasingly more cases recognized in immunocompetent hosts (Day, Hoang et al. 2011, Day, Qihui et al. 2017). Until now, it is still hard to treat cryptococcal infections with a mortality rate higher than 80%, both because of delayed diagnosis and because of limited antifungal treatment

options (Johnston and May 2013, Rajasingham, Smith et al. 2017). The standard treatment of cryptococcal infection requires a combination therapy of amphotericin B for two weeks with flucytosine followed a long-term fluconazole monotherapy (Zafar, Altamirano et al. 2019). However, according to both *in vitro* and *in vivo* studies *C. neoformans* have been shown to gain transient fluconazole resistance, and this resistance is controlled by gaining extra chromosomes 1, 4, 6, or 10 (Sionov, Chang et al. 2009, Sionov, Lee et al. 2010, Gerstein, Fu et al. 2015, Stone, Rhodes et al. 2019).

Cryptococcal cells are mostly observed in the environment or host body as yeasts or spores, and grow as encapsulated budding yeasts during culture in standard microbial media. However, in the late-20th century, there were two clinical reports about unusual morphology of cryptococcal cells, in which enlarged encapsulated yeasts were isolated from both lungs and brains of infected patients (Cruickshank, Cavill et al. 1973, Love, Boyd et al. 1985). These unusual cells' sizes shifted from >40μm when identified directly from patients to <20μm when cultured *in vitro* and back to >40μm in infected mice (Cruickshank, Cavill et al. 1973, Love, Boyd et al. 1985). At this point, the distinct capsule and cell wall structure of these enlarged cells were also noted by Cruickshank et al (Cruickshank, Cavill et al. 1973). These enlarged cells were named as "titan" cells for the first time in 2010, when they were determined to be present during host infection and shown to enhance *C.*

neoformans virulence (Okagaki, Strain et al. 2010, Zaragoza, Garcia-Rivera et al. 2010).

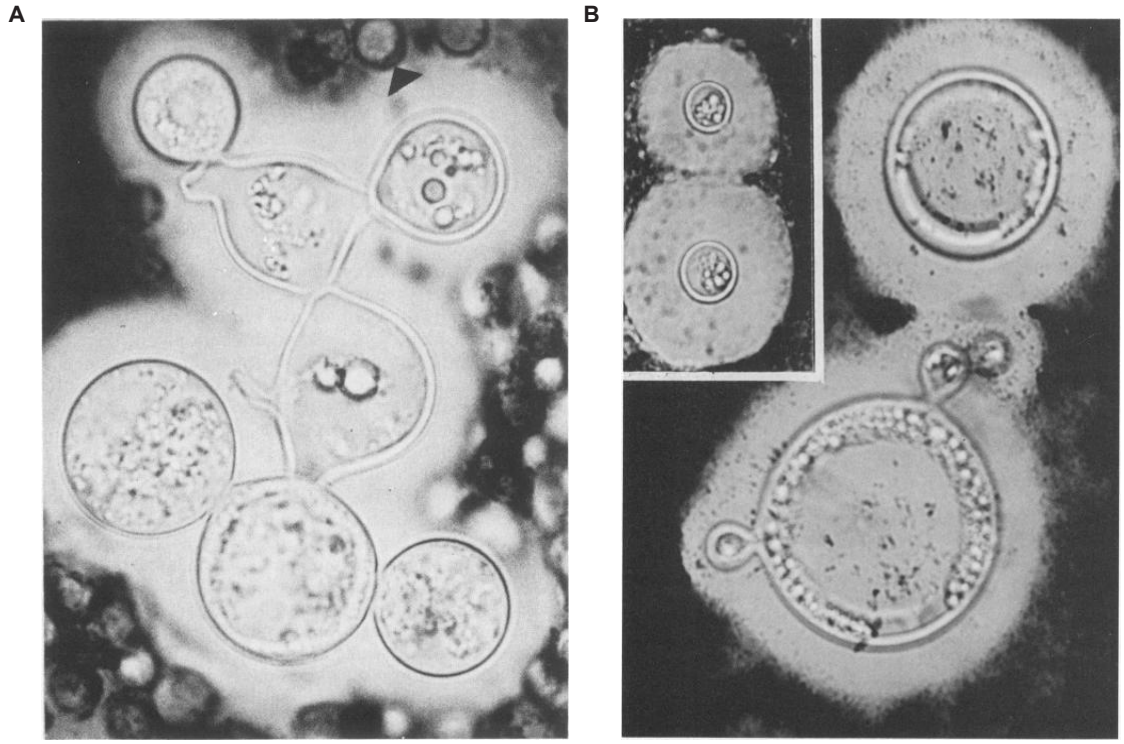


Fig 1.1: **Large yeast cells found from clinical reports**. Figures adopted from Love, Boyd et al. 1985. (A) Large yeast cells were seen from an infected patient, and cell sizes are between 40 to 60μm excluding capsule. (B) Large yeast cells were seen from mice infected with the patient isolate from (A), which range from 10 to 40μm. Cells isolated from mice infected with the laboratory strain were used as a control (5 to 15μm) (Love, Boyd et al. 1985).

1.1 Definition of titan cell

C. neoformans is usually inhaled into the host lung in the form of desiccated yeast or spores; then during the earliest stage of infection, *C. neoformans* undergoes an unusual yeast-to-titan morphogenic transition in

response to the infected lung environment (Giles, Dagenais et al. 2009, Okagaki, Strain et al. 2010, Okagaki, Wang et al. 2011). Titan cells are able to be observed 1-day post-infection in the lung and can comprise up to 20% of cryptococcal cells 3 days post-infection (Okagaki, Strain et al. 2010). The most obvious feature of titan cells is the enlarged cell size: they are usually larger than 10μm in diameter and can reach up 50 to 100μm, while typical yeast cells are around 5μm (Okagaki, Strain et al. 2010) (Fig 1.2A). At the same time, titan cells display increased DNA content, as they have high ploidy -- often tetraploid or octoploid -- and they can produce diploid or aneuploid daughters with typical yeast cell sizes (Okagaki, Strain et al. 2010, Zaragoza, Garcia-Rivera et al., 2010) (Fig 1.2B). In addition, a unique sub-population of cells were observed and described as micro-cells which are less than 1μm in cell diameter and have thick cell wall (Feldmesser, Kress et al. 2001).

More importantly, titan cells show altered virulence attributes: they have a highly compacted polysaccharide capsule which helps them to survive within phagocytes by physically or chemically blocking immune cells receptor binding sites, and altered Pathogen Associated Molecular Pattern (PAMP) exposure which can be recognized by pattern recognition receptors (PRRs) of phagocytes (Bose, Reese et al. 2003, Erwig and Gow 2016)(Fig 1.2C).

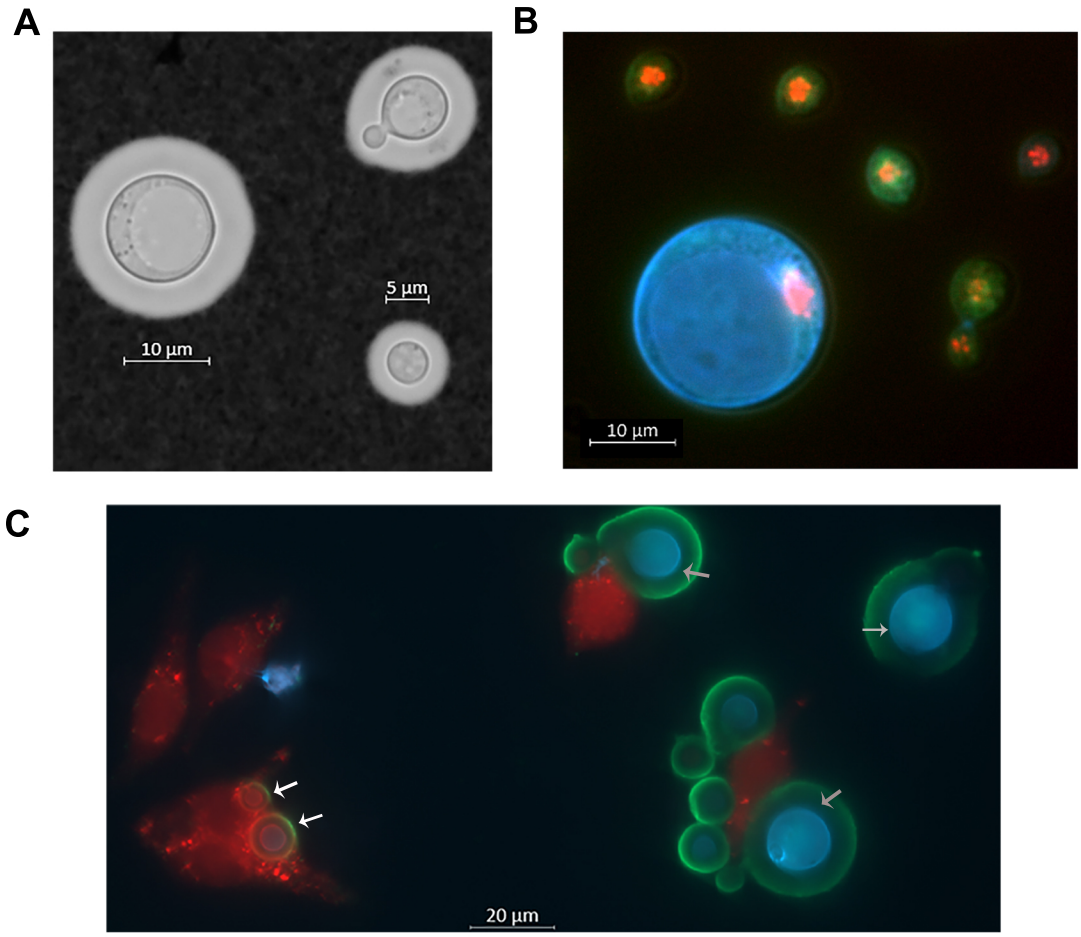


Fig 1.2: Heterogeneous populations of titans, yeasts, and titanides. A&C are adopted from Zhou and Ballou, 2018, and Zhou, May et al, 2018 Microbiology Today magazine. (A) stained with India ink to reveal capsule; (B) stained with calcofluor white(blue), red= Cse4-mCherry, kinetochore, and green=GFP-Ndc1, nuclear membrane. (C) Murine macrophages(J774) infected with *in vitro* titan induced cells. Red=macrophages, green=capsule, blue= calcofluor white. White arrows point at engulfed yeast cells, grey arrows point at unengulfed titan cells(Zhou and Ballou 2018).

1.2 Host immune response to cryptococcal infection

During infection, the interaction between host and fungal pathogens is complex, and their responses can directly determine disease outcome. As *Cryptococcus* cells enter into host lungs they will trigger host innate immune responses and encounter various phagocytic cells including neutrophils, dendritic cells, and macrophages here (Del Poeta 2004, Rohatgi and Pirofski 2015). As part of the mononuclear phagocyte system (MPS), blood monocytes are precursors of macrophages and can polarize into M1 macrophages under the stimulation of granulocyte-macrophage colony-stimulating factor (GM-CSF), while macrophage colony-stimulating factor (CSF-1) is mainly involved in M2 polarization (Italiani and Boraschi 2014). Among these effector cells, macrophage-derived phagocytosis is the key determinate for controlling *Cryptococcus* cell proliferation in the lungs (Baba 1988, Rohatgi and Pirofski 2015). Despite the fact, *Cryptococcus* cells can survive within macrophages or even escape via nonlytic vomocytosis and proliferate intracellularly (Johnston and May 2010, Johnston and May 2013).

More importantly, alveolar macrophages with internalized *Cryptococcus* cells are the link between host innate and adaptive immune response (Davis, Tsang et al. 2013, Rohatgi and Pirofski 2015). When the host mounts a T_H1-dominated immune response, it drives the accumulation of interferon gamma (IFN-γ) and macrophage M1 polarization which is highly associated with the fungicidal factor production (Zhang, Wang et al. 2009, Hardison, Ravi et al.

2010, He, Lyons et al. 2012). While T_H-2-dominated response is in favour of fungal infection with M2 polarization which is reported to be unable to control cryptococcal intracellular replication (Anthony, Urban et al. 2006, Osterholzer, Surana et al. 2009, Voelz, Lammas et al. 2009).

1.3 Role in virulence and impact on host interaction

For fungal pathogens, morphology alterations are quite common in response to environment changes or different host stimuli. Upon encountering the host environment, fungal pathogens can undergo morphogenic switches like yeast-to-hyphae to mediate tissue damage and influence immune evasion and dissemination. The *Candida albicans* yeast-to-hyphal switch and the *Histoplasm capsulatum* mycelial-to-yeast switch both contribute to invasion into host tissue and further growth inside the host (Maresca and Kobayashi 2000, Noble, Gianetti et al. 2017). Mutant strains that fail to make this switch show reduced virulence (Maresca and Kobayashi 2000, Noble, Gianetti et al. 2017). Similarly, *C. neoformans* adopted this unusual yeast-to-titan transition to mediate disease progression in order to successfully colonize in the lung and further disseminate into the central nervous system (CNS). Consistent with this, titan-defective mutants or low-titanizing strains exhibit reduced virulence with lower fungal and brain burdens (Crabtree, Okagaki et al. 2012). In addition, titanization also exhibits great impact on the host immune response as the higher proportion of titan cells is correlated with a non-

protective polarized Th2 type immune response in the mouse model (Garcia-Barbazan, Trevijano-Contador et al. 2016). As a significantly higher proportion of titan cells were found in T_H2-repsonse dominated C57BL/BL mice when compared to the CD1 mice which present T_H1-type response with high production of IFN-γ, TNF-α and IL17 (Garcia-Barbazan, Trevijano-Contador et al. 2016).

Titan cells themselves are more resistant to phagocytosis due to their large cell and capsule sizes, or altered PAMP exposure (Okagaki, Strain et al. 2010, Zaragoza, Garcia-Rivera et al. 2010, Crabtree, Okagaki et al. 2012). At the same time, titan cells can also confer protection to normal-sized cells to help them escape from being phagocyted and killed (Zaragoza, Garcia-Rivera et al. 2010). Besides that, titan cells are proved to survive better under phagocytes killing similar oxidative and nitrosative stresses (Okagaki, Wang et al. 2011). Together, the presence of titan cells contributes to establishment and persistence of the early infection in host lungs (Zaragoza and Nielsen 2013). In the past, titan cells were also shown to be able to promote the dissemination of small cells from lung into brain (Crabtree, Okagaki et al. 2012). Even though titan cells are thought to be unable to cross the blood-brain barrier (BBB) themselves because of their large cell size, it is believed that they can contribute to the further dissemination by producing small daughter cells (Okagaki, Strain et al. 2010, Crabtree, Okagaki et al. 2012,

Zaragoza and Nielsen 2013). According to *in vivo* data from mouse models, fungal cells observed in brains or that can cross BBB are yeast cells (Okagaki, Strain et al. 2010). Under both *in vivo* and *in vitro* titan-inducing conditions, a subpopulation of titan daughter cells ranging from 2 to 7μm is observed, which arises from normal yeast-phase budding and through asymmetric titan budding (Dambuza, Drake et al. 2018, Hommel B, Mukaremera L et al. 2018, Trevijano-Contador, de Oliveira et al. 2018, Zaragoza, Garcia-Rivera et al. 2010). Over time, this population represents the majority of the infection population and these small cells are available to be phagocytosed, then hijack phagocytes to achieve further dissemination in to brain (Denham and Brown 2018). Additionally, titan daughters, like their mother titan cells, have been shown to have similar resistance to stress, mainly because of their unbalanced ploidy (Gerstein, Fu et al. 2015). However, *in vitro* reports showed that hypo- and hyper-titanization strains had similar delayed dissemination into brain in the mouse model (Crabtree, Okagaki et al. 2012, Dambuza, Drake et al. 2018). Until now the mechanisms by which titan cells alter disease outcomes remains to be further explored.

1.4 *In vitro* titan cell induction models

In the past, one of the biggest challenges hampering further understanding of the molecular mechanisms driving titanization and their contribution to disease outcome was the lack of an *in vitro* titan cell induction protocol. The

process of titanzation is triggered by environmental stimuli from the host lung, and our group together other two groups reported that with host-relevant stimuli titan cells are able to be induced *in vitro* (Dambuza, Drake et al. 2018, Hommel B, Mukaremera L et al. 2018, Trevijano-Contador, de Oliveira et al. 2018, Zhou and Ballou 2018). These *in vitro* generated titan cells exhibited similar features to *in vivo* induced titan cells including: enlarged cell sizes, tightly compacted capsule, thicker cell wall, high ploidy and the presence of a single, large vacuole (Dambuza, Drake et al. 2018). Our *in vitro* titan cell induction protocol is a two-step process: first incubate *Cryptococcus* cells under nutrient starvation medium to mimic environmental conditions before entering into host, and then induce pre-starved cells with PBS+10%HI-FCS at low cell density (OD_{600}=0.001) (Zhou and Ballou 2018). Within 24h, the titanized population is highly heterogeneous, containing three distinguished populations based on differentiated cell sizes and DNA contents: titan cells, titanides, and typical yeast cells.

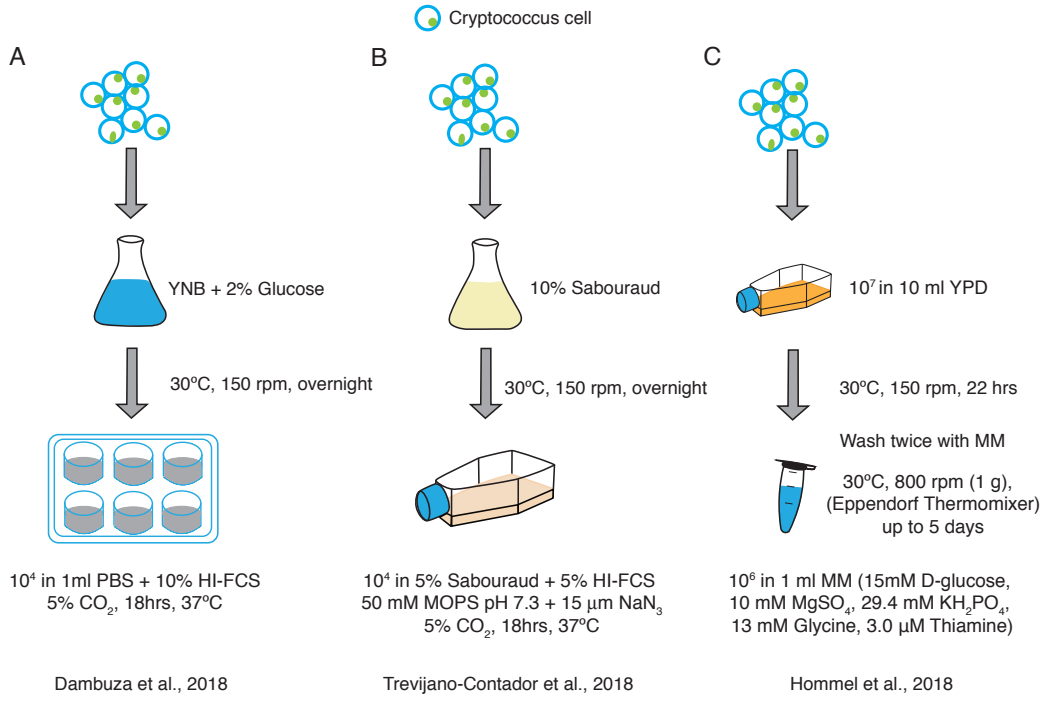


Fig 1.3: Schematic graph of three reported *in vitro* titan induction protocols (Zhou and Ballou 2018). Figure is adopted from Zhou and Ballou, 2018. (A) Induction of titan cells through pre-growth in minimal medium followed by exposure to 10% serum. (B) Induction of titan-like cells through pre-growth in minimal medium followed by exposure to serum + sodium azide. (C) Induction of Titan cells through continuous shaking under hypoxia. Relevant references for each method are indicated.

1.5 The molecular mechanism underlying titanization

Even though it has been proven that titanization plays a very important role in *C. neoformans* virulence, until now the mechanism underlying the titanization remains undescribed (Zaragoza and Nielsen 2013). Recently, as more elements involved in regulating titan cell formation have been identified,

we have begun to gain a rough idea about the signalling pathways controlling titanization, including cAMP-dependent and cAMP-independent pathways.

1.6 The cAMP pathway positively regulates titanization

Host-specific signals can induce pathogens to produce different microbial virulence factors which can help them to survive in the host environment (Alspaugh, Perfect et al. 1997). In eukaryotic cells, cAMP/PKA is a central signal transduction pathway controlling conversion of intracellular ATP to cyclic AMP (cAMP) (Alspaugh, Pukkila-Worley et al. 2002). It has been reported that in many pathogenic fungi the cAMP pathway plays a vital role in controlling pathogenicity: in *Ustilago maydis* cAMP controls establishment of filamentous growth (Andrews, Egan et al. 2000), in *Magnaporthe oryzae* *c*AMP signalling is required for appressorium formation (infection structure), and in *C. albicans* cAMP regulates filamentous growth and cellular stress (Bockmuhl and Ernst 2001, Giacometti, Kronberg et al. 2009). In *C. neoformans*, many virulence factors are also regulated by the cAMP pathway, including the antiphagocytic immunosuppressive polysaccharide capsule and the antioxidant melanin (D'Souza, Alspaugh et al. 2001, Alspaugh, Pukkila-Worley et al. 2002). In *C. neoformans*, this pathway is triggered when the Gα protein Gpa1 (guanine nucleotide-binding protein α subunit) activates the adenylyl cyclase protein Cac1 to produce cAMP, then cAMP targets downstream proteins via the Protein Kinase A catalytic subunit Pka1 and its

regulatory subunit Pkr1 to control virulence and mating (D'Souza, Alspaugh et al. 2001, Alspaugh, Pukkila-Worley et al. 2002).

Consistent with titanization as a virulence factor, Okagaki et al. pointed out that titan cell formation is controlled by the cAMP/PKA pathway, requiring two G-protein-coupled receptors: Ste3a pheromone receptor and Gpr5 protein (Okagaki, Strain et al. 2010, Okagaki, Wang et al. 2011). This conserved signalling pathway, in turn, mediates its effect on yeast-to-titan morphogenic change through activation of the Rim101 transcription factor (Okagaki, Wang et al. 2011). However, in previous studies the test for titanization ability was difficult because most cAMP/PKA pathway mutants are avirulent, and therefore easily cleared from the host lung (Okagaki, Wang et al. 2011). This leaves many questions about the cAMP/PKA pathway unexplored, like how this pathway is initially activated by host stimuli or how Rim101 interacts with downstream effectors. However, as our *in vitro* induced titan cells have been proved to be positively regulated by cAMP pathway similar to *in vivo* titan cells, it becomes much easier to further characterize the role of cAMP/PKA pathway (Dambuza, Drake et al. 2018).

1.7 Uncovering a second regulatory pathway

All findings about the cAMP pathway suggest that it plays a positive role in controlling titanization, as mutants in this pathway all showed defects in titan cell production. However, there is increasingly more evidence pointing

out that titanization is regulated by multiple signals. In 2011, Chrisman et al showed that phospholipids, in particular phosphatidylcholine can trigger titan cell production *in vitro* (Chrisman, Albuquerque et al. 2011). Later, it was reported that phospholipid-modifying enzyme Phospholipase B1 down-regulates titan cell formation, as the *plb1* mutant showed higher rates of titan cell formation compared with wild type both *in vitro* and *in vivo* (Evans, Li et al. 2015). Plb1, as a major virulence factor of *C. neoformans*, also effects cryptococcal pathogenesis throughout the entire infection process (Evans, Li et al. 2015). Moreover, the transcription factor Usv101 also influences titanizaiton. Usv101 was predicted to regulate Gpa1, but itself is not affected by cAMP (Gish, Maier et al. 2016). When *USV101* was knocked out, the mutant can produce more titan cells *in vitro* even though it exhibits defects in cytokinesis and bud morphology (Dambuza, Drake et al. 2018).

More interestingly, titan cell formation is also found to be regulated by multiple stress-response pathways, which include Rim and high-osmolarity glycerol (HOG) signalling pathway. In fungi, the Rim signalling pathway controls cellular response to environmental pH changes, which is reported to be essential for morphological transition (yeast to hyphae) and virulence for *C. albicans* (Davis 2003, Davis 2009, Bahn and Jung 2013). The key regulator of this pathway, Rim101 is a transcription factor that can be proteolytically cleaved at its C-terminus and activated in response to alkaline or neutral pH

(Selvig and Alspaugh 2011, Bahn and Jung 2013). In *C. neoformans*, Rim101 is involved in the regulation of titan cell formation as well as other important virulence factors like melanization and capsule production. (Liu, Chun et al. 2008, O'Meara, Norton et al. 2010, Okagaki, Wang et al. 2011, O'Meara, Holmer et al. 2013). CnRim101 is found to be regulated in a PKA-dependent manner, though this kind of regulation has not been seen in other fungi(O'Meara, Norton et al. 2010, Okagaki, Wang et al. 2011, Bahn and Jung 2013, O'Meara, Holmer et al. 2013). Therefore, Bahn and Jung pointed out that the upstream activators and sensors of CnRim101 need to be further explored (Bahn and Jung 2013). In the HOG pathway, Hog1 is a stress-activated mitogen-activated protein kinase (MAPK), playing a central role in regulating stress sensing and adaptation(O'Rourke, Herskowitz et al. 2002, Saito and Tatebayashi 2004, Hohmann, Krantz et al. 2007). CnHog1 has two putative transcription factor targets: Atf1 and Mbs1(Song, Lee et al. 2012, Bahn and Jung 2013). Despite the fact that disrupting CnHog1 has no effect on titan cell formation, deleting *CnMBS1* reduces the percentage of cells which titanize within the mice infection model(Song, Lee et al. 2012). Taken together, we predict that there is a second signalling pathway controlling titan cell formation, which is independent of the central cAMP pathway. Besides that, taking the fact that titanization is triggered by the host environment, we believe that stress responses of cryptococcal cells to varied host-derived

environmental and immune stress can also be part of the regulation mechanism of titanization.

Project Aims

In the host lung, the human fungal pathogen Cryptococcus neoformans undergoes a morphological switch from small haploid yeast to large polyploid titan cell. This unusual change contributes to C. neoformansvirulence as titan cells are less readily phagocytosed and can survive host nitrosative and oxidative stresses. With the built-up of in vitro titan induction protocol, this project aims to characterize key changes in clinical strains after titanization and further understand the roles of different titan sub-populations during the interactions with the host. After that, this project aims to apply in vitro induction protocol to uncover the molecular mechanisms that drive yeast-to-titan transition and investigate how host-derived immune signals can impact the degree and frequency of titanization. After revealing the key signal molecule which regulates this transition, this project aims to further determine the molecular mechanism including the role of key signal molecule in causing DNA damage, the relationship between DNA damage accumulation and titanizaiton, and central pathway which regulates DNA damage repairing and the yeast-to-titan transition.

Declaration

This chapter is adopted from an existing paper in which Xin Zhou is the first author, and Dr. Elizabeth Ballou is the corresponding author. This chapter only contains works that are conducted by Xin Zhou. This paper is currently available on bioRxiv: https://www.biorxiv.org/content/10.1101/2020.01.03.894709v2. "Host environmental conditions induce small fungal cell size and alter population heterogeneity in *Cryptococcus neoformans*"

Signature: Xin Zhou date: 13/12/2021

Signature:  date: 13 Dec 2021

Chapter 2

Mini introduction

Host environmental conditions induce small fungal cell size and alter population heterogeneity in *Cryptococcus neoformans*

The first clinical and murine model reports of cells consistent with giant/titan cells also reported significant size and morphological heterogeneity. Examination of cells from fungal abscesses revealed a highly heterogeneous population of cells ranging from 2-100 um(Cruickshank, Cavill et al. 1973, Love, Boyd et al. 1985).Consistent with this, infection of mice with laboratory strains yields a highly heterogeneous population comprised of large, polyploid titans and typical yeast as well as small, thick walled “micro” cells in lung extracts(Feldmesser, Kress et al. 2001, Okagaki, Strain et al. 2010, Okagaki, Wang et al. 2011, Evans, Li et al. 2015). However, replicating this heterogeneity *in vitro* presents a challenge to modelling *in vivo* infection. When cultured on rich medium, clinically heterogeneous populations become uniform, comprised of only typical yeast (Cruickshank, Cavill et al. 1973, Love, Boyd et al. 1985).

Moreover, this heterogeneity may be site specific within patients: clinical examination of *C. neoformans* isolates taken directly from CSF failed to identify cells that cross the defining 10 μm cutoff (Robertson, Najjuka et al.

2014). Whether this is because titan cells cannot escape the host lung or because the CSF environment is not supportive of *de novo* titan cell formation remains unclear (Hommel B, Mukaremera L et al. 2018, Zhou and Ballou 2018). Even during co-culture with immune cells that replicate host conditions and elicit titan cells, heterogeneity is not observed (Evans, Li et al. 2015).

Some degree of heterogeneity is observed under capsule inducing conditions: Fernandes et al. reported that 5 days exposure to DMEM (37°C, 5%CO2) yielded giant and micro cells and rare isolates that showed both giant and micro cells were significantly more virulent (Fernandes, Dwyer et al. 2016). Interestingly, these authors also reported wide variation in size and fungal morphology within and between isolates and across serotypes (Fernandes, Dwyer et al. 2016, Fernandes, Brockway et al. 2018). Mukaremera et al. also observed that strains that produce small cells were more virulent, using 5 days growth in DMEM plus serum (37°C, 5%CO2), conditions in which the high virulence titanizing laboratory isolate KN99a failed to produce titans. However, neither group report observing the wide variation in cell size observed in established titan inducing protocols, nor do they observe small oval cells consistent with titanides (Dambuza, Drake et al. 2018, Hommel, Mukaremera et al. 2018, Trevijano-Contador, de Oliveira et al. 2018). Despite this, these works, together with the findings of Denham et al reveal a role for small cells in infection progression (Denham, Verma et al.

2018). While it is established that the presence of titans can affect drug resistance and host immune responses, contributing to poor disease outcome, the role of small cells is less clear (Okagaki, Strain et al. 2010, Zaragoza, Garcia-Rivera et al. 2010, Okagaki, Wang et al. 2011, Crabtree, Okagaki et al. 2012). Therefore, a pressing question is the capacity of clinical and environmental isolates to generate population heterogeneity regardless of classic titanization capacity and the effect of this population heterogeneity on disease outcome.

Previous work defining titan cells has focused on identifying genetic regulators *in vivo* and *in vitro* as well as characterizing environmental and host-derived stimuli (Okagaki, Strain et al. 2010, Zaragoza, Garcia-Rivera et al. 2010, Okagaki, Wang et al. 2011, Crabtree, Okagaki et al. 2012, Evans, Li et al. 2015, Li and Nielsen 2017). However, the vast majority of this work has been done in the H99 laboratory strain. The extent of titanization in *C. neoformans* clinical isolates therefore remains unclear. Moreover, the relationship between the titanization capacity of a given strain and virulence remains poorly understood (Fernandes, Brockway et al. 2018, Mukaremera, McDonald et al. 2019). In order to study the impact of titanization on host interaction, we examined the capacity of non-H99 clinical strains to produce titan cells with our *in vitro* assays. A screen of clinical and environmental *C. neoformans* isolates representing VNI, VNII and VNB clades found wide

variation in the capacity of pathogenic strains to titanize (Dambuza, Drake et al. 2018). We therefore divided them into three groups: titanizing, non-titanizing and intermediate. In this thesis, we further characterized titanization in four strains, H99, Zc1, Zc8 and Zc12, selected based on their capacity to form titan cells *in vitro*. Upon in vitro induction, H99 and Zc8 produce highly heterogeneous populations comprising titans, titan daughters (titanides) and yeasts, while Zc1 and Zc12 are defective in titan formation. Titans account for about 15% of the H99 total population, but only approximately 2% in Zc8, where titan cells are defined as those >10μm. All four strains have been fully sequenced and genotyped and are genetic closely related (VNI). Strains from this clade are reported to be responsible for over three-quarters cryptococcal infections in Zambia (Vanhove, Beale et al. 2017).

Therefore, based on the differential capacity for titanization, this thesis applied *in vitro* titan cell induction protocol in these 4 strains, and studied the morphogenic differences across induced cells, including PAMP exposure, capsule structure and DNA content. Meanwhile, in order to better understand varied disease outcomes of these 4 strains in mice, this thesis also determined their interactions with macrophages *in vitro*. Therefore, these 4 strains can provide a window to understand the influence of titanization on the interaction with host.

Results

2.1 *In vitro* titan inducing conditions trigger a range of cell size and DNA content changes across four clinical isolates

During standard *in vitro* YPD culture, cells were uniform in size, generally round with no defects in budding, and cell size was similar across and within all strains (Fig 2.5A). To more fully characterize the impact of titan induction on all four strains, we first examined cell size distribution across the four clinical isolates under *in vitro* titanizing conditions. Consistent with our previous classification, H99 and Zc8 produce highly heterogeneous populations comprising titans (>10μm), yeasts (>4μm and <10μm), and titanides (>1μm and <3μm oval cells), while Zc1 and Zc12 populations are more uniform (Fig 2.1A)(Dambuza, Drake et al. 2018). After 24 hours, cells >10μm account for about 15% of the H99 total population, but only approximately 2% in Zc8 (Fig 2.1B). Moreover, induced non-titan Zc8 cells (<10μm) are smaller on average than induced non-titan H99 cells (3.80 μm ± 0.10 vs 7.15 μm ± 0.14 SEM, $p<0.0001$, $n>200$), and are smaller on average than Zc1 or Zc12 induced cells (4.44 μm ± 0.05, 4.57 μm ± 0.06 SEM, respectively, $p<0.0001$, $n>200$) (Fig 2.1B). Given the low frequency of titans detected in induced Zc8 cultures, which can easily be missed when relying on cell counts with small numbers (n=200), we assessed cell size spread and DNA content across the population of a large number of cells by flow

cytometry (up to n=10,000). Using this approach, for H99 we observed population structure characteristic of typical and titan populations, with a minority sub-population of cells that show distinguishable shoulder by forward scatter (FSC, a common proxy for cell size) (Fig 2.1Ci, n>8000) and DNA content >4C (12.3%, Fig 2.1D, see Fig 2.2A for matched YPD controls). However, while 6.4% of induced Zc8 cells had DNA content >4C, this FSC shift was not apparent as H99 (Fig 2.1Cii). Despite this overall reduction in frequency, a similar stepwise population of polyploid cells with a long tail to the right was apparent for Zc8 (Fig 2.1D). In addition, the median FSC of cells with >4C DNA content was lower than in the H99 population, suggesting these Zc8 polyploid cells may be smaller than H99 polyploid cells and have a lower ploidy.

Unlike H99, the vast majority of cells in titan-induced Zc1 and Zc12 populations had DAPI staining consistent with 1C DNA content. However, when we closely examined DNA content, we did identify rare polyploid 4C cells in Zc1 isolates (2.8%) and Zc12 (<1%). These cells were similar in FSC to H99 4C cells, suggesting the presence of rare titan cells in the Zc1 and Zc12 cultures, which likely require acquisition of larger sample size in order to detect (Fig 2.1C iii). These data suggest that exposure to titan inducing

conditions has a general impact on both clinical isolate ploidy and cell size regardless of whether titans are visible.

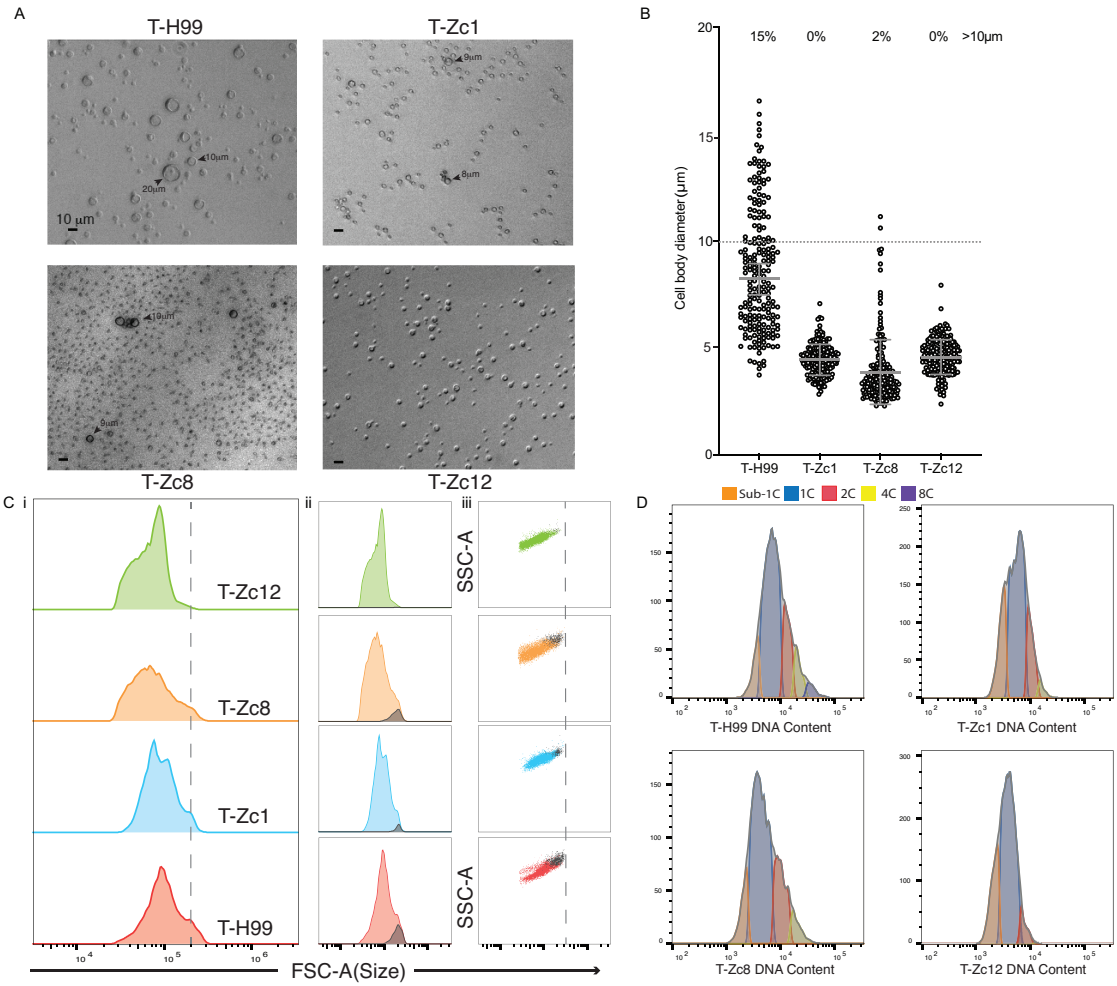


Fig 2.1. Titan cells formation varies among clinical isolates *in vitro*. (A) *C. neoformans* cells from all indicated strains after 24hrs titan induction, Scale bar: 10µm. (B) Cell body sizes of titan induced cells (n>200). (C) Flow cytometry for cells after titanization with FSC-A as a proxy for cell size. i) Histograms for cell size (FSC-A) are shown for all indicated isolates with a dotted line indicating the distinct shoulder of size increase. ii) The grey sub-population indicates the size threshold identified for cells with DNA content >4C. iii) FSC-A vs SSC-A scatter plots for all

indicated isolates with a dotted line indicating the threshold for H99 cell sizes (D) Flow cytometry analysis for DNA content after staining with DAPI. 1C and 2C populations were identified relative to YPD grown yeast cells from matched parent strains (Fig 2.2A). 4C peaks were established according to doubled MFI of DAPI staining relative to 2C. “T” indicates pre-titanized cells. Experiments were independently repeated at least three times (n>3) with a representative biological replicate is presented.

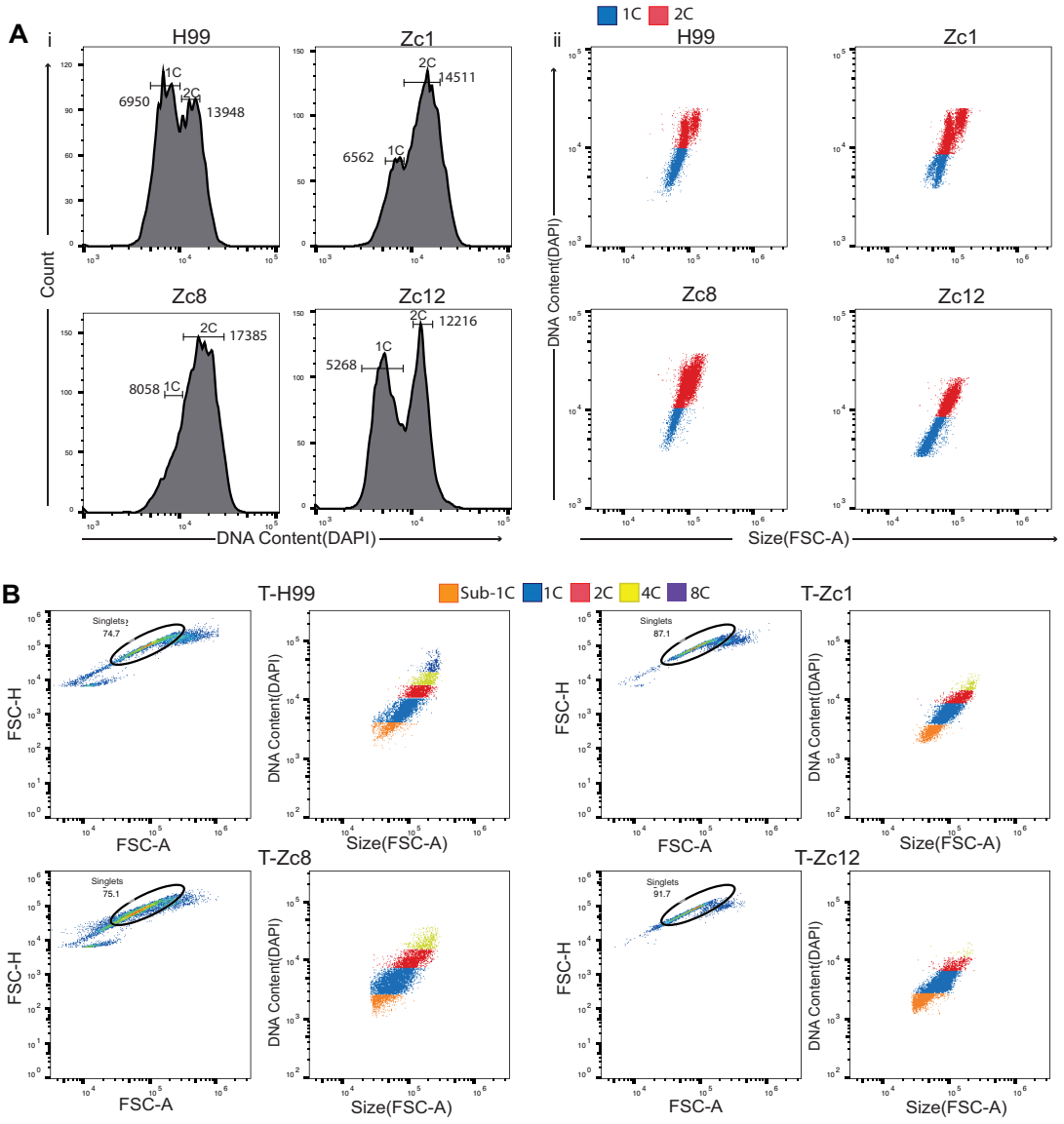


Fig 2.2. Supplemental information for DNA content analysis used Fig 2.1 (A) i) Histograms of DAPI staining intensity for YPD grown cells, and 1C and 2C peaks are indicated based on the MFI. ii)FSC-A vs DNA content scatter plots show the correlation of size increase with DNA content. (B) Single cells were identified by FSC-A vs FSC-H to remove doublets (n>8000 after gating), then were used for DNA content analysis (Left panel). FSC-A vs DNA content scatter plots show the correlation of size increase with DNA content (Right panel). “T” indicates pre-titanized

cells. Experiments were independently repeated at least three times (n>3) with a representative biological replicate is presented.

2.2 Induced cells exhibit changes in PAMP exposure

C. neoformans titan and typical cells recovered from mouse lung have different cell wall composition, with an increase in chitin and mannose (including mannan, mannoproteins, and capsular mannans) observed in cells >10 μm (Wiesner, Specht et al. 2015, Mukaremera, Lee et al. 2018). We therefore asked whether similar differences could be observed in *in vitro* induced cells. Chitin (Calcofluor white, CFW), chitosan (EosinY), and cell wall mannan (ConA) were measured following exposure to inducing conditions for 24 hours. Microscopy and flow cytometry revealed an overall decrease in PAMP exposure following titan induction relative to YNB (Fig 2.3A, 2.3Bi, H99 representative plot). Gating on positively staining cells only, chitin, mannan, and chitosan staining correlated with cell size, with larger cells staining more intensely than smaller cells, the majority of which were below the threshold of detection (Fig 2.3Bii). Moreover, distinct high chitin populations were apparent in H99, Zc1, and Zc8 cultures (Fig 2.4). Quantitative analysis by flow cytometry using the same approach to identify titan cells as taken in Fig 2.1C again revealed a sub-population of large cells in all four induced cultures (Fig 2.2). Similar to *in vivo*-derived H99 titan cells, *in vitro*-induced H99, Zc1, Zc8, and Zc12 cells displayed a distinct CFW-high population that correlated with

the largest cells (Fig 2.3B, Fig 2.4) (Wiesner, Specht et al. 2015, Mukaremera, Lee et al. 2018). The largest cells in all isolates had comparable chitosan and cell wall mannan staining to typical cells (Fig 2.4). Moreover, in long-term induced cultures (72 h), overall size heterogeneity was more apparent, with increased numbers of small cells and distinct high and low chitin peaks present in both Zc1 and Zc12 populations (Fig 2.3C). Together, these data suggest that changes in cell wall composition occur during low density growth in serum regardless of induction of cells larger than 10μm.

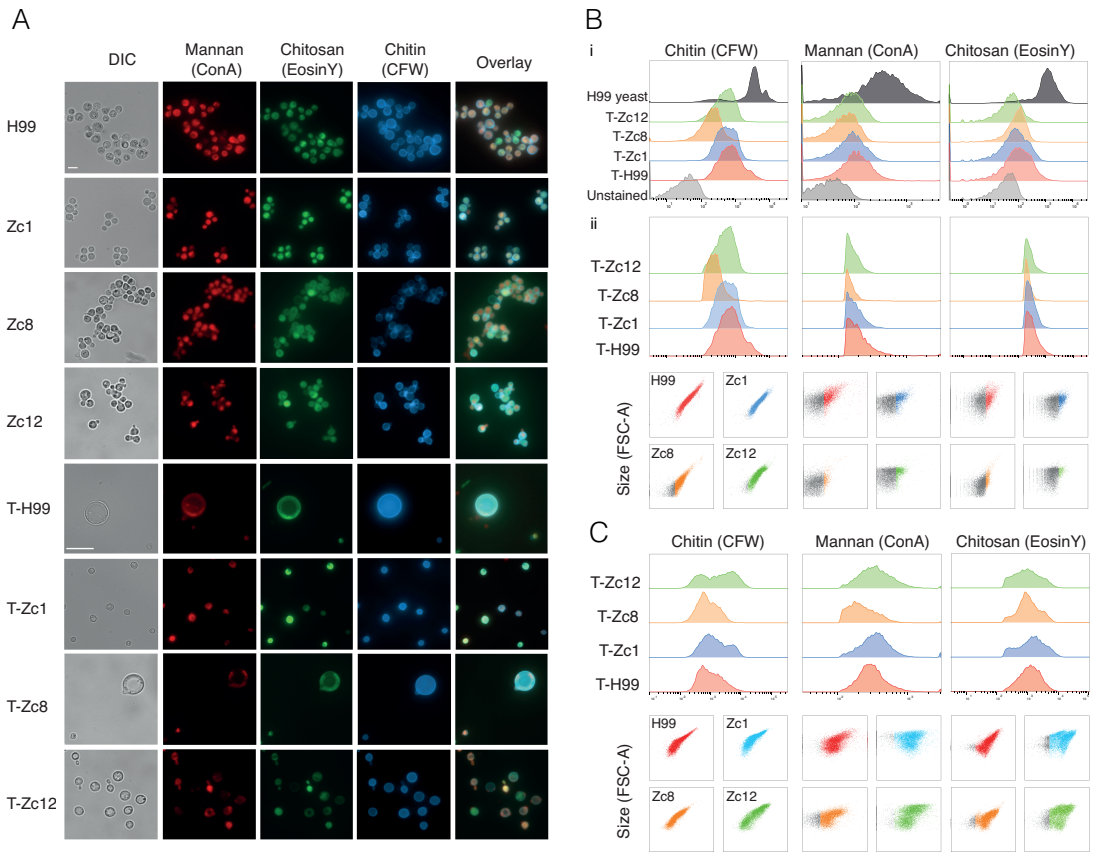


Fig 2.3. Non-titanizing strains also exhibit population heterogeneity. (A) PAMP staining for all indicated strains cells from both YNB yeast and 24hrs titan induction, Mannan (ConA, Red), Chitosan (EosinY, Green), Chitin (CFW, Blue). YNB grown

yeast scale bar 5μm; titanized cells scale bar 10μm. (B) Stained cells from (A) were analysed by flow cytometry to determine MFI indicating exposure of Chitin (CFW, right); Mannan (ConA, centre); and Chitosan (EosinY, left). (C) Flow cytometry analysis of PAMP staining for indicated cells from long-term(72hrs) titan inductions with MFI indicating exposure of Chitin (CFW, right); Mannan (ConA, center); and Chitosan (EosinY, left). “T” indicates pre-titanized cells. Experiments were independently repeated at least three times (n>3) with a representative biological replicate is presented.

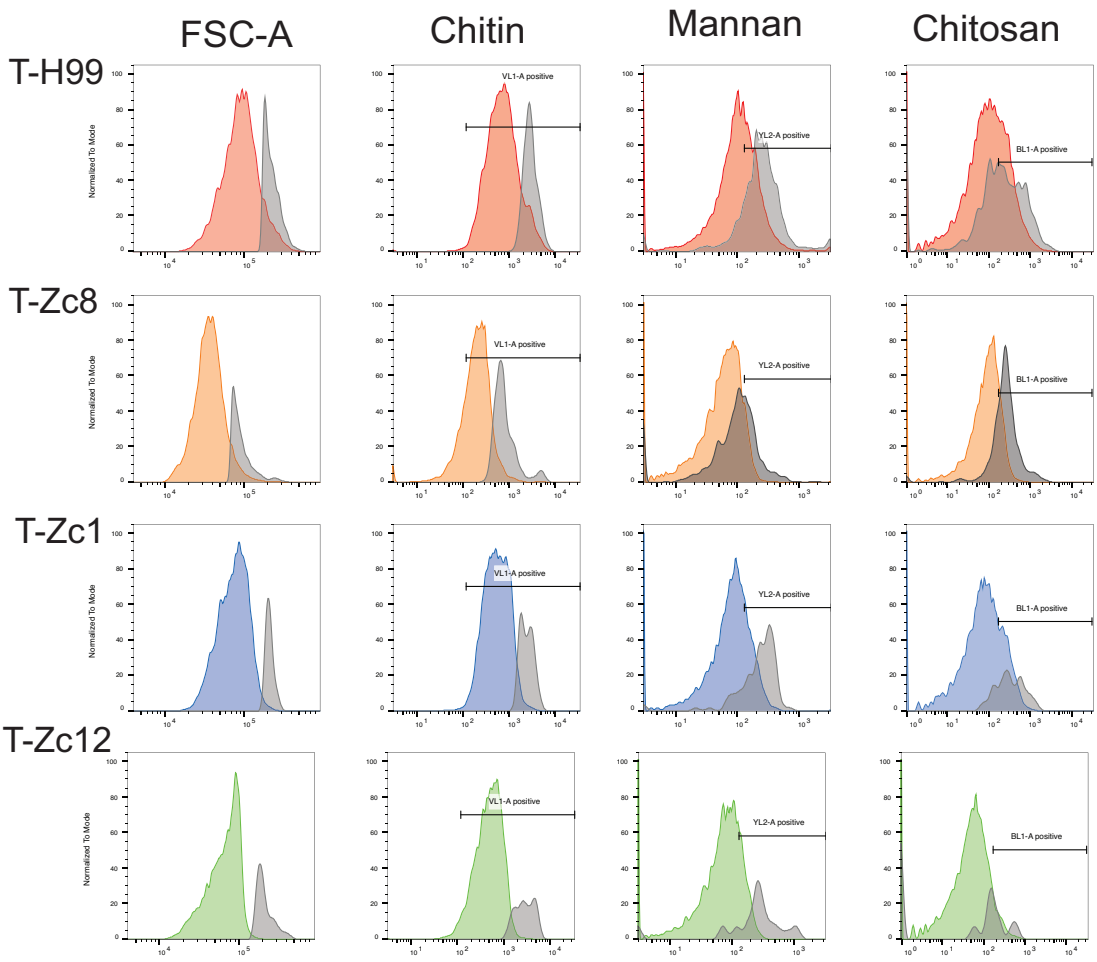


Fig 2.4. PAMP staining flow cytometry analysis of induced cells from Fig 2.3 with large cells sub-population highlighted in grey and MFI indicating exposure of Chitin

(CFW, right); Mannan (ConA, center); and Chitosan (EosinY, left). “T” indicates pre-titanized cells. Experiments were independently repeated at least three times (n>3) with a representative biological replicate is presented.

2.3 Cell density is sufficient to change capsule size and structure during capsule induction

To further explore the differences in disease outcome resulting from titan induction, we examined capsule structure from yeast-phase and titan-induced stages. The *C. neoformans* cell wall is covered by a protective capsule, which not only impairs phagocytosis by macrophages, but also masks PAMP from being engaged by host PRRs (Erwig and Gow 2016). We first examined growth during incubation in 10% FCS at high cell density (OD_{600} 0.1), conditions established to induce robust capsule but not titan cells (Dambuza, Drake et al. 2018). Capsule was visualized using india ink and the capsule to cell body ratio measured (Fig 2.5B, C). H99 and Zc12 showed an overall larger capsule size compared to Zc1 and Zc8 (Fig 2.5B) ($p<0.0001$, $n>100$). We previously showed that the anti-capsule IgM antibody Crp127 binds O-mannosylation sites in capsular polysaccharide (Probert, Zhou et al. 2019). In standard capsule inducing conditions, Crp127 binding was highly heterogeneous across and within all four strains, with both stained and unstained cells apparent (Fig 2.5C), consistent with our previous reports assessing binding during YPD and DMEM-induced growth (Probert, Zhou et

al. 2019). As assessed by flow cytometry, H99 spanned unstained to high binding, with 51.8% of cells showing intermediate or high binding. For Zc8, the vast majority stained with intermediate Median Fluorescence Intensity (MFI (67.7%)). For Zc1 the majority of cells are unstained (86.4%), while 48.1% of cells from Zc12 exhibited intermediate binding (Fig 2.5C).

Simply reducing the cell density leads to titan induction:10% FCS at OD_{600}=0.001. After induction, all isolates expressed robust capsule and were reactive to Crp127 IgM. Analysis of capsule to cell body ratio for each of the populations revealed that Zc12 cells display reduced capsule compared to the other isolates ($p<0.0001$, $n>100$) (Fig 2.6B). Across the four isolates, binding by Crp127 remained heterogeneous, but binding patterns changed compared to high density capsule induction (Fig 2.6A, C), consistent with our observation that Crp127 binding is dynamic throughout titan development (Probert, Zhou et al. 2019). Similar to high-density capsule induction, for H99 and Zc12, more than 50% of the total population was positive for IgM binding, but H99 staining was higher overall, while Zc12 remained more intermediate. For Zc1, which was predominately negative for IgM under high-density capsule conditions, ~40% of cells became positively stained. However, for Zc8 the pattern was reverse: only 5% of Zc8 cells, the largest cells present, were positive for IgM binding, whereas a majority of Zc8 cells were positive for IgM under high density capsule induction (Fig 2.6C, D). Together, these data

suggest that differences in cell density during exposure to inducing conditions (OD600 = 0.1 vs 0.001) significantly impact capsule structure, with a high potential for altered capsule expression and organization across genetically related clinical isolates, even in absence of large-scale cell size changes (Zc1, Zc12).

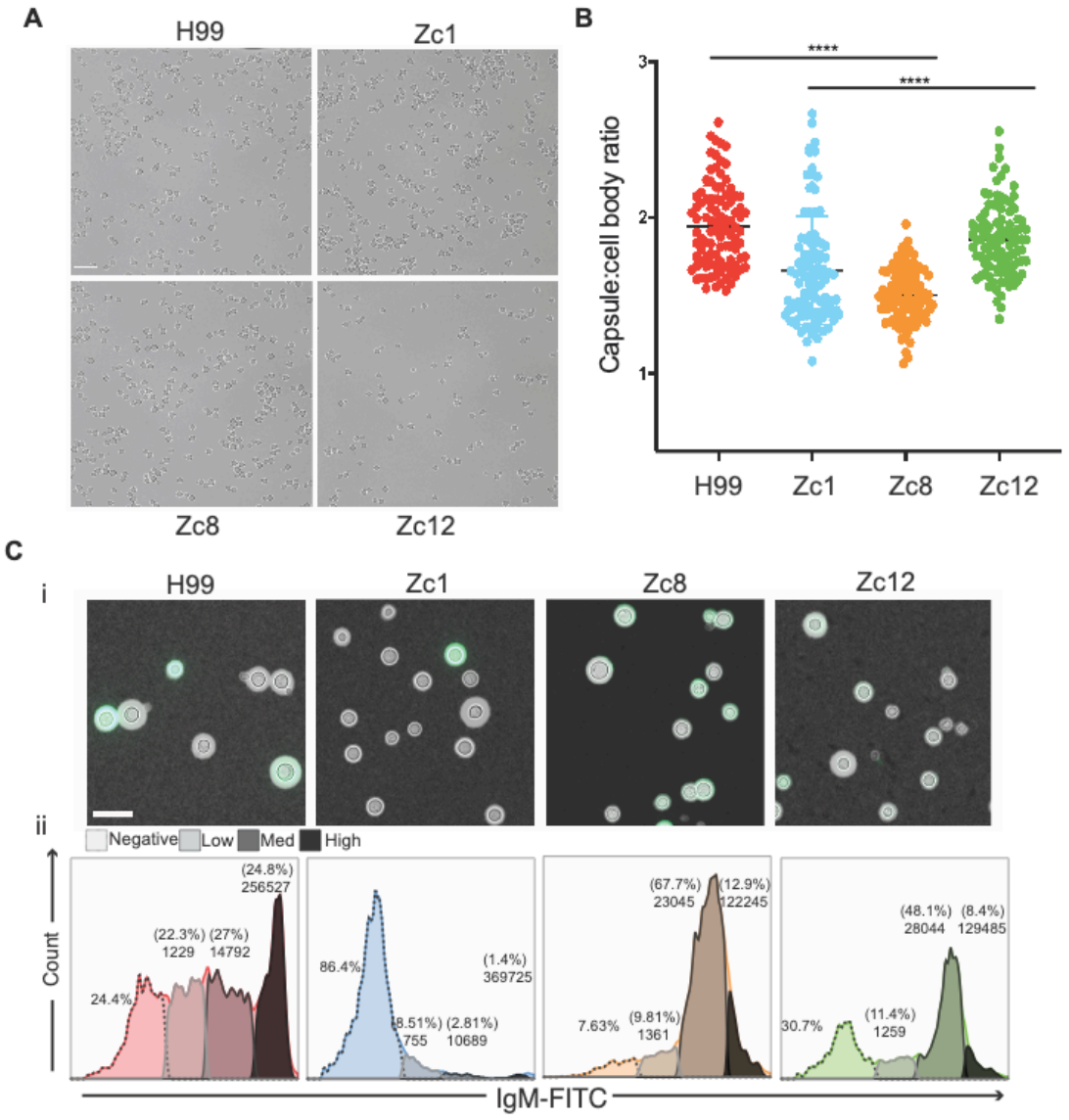


Fig 2.5. Phenotype characterization of clinical isolates at yeast phase. (A) *C. neoformans* cells from all indicated strains at yeast phase, Scale bar: 20μm. (B) Total capsule and cell body diameters were measured and a ratio reported for each cell.

(n>100). ****: p<0.0001. Data were assessed for normality by Shapiro-Wilk and analysed by One-Way ANOVA. (C) i) Representative images of capsule structure from capsule induction condition stained with both India ink and anti-IgM (Crp127) FITC(Green). ii) Histograms for IgM staining and gates show peaks for different levels of staining with corresponding frequency and MFI reported. Negative: cells failed to bind. Scale bar: 10μm. Experiments were independently repeated at least three times (n>3) with a representative biological replicate is presented.

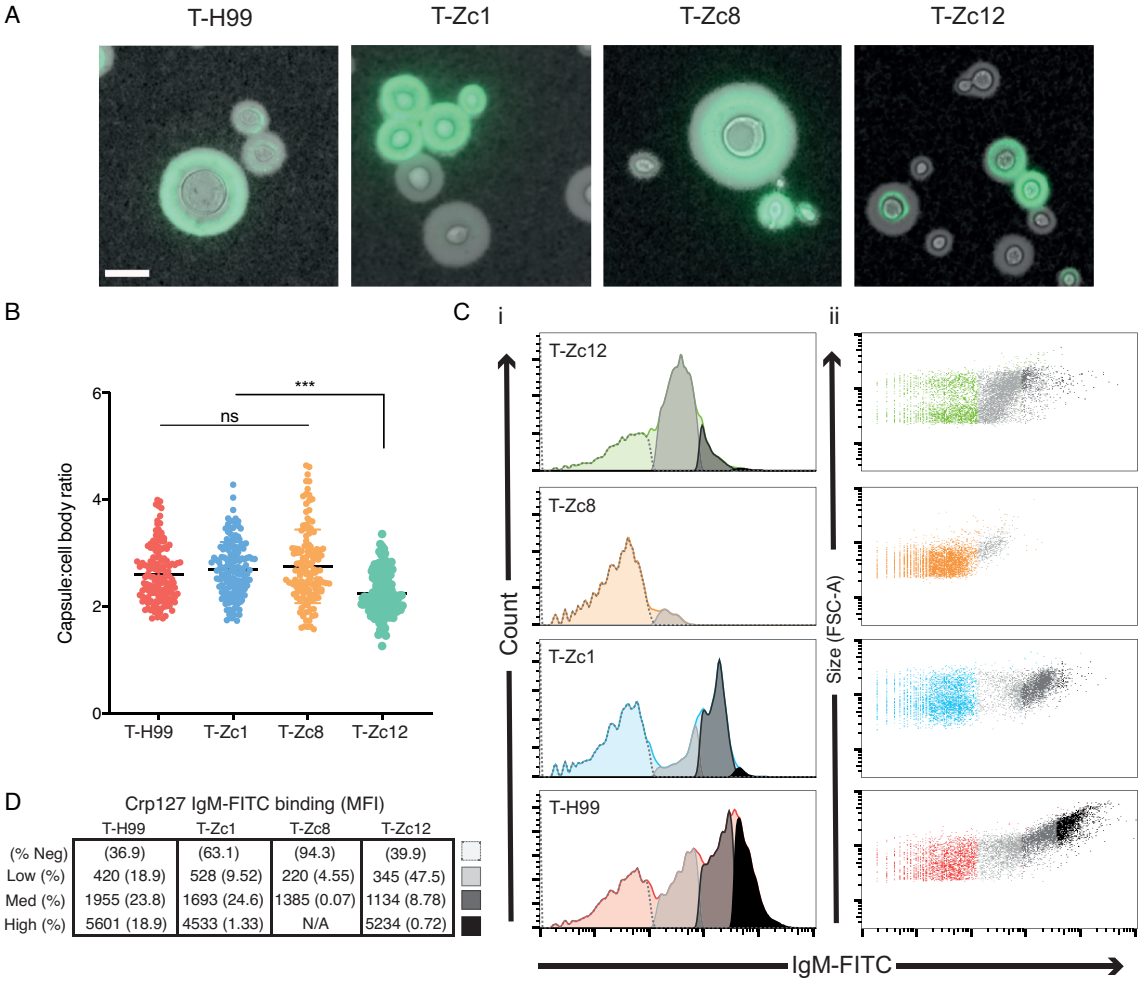


Fig 2.6. Capsule structure from titan induction(A) Representative images of capsule structure of titanized cells stained with India ink and anti-IgM (Crp127) FITC(Green); bar scale: 10μm. (B) Total capsule and cell body diameters were

measured and a ratio reported for each cell (n>100). ****: p<0.0001. Data were assessed for normality by Shapiro-Wilk and analysed by One-Way ANOVA. (C, D) Flow cytometry analysis of IgM staining with frequency and MFI reported. Ci) Gates show peaks for different levels of staining, with (D) corresponding MFI indicated. Cii) Size (FSC-A) vs IgM-FITC intensity, with different populations highlighted as in (Ci). "T" indicates pre-titanized cells. Experiments were independently repeated at least three times (n>3) with a representative biological replicate is presented.

2.4 What are titanides?

We previously identified a third distinct cell type in induced cultures: oval cells 2-3 μm in diameter with thin cell walls and a clear, well defined nucleus, which we termed titanides (Dambuza, Drake et al. 2018). These cells emerge 24 hrs after serum exposure and are the predominant cell type in H99 induced cultures after 3 days (Fig 2.1A, 2.7A). We observed titanide cells in Zc8 *in vitro* cultures that shared these features (Fig 2.1A, 2.7A) and in *in vivo* lung extracts (Fig 2.8A), where thick walled "micro" cells could also be observed. Viability analysis of individual cells isolated from *in vitro* cultures by microdissection was 100% within 48 hours of serum induction for both H99 and Zc8 titanides. Titanides are therefore distinct from previously described micro cells (<1 μm) and drop cells (5 μm), which have thick cell walls and, for the latter, disorganized nuclei and low viability (Feldmesser, Kress et al. 2001, Zaragoza 2011, Alanio, Vernel-Pauillac et al. 2015).

Examination of DNA content by flow cytometry for small cell populations revealed that when grown under inducing conditions, all four clinical isolates contained cells with apparent “sub-1C” DNA content, represented as stepwise peaks to the left (Fig 2.1D). These “sub-1C” populations were not present when cells were grown in YPD (Fig 2.2A ii). We speculated that these peaks might represent titanide cells, and in fact they are the smallest cells by FSC (Fig 2.2B). Microscopy to compare cell size in high density capsule inducing conditions vs. low density conditions also showed that these small cells are specifically generated under titan induction (Fig 2.7B).

Similar “sub-1C” peaks have been observed during flow cytometry-assisted cell cycle analysis of *Saccharomyces cerevisiae* and are representative of G0 or quiescent cells (Delobel and Tesniere 2014, Zhang, Martinez-Gomez et al. 2019). We speculated that this peak might therefore represent G0 quiescent cells, suggesting that titanides might share similarity to *C. neoformans* spores produced by mating, which are quiescent prior to germination. To test this hypothesis, we first established that quiescent *C. neoformans* spores exhibit sub-1C DNA content similar to *S. cerevisiae* quiescent cells. H99, Zc1, Zc8, and Zc12 MATalpha cells were crossed with KN99 MATa cells and incubated for 2 weeks to ensure robust sporulation. Zc1 and Zc12 formed robust hyphae and sporulating basidia after 7 days, comparable with H99. Zc8, a MATalpha isolate, exhibited a profound defect in

the formation of hyphae, with sporulating basidia rarely visible even after 3 months (Fig 2.8B). The mating front, representing hyphae, basidia, spores, and some contaminating yeast, was excised, and filtered through 40 um filters to exclude large particles. The resulting population was fixed, stained and analysed by flow cytometry alongside yeast-phase cells to identify 1C and 2C gates and a “sub-1C” background of <2.5%, set as a threshold for false positives using actively growing YPD cultures. This analysis revealed a “sub-1C” peak to be a major population in robust mating reactions (H99: 37%; Zc1:34%; Zc12:53%) and a minor population (10%) in the Zc8 mating front, in which basidia were rarely observed (Fig 2.7C, 2.8B). Direct comparison to titan-induced H99 cultures revealed a similar “sub-1C” peak (8%) suggesting that this population represents quiescent G0 cells specifically generated during titan induction.

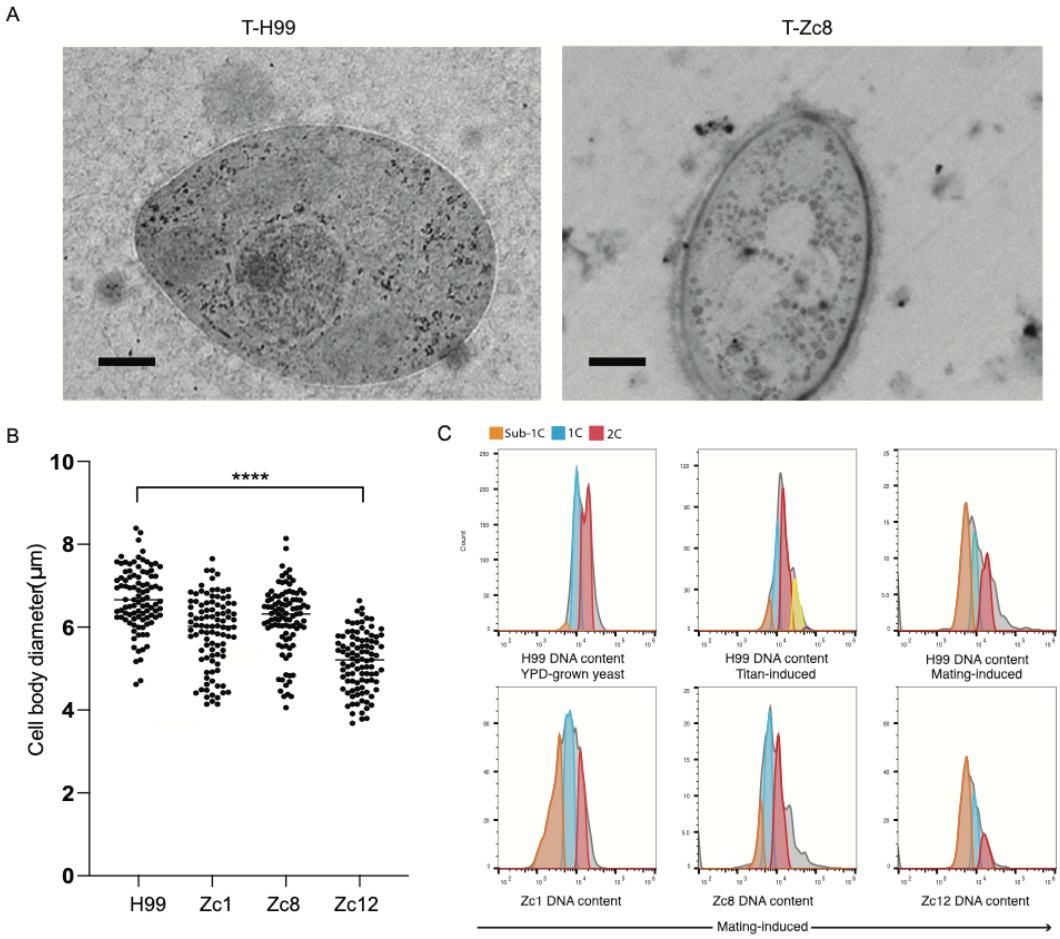


Fig 2.7. Titanides from both *in vivo* and *vitro* (A) TEM of titanide cells from H99 and Zc8 from titan induction. Scale bar:500nm. (B) Cell body sizes of all indicate strains after capsule induction(n>100, ****: p<0.0001). Data were assessed for normality by Shapiro-Wilk and analysed by One-Way ANOVA. (C) Flow cytometry for DNA content of mating fronts from the indicated isolates crossed with KN99a. 1C and 2C populations were identified relative to YPD-agar grown yeast cells from matched parent strains and MFI was recorded for sub-1C, 1C, 2C peaks. “T” indicates pre-titanized cells. Experiments were independently repeated at least three times (n>3) with a representative biological replicate is presented.

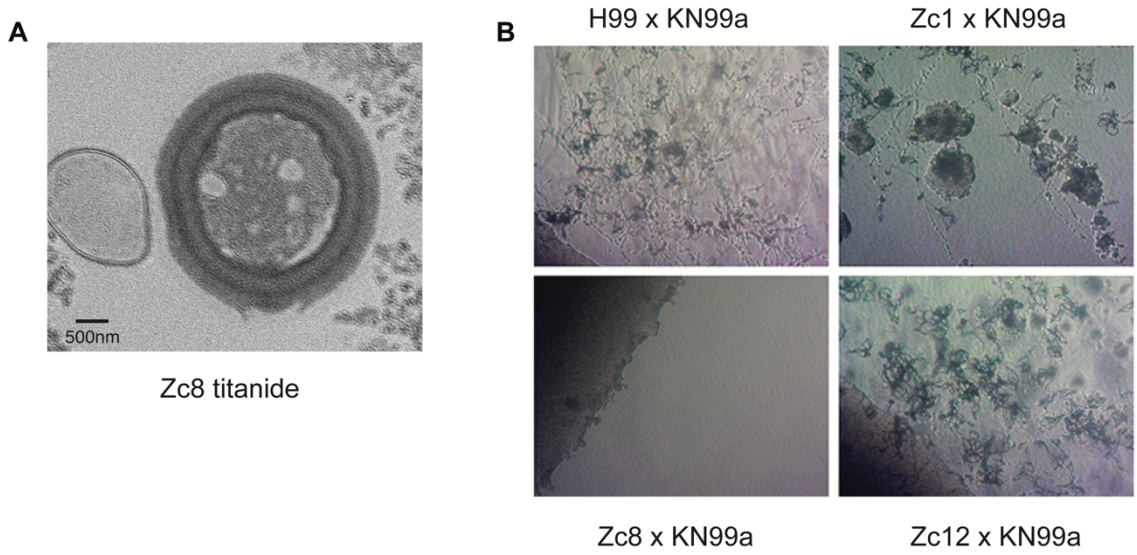


Fig 2.8 (A) TEM of Zc8 titanides recovered from mice lungs, scale bar: 500nm. (B) Mating plates from the indicated isolates crossed with KN99 MATa. The representative image is presented for a biological replicate (n>3).

2.5 Modelling fungal-phagocyte interaction *in vitro* reveals strain specific phenotypes

To better understand the impact of titan and small cells on disease development, we analyzed the infection process of all four strains following titan induction using an *in vitro* model. During initial cryptococcal infection in the host lung, the first immune cells to encounter *Cryptococcus* are resident alveolar macrophages, and the outcome of this interaction is predicted to determine the course of this infection (Johnston and May 2013). To model the impact of titanization on disease development, we first studied the *in vitro* interactions between these four strains and murine J774.1A macrophage-like cells, a commonly used proxy for *Cryptoccocus*-macrophage interactions (Ma,

Hagen et al. 2009, Gilbert, Seoane et al. 2017). Each of the four clinical isolates was incubated in titan-inducing conditions for 24 hours and then co-incubated with phagocytes for 2 hours. Cells incubated in YNB for 24 hours served as a control. To differentiate engulfed and un-engulfed cells, calcofluor white was added to the medium prior to fixation and imaging. We observed significant variation in the percent of macrophages containing at least one internalized *C. neoformans* cell across the four isolates, while YNB grown cells were phagocytosed similarly across the four isolates (Fig 2.9A). Among titan-induced cells, H99 showed the lowest macrophage infection rate and was significantly reduced compared to the other 3 strains (Fig 2.9A) (compared to H99: Zc1, p=0.0063; Zc8, p=0.0131; Zc12, p=0.0164). As shown in Fig 2.9B, for both H99 and Zc8, it appears most engulfed cells were typical cells (titanides and yeasts) rather than titan cells. Furthermore, capsule staining with 18B7 revealed that H99 titan cells physically associated with macrophages but were not engulfed (Fig 2.9D). We therefore asked whether the reduced uptake of H99 cells overall relative to Zc8 (Fig 2.9A) is a consequence of the higher proportion of titan cells in this population, similar to *in vivo* reports. Filtered titan (>10 μm) cells or typical (<10 μm) H99 cells were used to infect macrophages separately. When only titan cells were present, the average macrophage infection was 21.6% ± 5.5 (SEM), while for typical H99 cells the rate was 82.2% ± 1.6 (SEM) (Fig 2.9C, p=0.0002, n=500),

similar to uptake of the total populations for the three Zc strains. Mixed cultures of titanized cells were co-incubated with macrophages *in vitro* and observed via time-lapse imaging for 18h. Intracellular Proliferation Rate (IPR), frequency of vomocytosis (vomo %), and frequency of macrophage death (Mϕ death %) were measured. No significant difference in IPR was observed for the four strains, indicating that they maintain similar intracellular growth rates (Fig 2.9E). Zc8 induced the highest frequency of vomocytosis, although it was not statistically significantly different ($p=0.05$ vs. Zc12) (Fig 2.9F), but did induce significantly more macrophage death ($p<0.001$) (Fig 2.9G; n=400). This suggests that there is no correlation between titanization capacity and vomocytosis or macrophage death. These results are consistent with previous studies *in vivo* showing that titan cells are more resistant to phagocytosis and with the observation that these cells exert a protective effect on the uptake of smaller cells and further validate the overlap between *in vitro* induction and *in vivo* induction (Okagaki, Strain et al. 2010, Gerstein, Fu et al. 2015).

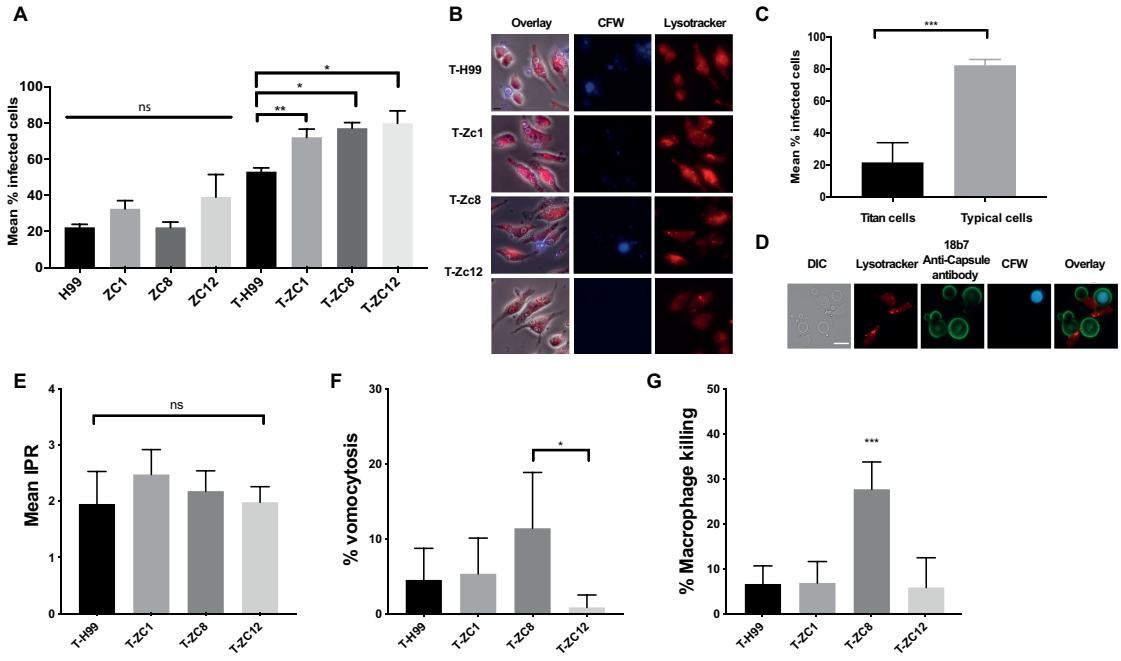


Fig 2.9: *In vitro* titan cells interaction with host immune cells (A) Infection rates for the 4 clinical strains, showing the percentage of macrophages infected with at least one internalized *C. neoformans* cell after 2h co-incubation. Data were assessed as not normal by Shapiro-Wilk and analysed by Welch's ANOVA with Dunnett's test for multiple comparisons. **p*<0.02; ****p*=0.0008. (B) Representative images showing macrophages (Red, Lysotracker) infected with cryptococcal cells (Blue, CFW). Scale bar: 10µm. (C) Macrophages infection rates infected with only titan or typical cells (typical cells <10 um, titan cells > 11 um). Data were assessed for normality by Shapiro-Wilk and analysed by Student's T-test with Welsh's correction for unequal variance (determined by F-test). ****p*=0.0002. (D) Representative images showing macrophages (Red)infected with H99 yeast and titan cells. Fungi were co-incubated with anti-capsule antibody 18b7 plus anti-mouse IgG-FITC (Green) and calcofluor white (CFW) for chitin (blue). Scale bar: 20µm. (**E-G**) Macrophages and pre-titanized

C. neoformans were co-incubated for 18 hours and assessed via live imaging for (**E**) IPR, (Trevijano-Contador, Pianalto et al.) (**F**) vomocytosis, and (**G**) macrophage lysis. (**E**) IPR: mean intracellular proliferation rate. Data were assessed for normality by Shapiro-Wilk and analysed by One-Way ANOVA. (Trevijano-Contador, Pianalto et al.) Mf death %: frequency of macrophage de ath indicated by cell lysis. Data were assessed for normality by Shapiro-Wilk and analysed by One-Way ANOVA. *p=0.05; ***p<0.001. (**G**) Vomo %: frequency of vomocytosis. Data were assessed as not normal by Shapiro-Wilk and analysed by Kruskal-Wallis with Dunn's correction. "T" indicates pre-titanized cells. Experiments were independently repeated at least three times (n>3) with a representative biological replicate is presented.

2.6 Titan cells enhance the production of TNF

Titan cells have previously been reported to enhance the production of TNF, a marker of M1 and T_H1 polarization required for successful *Cryptococcus* infection control and involved in ROS generation (Davis, Tsang et al. 2013, Leopold Wager and Wormley 2014). As shown in Fig 2.10A, after 24 hrs there was increased accumulation of TNF for macrophages infected with either induced H99 ($p<0.0001$) or Zc8 ($p=0.01$) cells compared to their un-induced controls. In particular, H99 titanized cells showed an almost 10-fold increase compared with Zc1 and Zc12 strains pre-cultured under titanizing conditions (Fig 2.10A). However, induced Zc8 cells also elicited increased TNF compared to induced Zc1 ($p=0.004$) or Zc12 ($p=0.0002$). This

increase can primarily be explained by the presence of titan cells: when macrophages were infected with filtered H99 titan cells, there was significantly higher accumulation of TNF compared to a mixed infection ($p<0.0001$) or to pre-induced typical cells alone ($p<0.0001$) (Fig 2.10B). Circulating blood monocytes are increasingly recognized as essential players in innate and adaptive immune responses against a wide range of microbes (Serbina, Jia et al. 2008, Lauvau, Loke et al. 2015, Heung and Hohl 2019). Human monocytes derive from progenitors in the bone marrow and can supply tissues with macrophages and dendritic cell (DC) precursors that contribute to antimicrobial defense (Taylor and Gordon 2003, Gordon and Taylor 2005, Lauvau and Soudja 2015) However, Heung et al. recently showed that during infection, *C. neoformans* can influence inflammatory monocyte polarization to an alternatively activated M2-like profile which are poor producers of ROS and are detrimental to the host response (Heung and Hohl 2019). To investigate the impact of titan cells on monocyte activation, we determined TNF production by human blood-derived monocytes infected with each of the 4 strains pre-grown under titanizing conditions (Fig 2.10C). As early as 4hrs following incubation, H99 titanized cells showed higher production of TNF compared with the other three strains (Compared with T-H99: all $p<0.0001$) which substantially increased by 24hrs of culture (Fig 2.10C; Compared with T-H99: all $p<0.0001$). As shown in Fig 2.10C, monocytes infected with H99

titanized cells showed higher production of TNFα compared with the other three strains (Compared with T-H99: all $p<0.0001$). Together, by comparing TNF production among clinical isolates, and between filtered cell populations, this thesis demonstrate that *in vitro* titan cells are immunologically distinct from typical cells and their capacity to robustly modulate a pleiotropic cytokine like TNF suggest that titan cells may influence disease outcome in a heterogeneous infection.

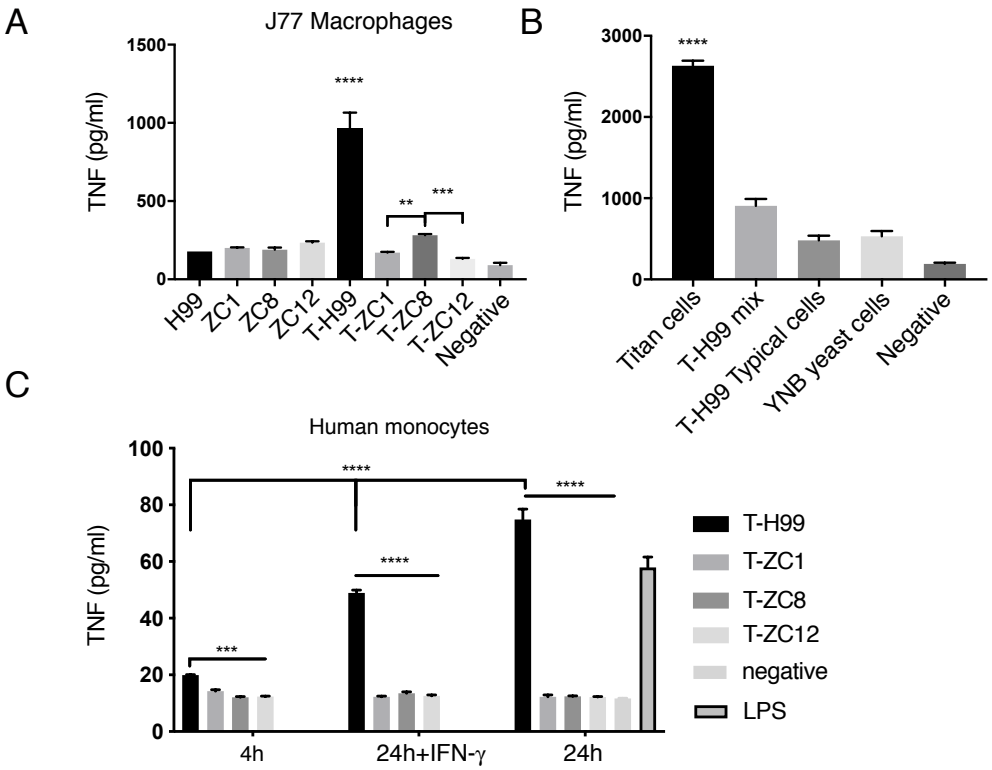


Fig 2.10. Titan cells enhance the production of TNF. (**A**) J774.1 Macrophages and YNB-grown or pre-titanized *C. neoformans* of the indicated strains were co-incubated for 24 hours in triplicate. Supernatants were collected and TNF measured. Data were assessed for normality by Shapiro-Wilk and analysed by One-Way ANOVA with

Holm-Sidak's correction for multiple comparison. **p=0.004; ***p<0.001; ****p<0.0001. (**B**) J774.1 Macrophages were co-incubated with pre-titanized H99 *C. neoformans* that had been filtered by size (typical cells <10 um < titan) for 24 hours in triplicate. Supernatants were collected and TNF measured. Data were assessed for normality by Shapiro-Wilk and analysed by One-Way ANOVA with Tukey's correction for multiple comparison. (**C**) Human monocytes from whole blood and YNB-grown or pre-titanized *C. neoformans* of the indicated strains were co-incubated for 4 or 24 hours plus or minus IFN-γ10U/ml in triplicate. LPS-treated monocytes (100ng/ml 24hr) served as a positive control. Supernatants were collected and TNFα measured. Data were analysed by Two-Way ANOVA with Tukey's correction for multiple comparison. Experiments were independently repeated at least three times (n>3) with a representative biological replicate is presented.

2.7 *In vivo* titan inducing conditions match *in vitro* predictions

Overall, *in vitro* phenotyping by microscopy and flow cytometry for cell size and DNA content predicts that: 1) H99 and Zc8 isolates will form titans *in vivo*, with the overall size of Zc8 populations smaller than that of H99, 2) a minority of Zc1 titan cells might be detected, 3) Zc12 will fail to produce detectable titans *in vivo*, and 4) small cells will be apparent for all four isolates and will proliferate to a similar degree within phagocytes. We therefore assessed all four strains in a murine inhalation model of cryptococcosis, the gold standard for determining titan capacity. C57BL/6 female mice were

infected intra-nasally with $5x10^5$ cells pre-cultured in sabouroud dextrose medium according to standard infection protocols, and brain and lung fungal burdens were measured after 10 days. Work using H99-derived mutants has demonstrated a role for titan cells in survival and proliferation in the pulmonary environment as early as day 7 (Crabtree, Okagaki et al. 2012). When fungal cells from lung homogenates were analysed microscopically for titanization *in vivo*, similar size distributions were observed as seen *in vitro* (Fig 2.11A). Specifically, robust titanization was observed for both H99 and Zc8 (65% and 68% of cells recovered from the lung, respectively, >10 um), with Zc8 population covering a significantly smaller size range than H99 (Kolmogorov-Smirnov test for cumulative distribution, p=0.0001). A minority (8%) of Zc1 cells were >10 um. No Zc12 cells >10 um was observed. Similar to *in vitro* induced Zc1 and Zc12 cells, the *in vivo* populations as a whole were smaller and more uniform overall. All four clinical strains showed similar fungal burdens in the lungs on day 10 (Fig 2.11B, $p>0.05$) as assessed by CFUs, demonstrating similar capacities to proliferate early during infection. Moreover, brain CFUs analysed at day 10 post infection were comparably low across all four isolates, with Zc1 CFUs slightly higher than the others (Fig 2.11C; $p<0.01$). Taken together, these results support our predictions that *in vitro* titanization reflects *in vivo* titanization.

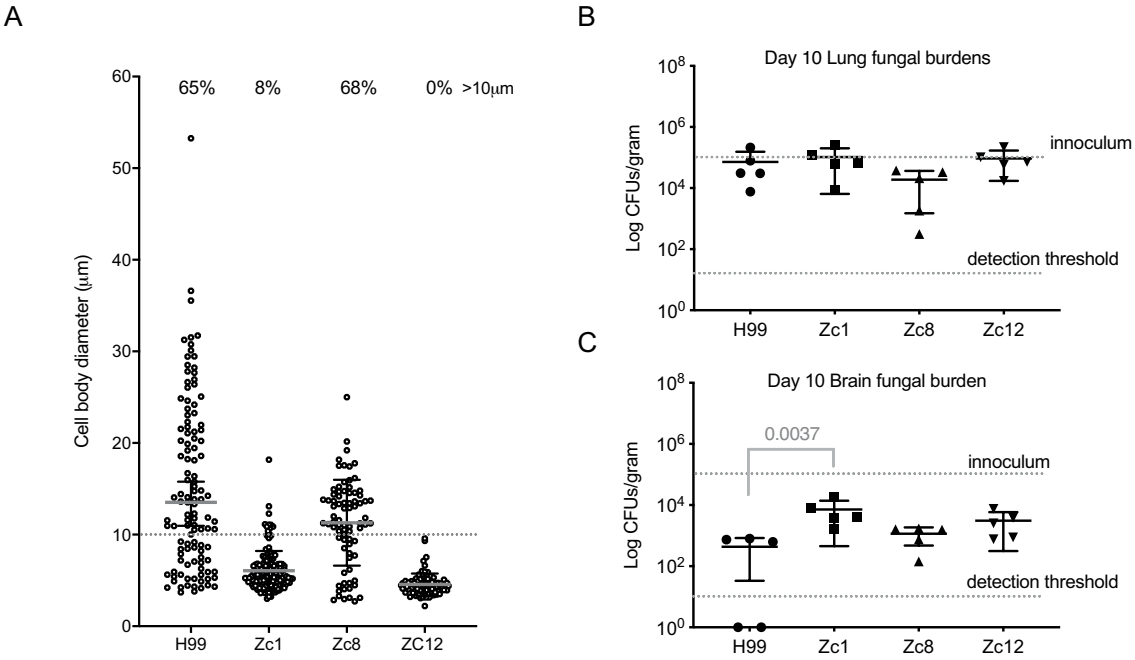


Fig 2.11. Titanizaiton and disease outcomes on mouse model. (A) Cell body sizes of fungal cells collected from murine lungs (n>70 cells for each isolate). (B, C) Infectious burdens for the indicated strains. Murine lungs (B) and brains (C) were assessed for dissemination 10 days post-infection via colony forming units of total homogenates (n=5 per strain). Data are presented as Log CFU/gram. (B) Data were assessed as normal by Shapiro-Wilk and analysed by One-Way ANOVA with Holm-Sidak's multiple comparisons test. Data are presented as Log CFU/gram. (C) Data were assessed as not normal by Shapiro-Wilk and analysed by Kruskal-Wallis ANOVA with Dunn's correction for multiple comparisons.

2.8 Clinical isolates show different capacities to produce aneuploid colonies

In vivo polypoid titan cells were reported to be able generate aneuploid progeny with improved stress resistance compared to typical cells from the

same culture (Gerstein, Fu et al. 2015). Our *in vitro* model predicts that high titanizing isolates H99 and Zc8 will yield greater aneuploidy *in vivo.* It remains unclear whether ploidy variation in CNS cryptococcosis reflects the degree of ploidy variation observed in the lung. However, because titan daughter cells are smaller on average and readily phagocytosed, we predict that ploidy variation following dissemination to the brain will reflect the degree of ploidy variation observed in the lung. To test this, we determined the impact of titanization on the genetic diversity of offspring and the impact on different sites. We examined the ploidy of individual colonies originating from lung and brain CFUs for all four isolates (Fig 2.12A, n=30 for lung CFUs, n≥10 for brain CFUs, across 3 mice per isolate). Colonies were assessed within 72 hours of recovery from mice, at the point when a small colony was just visible on YPD agar (~36 generations), a measure of stable aneuploidy in the absence of environmental stress. Fig 2.12A shows the ploidy of individual colonies relative to the median ploidy of all colonies from that particular lineage. Interestingly, ploidy variation occurred for all isolates, including Zc12. There was no significant difference in relative ploidy between colonies from lung vs. brain isolates for any of the isolates. We observed that ploidy of H99 and Zc8 colonies varied widely, while Zc1 colonies were more uniform ($p=0.02$ compared to H99). This is consistent with a high degree of titanization driving aneuploidy in H99 and Zc8 infections, and relatively low titanization in the Zc1

isolate. However, we also observed widespread instances of aneuploidy in Zc12 CFUs, despite finding no evidence of true titanization in this strain either *in vitro* or *in vivo*.

Aneuploidy is associated with increased resistance to fluconazole, which continues to be used as a frontline antifungal in resource limited settings. Fluconazole resistance in *C. neoformans* is linked to aneuploidy of chromosomes 1, 4, 6, and 10 due to the presence of genes on these chromosomes that directly enable fluconazole resistance, however the contribution of titanization to resistance remains unclear (Zafar, Altamirano et al. 2019). We therefore assessed the impact of altered ploidy on drug resistance of individual colonies isolated from the lungs and brains of infected mice (Fig 2.12B). Relative to parent isolates, we observed a wide range in capacity to proliferate in the presence of fluconazole. The distribution of resistance for Zc12-derived colonies was significantly limited compared to those of H99, Zc8, or Zc1 ($p \leq 0.0002$). For H99, both fluconazole resistant and sensitive colonies were identified. For Zc8, colonies with increased resistance to fluconazole tended to have increased ploidy, but a colony with reduced overall ploidy and increased drug resistance was also observed. For Zc1, aneuploid colonies were more sensitive to the drug. Within individual lineages there was no correlation between increased or decreased ploidy and degree of fluconazole resistance ($R^2<0.3$ in all cases). This is consistent with

titanization facilitating ploidy shifts in progeny and with aneuploidy in these isolates being random rather than specific amplification of chromosomes involved in fluconazole resistance occurring prior to drug exposure.

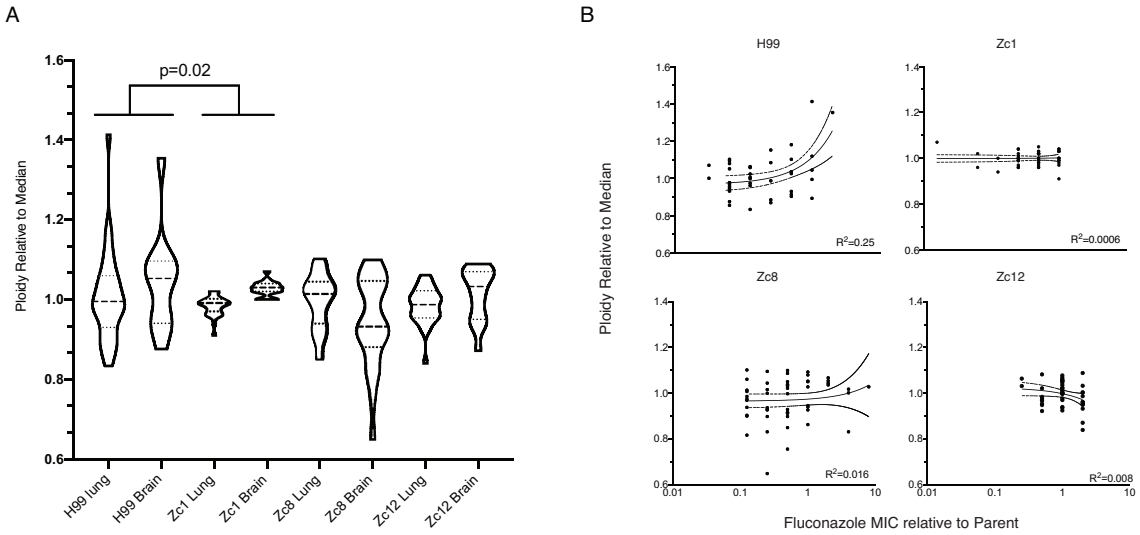


Fig 2.12: Clinical isolates produce aneuploid daughter cells with altered drug resistance *in vivo*. (A) Degree of heterogeneity in ploidy across the individual colony forming units recovered from host tissue. 1C and 2C populations were identified relative to YPD-grown colonies from matched parent strains and MFI was recorded for 1C and 2C peaks. Data are presented relative to median 1C MFI for all colonies for a given isolate. Data were assessed as not normal by Shapiro-Wilk and analysed by Kruskal-Wallis ANOVA compared to H99 with Dunn's correction for multiple comparisons. (B) Fluconazole resistance relative to parent for individual colonies aggregated in (A). Data are plotted relative to parent MIC and as a function of colony ploidy as assessed in (A). Data were assessed as not normal by Shapiro-Wilk and analysed by Kruskal-Wallis ANOVA with Dunn's correction for multiple comparisons

Discussion

The yeast-to-titan transition is an important morphogenetic switch for *C. neoformans* that can affect drug resistance and host immune responses, contributing to poor disease outcomes (Okagaki, Strain et al. 2010, Zaragoza, Garcia-Rivera et al. 2010, Okagaki, Wang et al. 2011, Crabtree, Okagaki et al. 2012). In a common laboratory strain (H99), *in vitro* and *in vivo* titan induction yields a heterogeneous population including >10 μm titan cells, 5-7 μm yeast cells, and 2-4 μm titanides. Previous reports have shown that titan cells are associated with enhanced virulence and the generation of aneuploid cells that facilitate stress adaptation and drug resistance, while small (>10 μm) cells are associated with increased dissemination. However, the relationship between titan cells, small cells, and titanides remains unclear. With the development of robust *in vitro* titan cell induction models, we are now able to reproduce titan cells *in vitro* using host-relevant environment signals. Here, we characterize key changes in clinical strains after titanization, revealing that non-titanizing strains also show high population heterogeneity both *in vitro* and *in vivo*. we characterize titanides and small cells in H99 and three clinical isolates and show that titanides share G_0 quiescent-like DNA staining of mating spores. In addition, we show that both titanizing and non-titanizing isolates exhibit altered capsule structure and PAMP exposure over time during *in vitro* culture, and generate aneuploidy *in vivo.*

2.9 Investigating population heterogeneity *in vitro*

Here, we expand upon the *in vivo* definition of titan cells to encompass the wide phenotypic diversity observed during *in vitro* induction of three clinical isolates from the ACTA Lusaka Trial in Lusaka, Zambia (Vanhove, Beale et al. 2017, Molloy, Kanyama et al. 2018). Our data add to existing knowledge by specifically studying clinical isolate titanization using an established *in vitro* titan induction protocol. After *in vitro* titanization, *C. neoformans* populations are highly heterogeneous with multiple sub-populations: titan (>10μm), typical/small (>4μm), and titanide (2-4μm) cells, as well as micro (1μm) cells (Cruickshank, Cavill et al. 1973, Love, Boyd et al. 1985, Feldmesser, Kress et al. 2001, Okagaki, Strain et al. 2010, Evans, Li et al. 2015, Dambuza, Drake et al. 2018). Building on our previous findings, we used 4 clinical strains from the same genetic clade (VNI) which we previously identified as having different capacities to produce titan cells (Dambuza, Drake et al. 2018). These four strains are closely related based on genome analysis, however evolved variation still exists between them.

All 4 strains demonstrated significant population heterogeneity after exposure to inducing conditions, regardless of titan status. Relative to Zc8, H99 is strongly titanizing *in vitro* when the *in vivo* definition (> 10 μm) is applied, but Zc8-induced cells exhibit overall population structure consistent with titanization, including polyploidy (>4C), a relative increase in cell size,

and overall changes in PAMP organization. By combining microscopy and flow cytometry, we propose a model in which predictive outcomes can be made about *in vivo* strain “titan-signature” status. We additionally note that researchers can readily identify titan cells through visual inspection of liquid cultures in tissue culture plates using bright-field microscopy, with titans being large cells with a single vacuole and an intensely dark cell wall apparent in H99, Zc8, and Zc1 cultures, but DNA content analysis offers important information about overall population structure (Fig 2.1A, D).

2.10 Variation in cell size and morphology and impact on host cell interaction

Population heterogeneity appears to be a general feature of titanizing isolates. Here we observed that both titanizing strains H99 and Zc8 are highly heterogeneous after induction, with three sub-populations that maintain distinct cell sizes and DNA contents. Moreover, titan cells from both strains exhibit changes in PAMP exposure and capsule size and composition, features important for the virulence of *C. neoformans*. Surprisingly, non-titanizing induced strains Zc1 and Zc12 also show population heterogeneity as measured by DNA content and cell wall structure, despite a lack of true titan cells. Consistent with previous findings, we directly showed that the presence of titan cells leads to decreased phagocytosis rates of small cells (Okagaki, Strain et al. 2010, Gerstein, Fu et al. 2015). Denham et al. showed

that at later infection stages, in both lungs and brains the predominant population is the smaller cryptococcal cells around 10μm in total diameter(Denham, Verma et al. 2018). This matches our *in vitro* observation that in later titan-induced cultures, the proportion of small cells increases, consistent with the increased replication rate of titan mothers and the impact of cell culture density on the generation of new titan mothers(Dambuza, Drake et al. 2018, Hommel, Mukaremera et al. 2018, Trevijano-Contador, de Oliveira et al. 2018).

We additionally observed changes in capsule and IgM binding upon titan induction relative to other capsule inducing protocols. IgM mediates complement-dependent phagocytosis and has been shown to specifically inhibit the yeast-to-titan transition (Aslanyan, Ekhar et al. 2017, Trevijano-Contador, Pianalto et al. 2020). Interestingly, IgM has been shown to be particularly important in the clearance of small particles (2-5 μm) (Litvack, Post et al. 2011). Our data here suggest differences in epitope exposure on small vs. large cells may exert a protective effect by reducing overall phagocytosis. Future work will examine the impact of titan induction on complement-dependent, opsonin-independent uptake and will address the relative pathogenic potential of titanide vs yeast vs spores in murine models of infection.

2.11 How do titanides contribute to disease progression?

There is growing evidence of a high degree of genome plasticity during *C. neoformans in vivo* growth (Semighini, Averette et al. 2011, Morrow, Lee et al. 2012, Gusa, Williams et al. 2020). Semighini *et al*. previously demonstrated, using comparative genome hybridization arrays in H99-derived strains, that passage through mice in the absence of drug stress results in large scale genome alterations, including aneuploidy, insertions, and deletions (Semighini, Averette et al. 2011). Gusa *et al.* recently demonstrated that host temperature is sufficient to induce transposon-mediated rearrangements in the *C. neoformans* genome (Gusa, Williams et al. 2020). However, titanization adds to and enhances this variation: titan cells produce aneuploid daughter cells that promote *in vitro* stress resistance relative to yeast in the same population (Gerstein, Fu et al. 2015). We add to these previous reports by showing that high titanizing H99 and Zc8, low-titanizing Zc1 and non-titanizing Zc12 isolates all yield aneuploid daughters to some degree when exposed to the host microenvironment. We reveal that titanization can drive the emergence of aneuploid offspring in the host by comparing the ploidy distribution of cells recovered from infected mice. We observed large scale changes in genome content relative to parent isolates, and this weakly correlates with degree of titanization (H99>Zc8>Zc1>Zc12). We hypothesize that, in addition to strongly inducing titanization, during infection, the host microenvironment itself is sufficient to induce aneuploidy and exerts a

selective pressure, as has been observed for *C. albicans* (Hickman, Zeng et al. 2013). In line with this, we previously reported that daughter cell colonies derived from *in vitro*-induced titan cells are mostly diploid, in conflict with reports from Gerstein *et al*. that colonies derived from *in vivo*-derived titan cells are haploid or aneuploid (Gerstein, Fu et al. 2015, Dambuza, Drake et al. 2018). This suggests that daughter cells derived from the two conditions may differ in their tolerance to aneuploidy or capacity for genome maintenance. Fluconazole exposure, oxidative stress, and high temperature drive *in vivo C. albicans* aneuploidy, including whole ploidy reduction (diploidy to haploidy), individual chromosome aneuploidy (Chr 5), and segmental aneuploidy, and the same is likely true for *C. neoformans* even in the absence of titanization (Forche, Abbey et al. 2011, Hickman, Zeng et al. 2013, Forche, Cromie et al. 2018, Todd, Wikoff et al. 2019). Future work will more fully probe the molecular mechanisms differentiating these clinical isolates and their impact on virulence.

2.12 What is the environmental significance of "sub-1C" cells?

Ashton et al. recently suggested that the existence of robust quiescent cells such as spores might contribute to the broad ecological distribution of specific sub-clades, however the rarity of MATa *C. neoformans* isolates in the environment suggests an alternate origin for these cells (Litvintseva, Kestenbaum et al. 2005, Ashton, Thanh et al. 2019). Here, we demonstrate

that titanides observed in induced cultures originate from titan mothers and that these cells exist in a in G0-like state similar to spores generating by mating. Titanide cells have unique features including oval shape, smaller size and altered DNA content compared with typical yeast cells. The ability to induce titan cells in conditions likely to be encountered by *Cryptococcus* in the environment make it plausible that titan cells may form in the environment and are not just limited to patient lungs. In addition, we also we detected “sub-1C” populations from the Zc12 isolate in titan-inducing conditions, suggesting that the capacity to produce quiescent cells is not simply a consequence of high ploidy mothers. This raises the hypothesis that “quiescent” cells proposed to drive population expansion in environmental isolates may be generated via regulatory pathways driving titanization (Ashton, Thanh et al. 2019).

2.13 Impact of population heterogeneity on drug resistance

Gerstein *et al.* previously demonstrated that *in vivo*-derived titans provide daughters with a survival advantage compared to *in vivo*-derived typical cells (Gerstein, Fu et al. 2015). Therefore, we predict the presence of titanides also contributes to disease progression by affecting drug resistance and stress adaption. Titan-derived colonies are resistant to fluconazole via aneuploidy of chromosomes 1, 4, 10, 11, and/or 12 when propagated in the presence of fluconazole, suggesting that titanization drives fluconazole resistance *in vivo* (Gerstein, Fu et al. 2015, Zafar, Altamirano et al. 2019). Our

data support these findings, with overall increases in population diversity in titanizing strains compared to non-titanizing strains following passage through mice (Fig 2.9A). However, we observed no specific correlation between increased ploidy and increased fluconazole resistance (Fig 2.9B). This is consistent with *in vivo*-induced aneuploidy being random with regard to particular chromosomes, rather than a specific increase of chromosomes involved in fluconazole resistance. Finally, induced but not un-induced cells from all isolates showed high but similar virulence when using the galleria model (data not show) and we found no differences in capacity to control early lung fungal burdens during a mouse model of cryptococcosis. Our data therefore demonstrate that in response to the host environment signals both non-titanizing and titanizing isolates generate heterogeneous populations which will have implications for drug resistance and host cell interactions. Future studies will investigate their impact on long term immune responses including investigation of T cell polarization mediated by the different clinical isolates.

Declaration

This chapter is adopted from an existing paper in which Xin Zhou is the first author, and Dr. Elizabeth Ballou is the corresponding author. This chapter only contains works that are conducted by Xin Zhou. This paper is currently available on bioRxiv : https://www.biorxiv.org/content/10.1101/2021.03.01.433276v1." Host-derived Reactive Nitrogen Species mediate the *Cryptococcus neoformans* yeast-to-titan switch via fungal-derived superoxide"

Signature: Xin Zhou date: 13/12/2021

Signature:  date: 13 Dec 2021

Chapter 3

Mini introduction

Host-derived Reactive Nitrogen Species mediate the *Cryptococcus neoformans* yeast-to-titan switch via fungal-derived superoxide

3.1 Nitrosative and oxidative stress during host-interaction

In the host lung, *C. neoformans* yeast proliferate both extracellularly and within phagocytes (Coelho, Bocca et al. 2014, Erwig and Gow 2016). Successful control of infection requires a robust adaptive response, including T-cell mediated activation of phagocytic macrophages, which bind and internalize fungal cells (Davis, Tsang et al. 2013, Leopold Wager, Hole et al. 2016). Activated macrophages are polarized (M1/M2) and this polarization is dynamic, with an early M2 profile shifting to a protective M1 profile over the course of infection (Arora, Olszewski et al. 2011, Leopold Wager, Hole et al. 2016). Among other responses, M1 cells express NADPH oxidase 2 (Nox2), which generates superoxide anion (O_2^-) and other oxygen-derived intermediates, and inducible nitric oxide synthase (iNOS), which generates nitric oxide and its derivatives (Leopold Wager and Wormley 2014). These host-derived reactive oxygen and reactive nitrogen species (ROS/RNS) are well recognized for their important roles in controlling pathogens by causing

extensive damage to DNA, proteins and lipids (Brown, Haynes et al. 2009, Cadet and Wagner 2013). For *C. neoformans* in particular, host-derived ROS and RNS play important roles in controlling fungal proliferation and dissemination (Coelho, Bocca et al. 2014).

3.2 Fungal cell oxidative and stress response

In response to host oxidative and nitrosative stresses, *C. neoformans,* like other pathogenic fungi, has evolved stress resistance responses that enable fungal survival and lead to disease (Nikolaou, Agrafioti et al. 2009, Brown, Budge et al. 2014, Dantas, Day et al. 2015, Warris and Ballou 2018). Typical fungal responses involve the expression of ROS/RNS detoxification enzymes including superoxide dismutase (SOD), catalase (CAT), glutathione peroxidases, thioredoxin, and peroxiredoxins (Aguirre, Hansberg et al. 2006, Missal, Pusateri et al. 2006, Brown, Haynes et al. 2009, Upadhya, Campbell et al. 2013, Warris and Ballou 2018). These enzymes are required for fungal cells to detoxify intracellular ROS or RNS and play important roles in fungal biology and pathogenicity. For example, in *C. neoformans*, *C. albicans*, and *Aspergillus fumigatus,* the loss of SOD activity has been shown to have direct consequences for fungal virulence (Hwang, Rhie et al. 2002, Cox, Harrison et al. 2003, Giles, Batinic-Haberle et al. 2005, Lambou, Lamarre et al. 2010). *C. neoformans* additionally detoxifies host ROS through the expression of polysaccharide capsule and melanin (Zaragoza, Chrisman et al. 2008).

3.3 Fungal endogenous ROS production

In addition to exogenous ROS/RNS, mitochondria are a major source of endogenous ROS within the fungal cell. During phagocytosis, it is predicted that NO^-, the main product of the iNOS pathway, targets fungal mitochondria leading to the accumulation of Complex III-derived O_2^- within the fungal cell (Iglesias, Bombicino et al. 2015). Consistent with this, host-derived RNS blocks *C. neoformans* proliferation, and iNOS activity is required for host survival (Alspaugh and Granger 1991, Aguirre and Gibson 2000). Detoxification of RNS via nitric oxide dioxygenase and S-glutathione dehydrogenase as well as nitrosative stress responsive transcription factors are required for *C. neoformans* virulence (de Jesus Berrios, Liu et al. 2003, Missall and Lodge 2005, Missal, Pusateri et al. 2006).

Endogenous ROS also act as signalling molecules regulating different biological and physiological processes (Lara-Ortiz, Riveros-Rosas et al. 2003, Takemoto, Tanaka et al. 2007, Semighini and Harris 2008, Tudzynski, Heller et al. 2012, Schieber and Chandel 2014, Rossi, Gleason et al. 2017, Warris and Ballou 2018). In *A. nidulans* and *C. albicans*, the endogenous generation of a superoxide gradient was shown to regulate polarised growth and sexual development, and filamentation, respectively (Lara-Ortiz, Riveros-Rosas et al. 2003, Semighini and Harris 2008, Rossi, Gleason et al. 2017). In addition, ROS (H_2O_2) can trigger the antioxidant response through activation of

transcription factor Yap1 at cysteine residues, and this TF is involved in the regulation of genes involved in oxidative stress, nutrient assimilation, secondary metabolism, and virulence (Mendoza-Martínez, Cano-Domínguez et al. 2020). In both *A. fumigatus* and *A. nidulans*, *YAP1* homologous mutants showed growth defects in the presence of oxidants such as H_2O_2 and menadione (Lessing, Kniemeyer et al. 2007, Mendoza-Martínez, Lara-Rojas et al. 2017). While in *A. parasiticus*, YapA is required for the activity of antioxidant enzymes like SOD, glutathione peroxidase, and hydrogen peroxide reducing enzymes (Reverberi, Zjalic et al. 2008). A similar role for endogenous superoxide has not yet been described in *C. neoformans.*

Here, this thesis examined the *in vitro* interaction of host phagocytes with titanized cells (Dambuza, Drake et al. 2018, Zhou, Zafar et al. 2020). Upon co-culture, we observed a significant further increase in cryptococcal cell size and an increase in endogenous superoxide, the generation of which is required for titanization. Through mutant analysis and live cell imaging we begin to dissect the molecular mechanisms governing this process. We demonstrate that, rather than simply killing fungal cells or inhibiting fungal growth, host phagocyte iNOS activity can augment the formation of large titan cells, with implications for host survival.

Results

To study the yeast-to-titan transition, fungal cells can be induced to form titan cells using our established protocol: growth in minimal media followed by exposure for 24 hr to 10% Fetal Calf Serum (FCS), a source of bacterial peptidoglycan (Dambuza, Drake et al. 2018, Zhou and Ballou 2018). This yields a mixed culture of cells proliferating either via titan (15-20%, >10μm) or yeast (<10μm) growth patterns, and throughout this thesis we define cultures primed in this way as “titanized”. To study how this transition is impacted by interaction with the host, we performed time-lapse imaging of titanized cells subsequently co-cultured with murine J774.1 macrophage cell line stimulated with interferon gamma (IFN-γ) (to simulate M1-like conditions) (Fig 3.1A, B and Fig 3.2A). We observed that engulfed H99 titan cells continue to undergo cell enlargement within the phagolysosome. In addition, we noticed an overall increase in the maximum size and frequency of titan cells following co-culture relative to growth without macrophages (Fig 3.1C) (Dambuza, Drake et al. 2018, Zhou and Ballou 2018). This increase was not observed for control cells that had not been primed by previous exposure to FCS were co-incubated with phagocytes, indicating that host phagocytosis alone is not sufficient to trigger titanization (Fig 3.2B). This striking observation raised the possibility that, in addition to a role for nutrient limitation and bacterial peptidoglycan, host factors may also impact the degree and frequency of the yeast-to-titan

switch in the context of the host. We therefore set out to understand the molecular mechanisms driving this fungal response to the host environment.

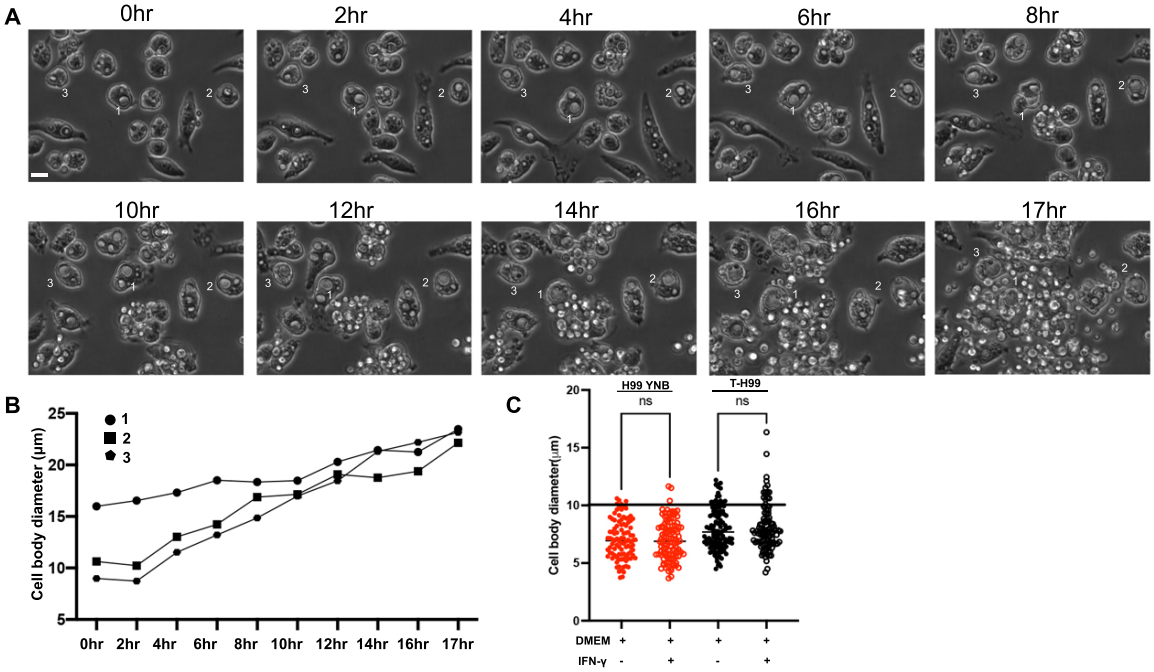


Fig 3.1: Time-lapse images from co-incubation of pre-induced H99 with macrophages. *C. neoformans* cells were incubated under titan inducing conditions for 24hr then co-incubated with J774 murine macrophages. Co-cultured cells were imaged for 18hr. (A) Representative micrographs are shown at 2 hr intervals; Indicate cells are representative of engulfed cryptococcal cells that increased in size. (B) Quantification of cell diameter for indicated cells over time. (C) Control cells were grown in DMEM plus or not IFN-γ in absence of macrophages. *C. neoformans* cell size was assessed for individual cells (cell body diameter, excluding capsule; n>100). Data were assessed for normality by Shapiro-Wilk and analysed by one-way ANOVA. “T” indicates titanized. Experiments were independently repeated at least three times (n>3) with a representative biological replicate is presented.

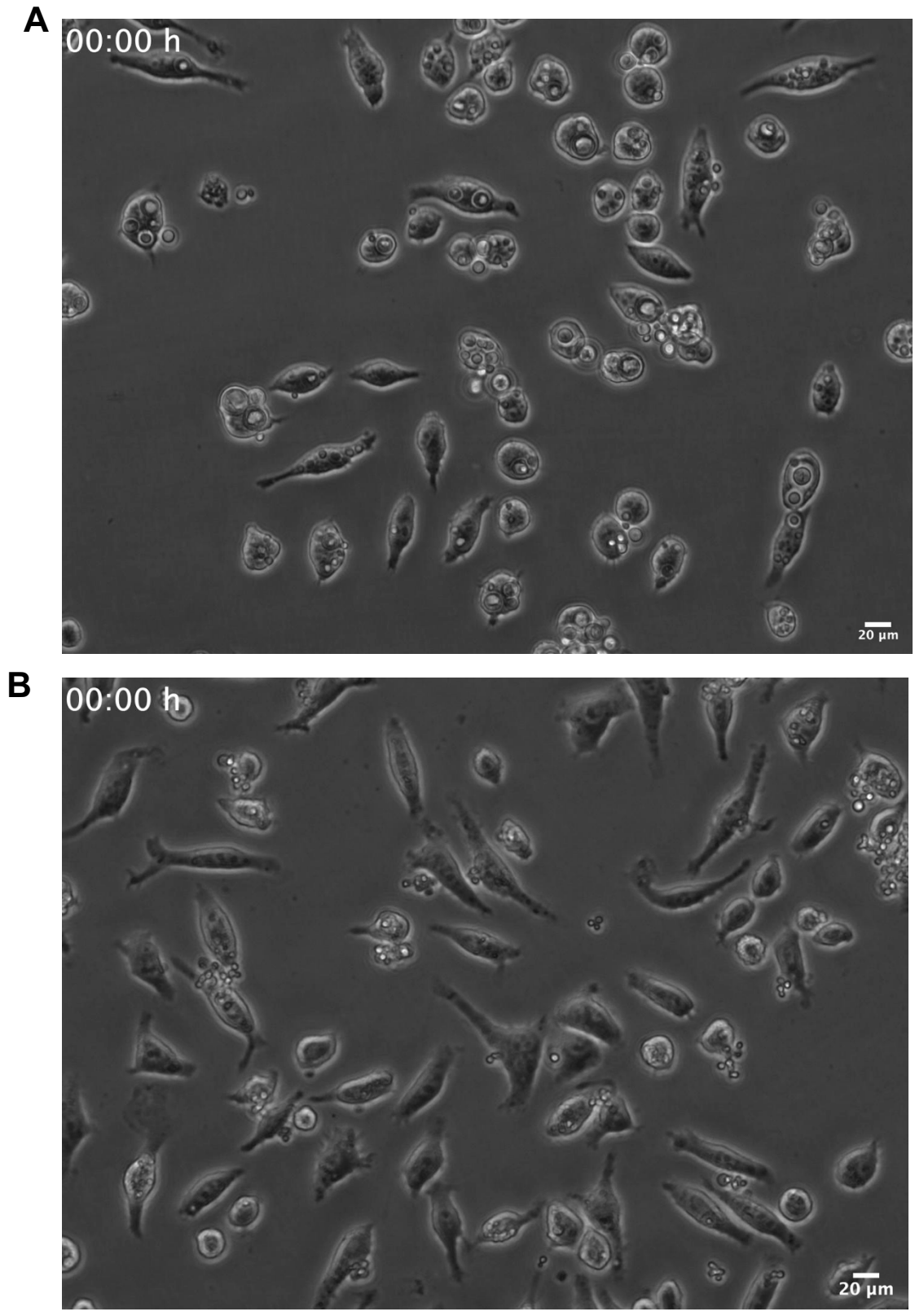


Fig 3.2: Time-lapse movie of interaction between macrophages and *C. neoformans* cells. (A)*(top)* 18hr time-lapse imaging of interaction between macrophages and H99 titanized or (B)*(down)* YNB-grown cells. “T” indicates

titanized. Three biological replicates were performed and a single representative replicate is presented (n>3).

3.4 Host-derived immune signals induce formation of large titan cells

We first asked whether activation of host immune cells is required to amplify fungal cell size. We used murine bone marrow derived macrophages (BMDMs) isolated from C57BL/6 (WT) to repeat the co-incubation assays. BMDMs are professional phagocytes that can be primed to be either M1 or M2, where M1 cells are strong producers of NO^-, TNF, and IFN-γ, factors important for the control and clearance of cryptococcal cells (Mills, Kincaid et al. 2000, Johnston and May 2013). Treatment with LPS and IFN-γ stimulates M1 polarization, which is associated with macrophage-mediated fungal killing via increased phagosomal ROS and NO^- (Davis, Tsang et al. 2013). In contrast, treatment with IL-4 stimulates an M2 polarization associated with macrophage mediated clearance.

As shown in Fig 3.3A, cryptococcal cells co-incubated with basally activated murine BMDMs increased in size relative to fungal cells alone, similar to co-incubation with J774.1 macrophages (Fig 3.3A). Of the engulfed fungal cells, approximately 50% increased further in cell size, while the remainder either proliferated as yeast or were controlled for their survival and growth. We then activated BMDMs with either LPS, IFN-γ, or both LPS and IFN-γ, priming M1 polarization, and examined fungal cell size by live cell

imaging for 18 hr (Fig 3.3A). There was a significant increase in fungal cell size (>10 μm) when co-incubated with unstimulated BMDMs compared to growth in matched medium alone ($p<0.0001$). Stimulating BMDMs with either LPS or IFN-γ or with both LPS and IFN-γ further increased fungal cell size compared to fungal cells in matched media (Fig 3.3A, $p<0.0001$). Representative images are shown in Fig 3.3B. There was no statistically significant difference between fungal cell populations incubated with either BMDM alone or BMDMs stimulated with LPS and IFN-γ, however we consistently observed an increase in frequency of very large titan cells (>15 μm) in co-stimulated cultures (Fig 3.3C). Flow cytometry of fungal cells after lysis and gating to exclude BMDMs confirmed the observed increase in fungal cell size, with the most dramatic size increase occurring after dual activation (FSC-A) (Fig 3.3D, gating strategy Fig 3.4A).

We asked whether stimulation with IL-4 impacted the capacity of BMDMs to increase fungal cell size. Fungal cell size was determined by flow cytometry following gating to exclude BMDMs as above. In contrast to stimulation with LPS and IFN-γ treatment with IL-4 reduced the proportion of very large titan (>15 μm) cells upon co-incubation with BMDMs (Fig 3.4B, C, D). Together, these data suggest that exposure to stimulated M1, but not M2, immune cells, can induce the formation of large titan cells.

M1-polarized phagocytes are strong producers of phagosomal O_2^- and NO^-, factors important for control and clearance of *Cryptococcus* cells (Davis, Tsang et al. 2013, Coelho, Bocca et al. 2014). Intriguingly, we observed that superoxide levels within cryptococcal cells increased in parallel with cell size after co-incubation with BMDMs. As shown in Fig 3.3D, cryptococcal cells exposed to BMDMs showed higher levels of superoxide compared with *in vitro* titanized cells alone, and the most dramatic increase in superoxide was observed for co-stimulated cells (Fig 3.3C top panel). The shift in superoxide correlated with increased cell size for fungal cells co-incubated with BMDMs for all conditions compared to fungal cells exposed to LPS and/or IFN-γ in the absence of BMDMs, further demonstrating that this effect was mediated by BMDM activity (Fig 3.3C).

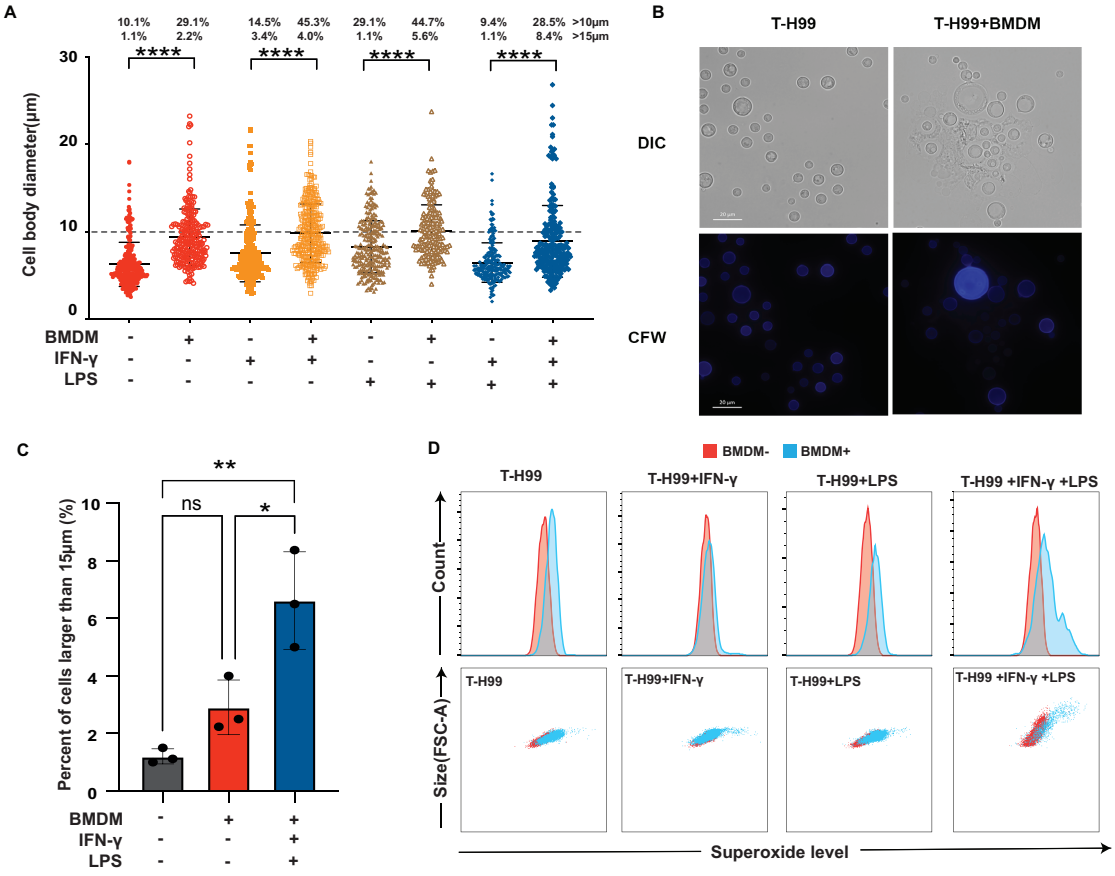


Fig 3.3: Fungal cell size increases after co-incubation with BMDMs and is influenced by BMDM activation. (A) *C. neoformans* titanized cell size changes after different incubation assays: *C. neoformans* were grown in RPMI in presence or absence of BMDMs, IFN-γ and/or LPS. *C. neoformans* cell size was assessed for individual cells (cell body diameter, excluding capsule; n>200). Data were assessed for normality by Shapiro-Wilk and analysed by one-way ANOVA, ****p<0.0001. (B) Microscopy images of cells grown in RPMI (*left*), or after co-incubation with BMDMs activated with IFN-γ and LPS (*right*, BMDMs lysed with cold sdH_2O); Cells were stained with calcofluor white (CFW) for cell wall (*blue*). Scale bar: 20µm. (C) Quantification of the percentage of cells assessed in A&B which are larger than 15µm. For each repeat 100 cells (n>100) were assessed for cell size and three

independent biology repeats for each condition were conducted for statistical analysis. Data were assessed for normality by Shapiro-Wilk and analysed by one-way ANOVA, ** p=0.0026, * p=0.0164. Each error bar indicates the standard deviation among the three independent repeats. (D) Flow cytometric analysis of cell size and superoxide staining distribution. Fungal cells were identified using gates for the capsule (Fig 3.4A). Single cells were identified by FSC-A vs FSC-H to remove doublets. Histograms for superoxide levels for fungal cells from indicated conditions (*top panel*); size (FSC-A) vs superoxide level scatter plots for cells from indicated conditions (*bottom panel*). (A, B, D) Three biological replicates were performed and a single representative replicate is presented. “T” indicates titanized.

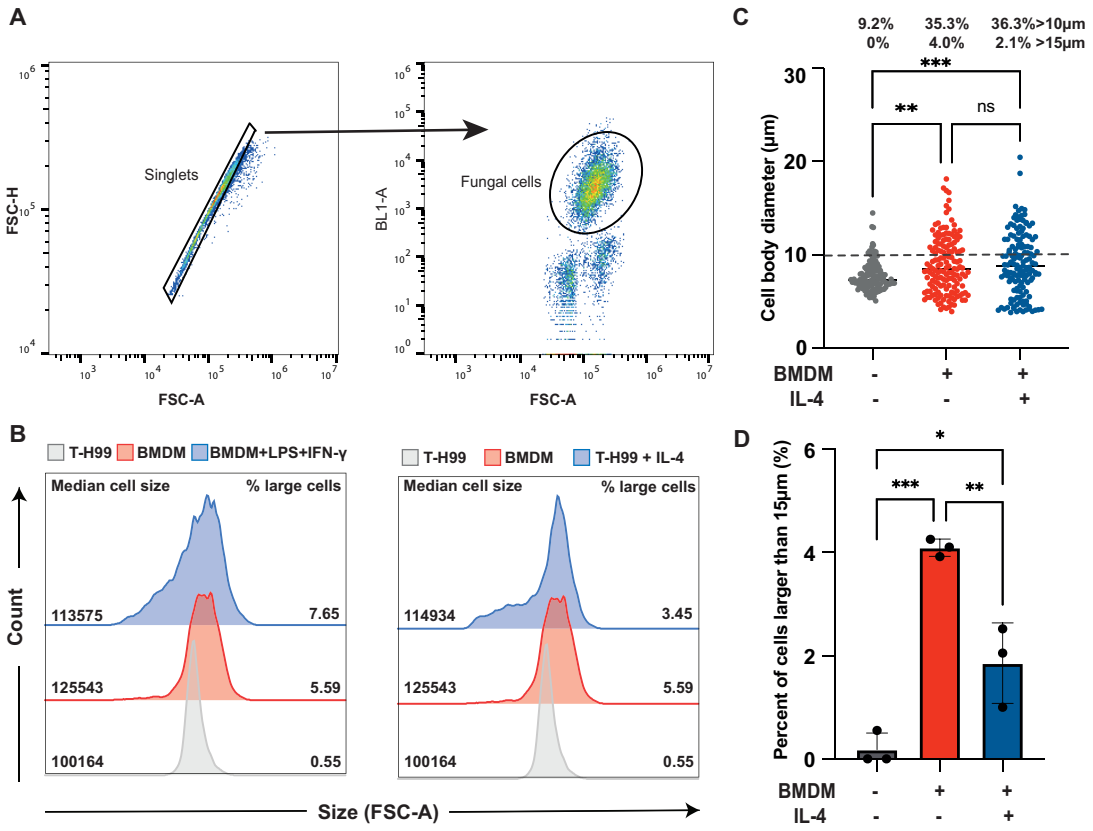


Fig 3.4: (A) Flow cytometric gating for identification of fungal cells. Single cells were first identified by FSC-A vs FSC-H, then fungal cells were gated by FSC-A vs BL1-A (capsule staining). (B, C) Fungal cell size change was not affected by IL-4 stimulation. (B) Flow cytometric analysis of cell size and (C) individual cell body size measurement, after incubation in RPMI in the presence or absence of BMDMs, IL-4. *C. neoformans* cell size was assessed for individual cells (cell body diameter, excluding capsule; n>200). Data were assessed for normality by Shapiro-Wilk and analysed by one-way ANOVA, ****p*=0.0009, ***p*=0. 0049. (A, B, C) Three biological replicates were performed and a single representative replicate is presented. (D) Quantification of the percentage of cells assessed in A&B which are larger than 15µm. For each repeat 100 cells (n>100) were assessed for cell size and three

independent biology repeats for each condition were conducted for statistical analysis. Data were assessed for normality by Shapiro-Wilk and analysed by one-way ANOVA, ** p=0.0036, * p=0.0143, *** p=0.0002. Each error bar indicates the standard deviation among the three independent repeats. “T” indicates titanized.

3.5 Exogenous nitrosative stress is sufficient to further potentiate titanization

The observation that co-incubation with M1 but not M2 macrophages concomitantly increased superoxide and cell size raised the hypothesis that host-derived ROS/RNS influence fungal morphogenesis. To investigate the roles of host-derived ROS and RNS in titanization, we directly added exogenous reactive oxygen (H_2O_2) or nitrogen (NO^-) species donors (Glucose oxidase or DPTA NONOate) at levels consistent with the host environment to titan cultures at the time of induction(Ramachandran, Moellering et al. 2002, Rossi, Gleason et al. 2017). Treatment with exogenous H_2O_2 was associated with increased superoxide staining within fungi, suggesting that the cells are under ROS stress, and moderate changes on cell size were observed (Fig 3.5A, B). In contrast, the presence of exogenous NO^- stimulated increased O_2^-, and DNA content, and nearly 10% increased titan cells proportion (>10um) (Fig 3.5A, B). These data suggest that host-derived RNS, and to a lesser extent ROS, can further potentiate titanization.

To determine the physiological relevance of the roles of exogenous ROS vs. RNS, we co-incubated titanized fungal cells with BMDMs from mice lacking either NOX (O_2^-, *Cybb*$^{-/-}$) or iNOS (NO^-, *Nos2*$^{-/-}$) activity (Fig 3.5C, D). Fungal cell size was examined both by flow cytometry (Fig 3.5D) and microscopy (Fig 3.5C). In the absence of LPS and IFN-γ stimulation, there was no difference in cell size distribution between wild type BMDMs and BMDMs from iNOS-deficient mice (Fig 3.5C). *Cybb*$^{-/-}$ BMDMs lacking the $Gp91^{PHOX}$ protein required for O_2^- production were moderately less able to induce titan cell size increases compared to *Cybb*$^{+/+}$ BMDMs (Fig 3.5C, D, E), but induced comparable endogenous superoxide. This suggests that host-derived ROS are minor contributors to fungal cell size increase (Pollock, Williams et al. 1995, Kassim, Fu et al. 2005). In contrast, when titanized fungal cells were incubated with stimulated BMDMs lacking *NOS2* (iNOS-), there was a profound defect in fungal cell size increase relative to WT BMDMs (Fig 3.5C, D, E). In addition, endogenous superoxide was markedly lower in fungal cells co-incubated with iNOS-deficient mice (Fig 3.5D). Together, these data confirm that both host-derived RNS and ROS can contribute to the observed increases in fungal cell size, with RNS as the major contributor.

3.6 Exogenous RNS increases mitochondrial potential

Exogenous and endogenous ROS/RNS can cause dysfunction of mitochondria leading to cell death, however moderate exposure to exogenous RNS has been shown to increase cell respiration and endogenous ROS formation (Poderoso, Carreras et al. 1996, Poderoso, Lisdero et al. 1999, Beltrán, Mathur et al. 2000, Brown, Haynes et al. 2009, Kaludercic and Giorgio 2016). While the impact of exogenous ROS and RNS on *C. neoformans* stress responses has been studied at the phenotypic, transcriptional and translational levels, their specific impact on mitochondrial function and morphology remains unclear (Cox, Harrison et al. 2003, Giles, Stajich et al. 2006, Missal, Pusateri et al. 2006, Upadhya, Campbell et al. 2013, Leipheimer, Bloom et al. 2019). In order to determine whether exogenous RNS impacts *C. neoformans* mitochondrial function, we measured mitochondrial membrane potential, an indicator of mitochondrial oxidative phosphorylation, during exposure to physiological concentrations of nitric oxide(Ramachandran, Moellering et al. 2002). We used the fluorescent probe JC-1, which exists as monomer and emits green fluorescence at low membrane potential. In mitochondria with high membrane potential, JC-1 forms aggregates and emits orange-red fluorescence (Fig 3.6A). As shown in Fig 3.5F, treatment with NONOate increased the mitochondrial potential of titanized cells, with a clear increase in JC-1 aggregates relative to untreated titanized cells, while cells treated with glucose oxidase showed decreased

mitochondrial potential with unchanged morphology. This suggests that exogenous RNS increases mitochondrial potential and mitochondrial ROS production, while exogenous ROS increases ROS production through posing oxidative stress instead of affecting mitochondrial activity.

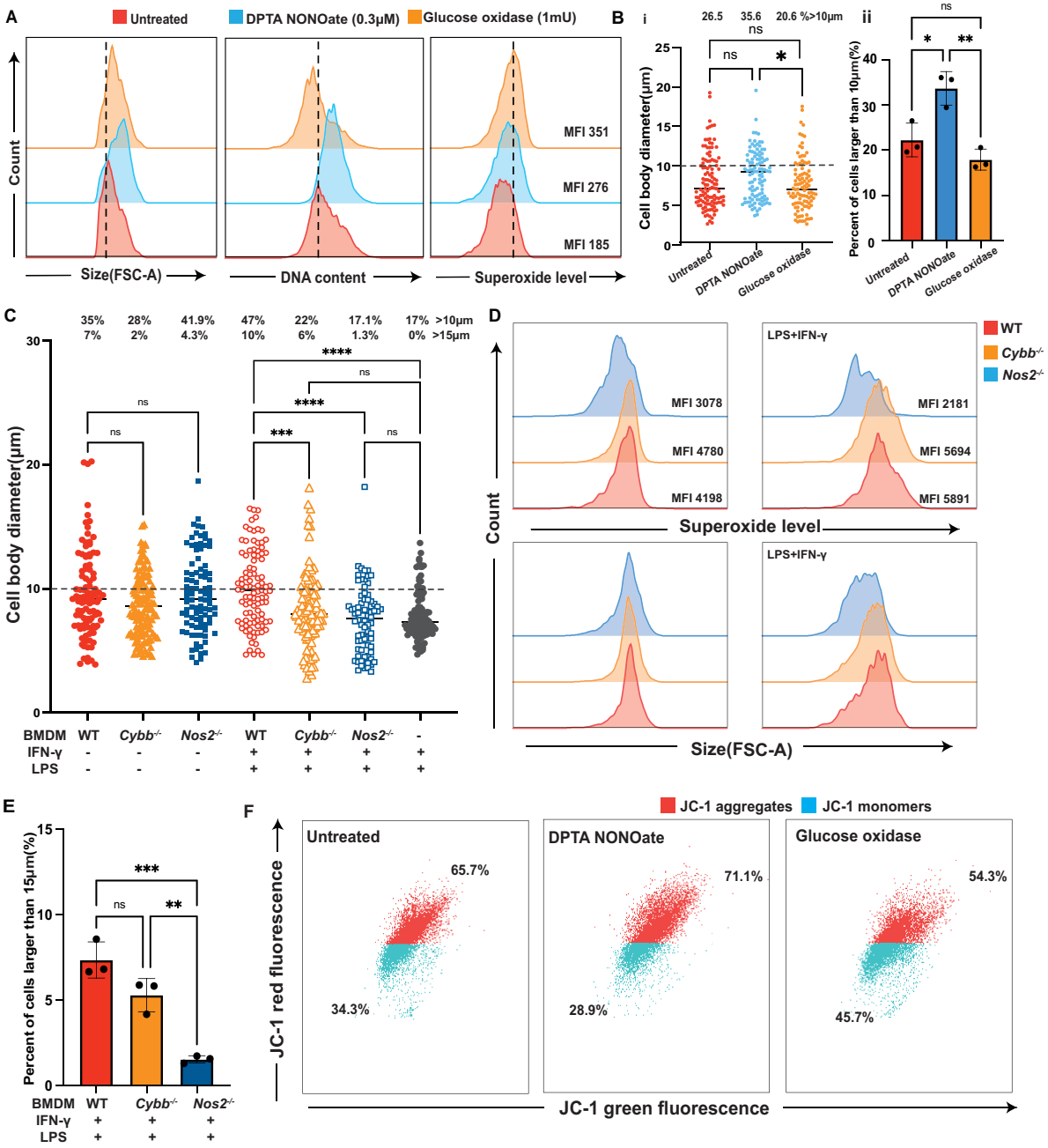


Fig 3.5: Exogenous RNS treatment correlates with increases in both cell size and superoxide level. (A) Histograms of size (FSC-A) and superoxide levels of

titanized cells from untreated (*bottom*), DPTA NONOate (0.3μM) treated (*middle*), and Glucose oxidase (1mU) treated (*top*), Dotted lines indicate median fluorescence intensity (MFI) of untreated cells. (B) i) *C. neoformans* titanized cell size changes treated with DPTA NONOate or Glucose oxidase. ii) Quantification of the percentage of cells assessed in i) which are larger than 10μm. Three independent biology repeats for each condition were conducted for statistical analysis. Each error bar indicates the standard deviation among the three independent repeats. ** p=0.0027, i) *p=0.0137, ii) *p=0.0131 (C) *C. neoformans* titanized cell size changes after different incubation assays: *C. neoformans* were grown in RPMI in presence or absence of WT or *Cybb*$^{-/-}$ or *Nos2*$^{-/-}$ BMDMs activated or not with IFN-γ and LPS. ****p<0.0001, ***p=0.0010 (D) Flow cytometer results of cell sizes and superoxide levels: C. neoformans cells were gated by capsule staining, then checked for superoxide level and size (FSC-A). Histograms of superoxide levels (*top panel*) and size (FSC-A) (*bottom panel)* for cells from different culture conditions. (E) Quantification of the percentage of cells assessed in i) which are larger than 15μm. Three independent biology repeats for each condition were conducted for statistical analysis. Each error bar indicates the standard deviation among the three independent repeats. ***p=0.0004, **p=0.0037. (B, C, E) Cell size was assessed for individual cells (diameter) for the cell body (capsule excluded; n>100). Data were assessed for normality by Shapiro-Wilk and analysed by one-way ANOVA. (F) JC-1 green fluorescence vs red fluorescence scatter plots of titanized cells from untreated,

NoNoate and Glucose oxidase treated cultures. Gating for JC-1 aggregates (red dots) and monomers (green dots) is indicated in Fig 3.6B. (C, D) Cells were stained with superoxide detector or JC-1, then analysed by flow cytometer. Single cells were identified by FSC-A vs FSC-H to remove doublets. Three biological replicates were performed and a single representative replicate is presented. “T” indicates titanized.

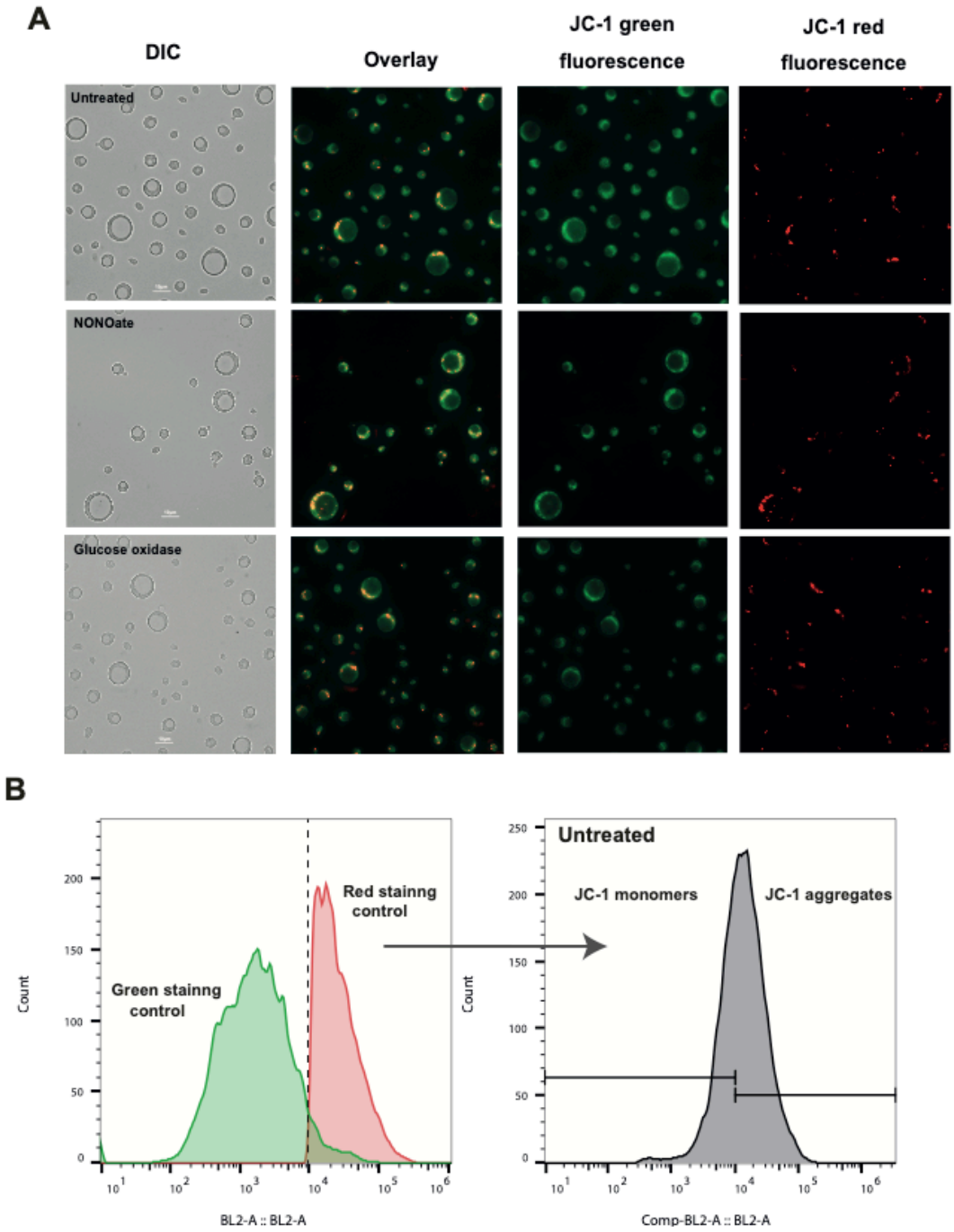


Fig 3.6: JC-1 staining within titanized cells. (A)Representative micrographs for JC-1 staining of untreated, NONOate, and Glucose oxidase treated titanized cells, green: JC-1 green fluorescence, red: JC-1 red fluorescence. Scale bar: 10µm. T" indicates titanized. (B) Gating for JC-1 monomers and aggregates. Gate is generated based on the red (mito tacker red) or green (mito tracker green) single staining cells,

and this gate is applied to JC-1 staining cells to differentiate JC-red(aggregates) and green(monomers) fluorescence. Three biological replicates were performed and a single representative replicate is presented.

3.7 Endogenous superoxide levels are dynamic throughout titanization and correlate with the capacity of isolates to form titan cells

Together, our data suggest that host-derived RNS, and to a lesser extent ROS, influence endogenous fungal superoxide, resulting in fungal size increase. We hypothesised that endogenous fungal superoxide influences the changes in fungal cell size observed during the 24hr yeast-to-titan switch, even in the absence of host stimulation. We therefore characterised endogenous superoxide levels over the course of titanization. We monitored endogenous superoxide using a superoxide-specific dye from 4hr post-induction, when titan cells are not apparent, until 24hr, when titan cells comprise 15% of the population. Flow cytometry showed that endogenous superoxide levels are initially high, then decrease 8hr post-induction, becoming bi-phasic (Fig 3.7A). From 13 to 18 hr, there is an overall shift to the right, and a minority of cells generate high levels of superoxide (Fig 3.7A). This minority population is maintained over the subsequent 12 hr, at which point overall superoxide is stabilized at an intermediate level. After 24 hr, the subset of cells with very high ROS correlate with the largest cells in this population (Fig 3.7A). When we monitored mitochondrial activity over time

using the JC-1 probe, we observed a similarly high initial potential (red fluorescence) that decreased by 8 hr and then stabilized and was maintained at a high level from 13 hr (Fig 3.7B). We conclude that during titanization, endogenous superoxide levels are dynamic across the population and are reflective of high mitochondrial activity.

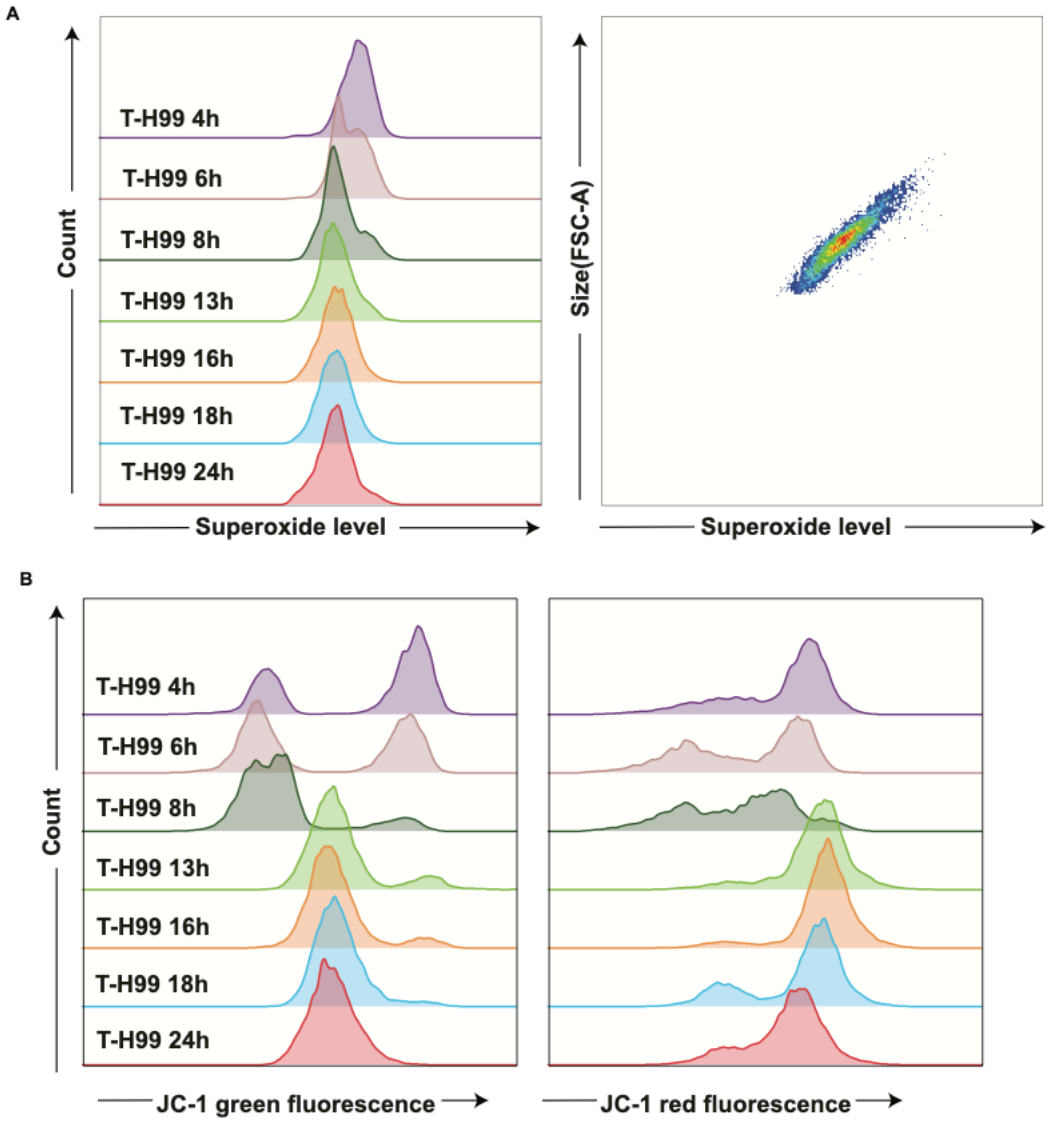


Fig 3.7: Superoxide accumulation is dynamic during titanization. (A) Histograms of superoxide levels of *C. neoformans* cells from different time points over titanization from 4hr to 24hr post-induction. size (FSC-A) vs superoxide level scatter plots for

cells from 24hr post-induction. Cells were stained with superoxide detector and analysed by flow cytometer. (B) Histograms of JC-1 green fluorescence (*left*) and JC-1 red fluorescence (*right*) of *C. neoformans* cells from different time points over the yeast to titan transition from 4hr to 24hr post-induction. Cells were stained with superoxide detector or JC-1, then analysed by flow cytometer. Single cells were identified by FSC-A vs FSC-H to remove doublets. Three biological replicates were performed and a single representative replicate is presented. “T” indicates titanized.

The dynamic nature of superoxide levels suggests that ROS detoxification is also important to fungal morphogenesis. Consistent with this, titan-induced H99 cells were more sensitive to killing by exogenous H_2O_2 than YNB-grown H99, suggesting titanized cultures are under increased endogenous oxidative stress (Fig 3.8A). Moreover, we observed a correlation between the capacity of clinical isolates to undergo titanization and sensitivity to exogenous H_2O_2 when grown under titan-inducing conditions: The clinical isolate Zc8, like H99, forms titans and becomes sensitive to H_2O_2 upon titan induction. In contrast, after exposure to titan conditions the Zc1 hypo-titanizing isolate and Zc12, which does not form titans, are no more sensitive than uninduced cells (Fig 3.8A). Microscopy and flow cytometry to measure superoxide levels in induced cells revealed that, after *in vitro* titan induction, H99 and Zc8 exhibit higher endogenous superoxide levels compared to non-titanizing isolates (Fig 3.8B, C). Co-incubation of the clinical isolates with

human blood monocytes revealed that the impact of phagocytes on fungal cell size also correlates with the capacity to titanize. After 24hr co-incubation with monocytes, H99 and Zc8 increased in maximum cell size up to >25 μm (H99) and >15 μm (Zc8) (Fig 3.8D), sizes which were only detected *in vivo* previously (Zhou, Zafar et al. 2020). In contrast, Zc1 and Zc12 did not exceed the 10 μm threshold even after co-incubation with human monocytes (Fig 3.8D).

Finally, we visualized endogenous ROS in fungal cells after co-culture with monocytes: superoxide was apparent as bright cytoplasmic foci and in the nucleus in H99 and Zc8 titan cells, yet was localised to diffuse puncta in H99 and Zc8 yeasts and titanides. Similar diffuse puncta were observed in all cells in the non-titanizing Zc1 and Zc12 isolates (Fig 3.8B). Overall, these data suggest that both level and localization of superoxide dictate phenotypic outcome and that this occurs regardless of genetic background.

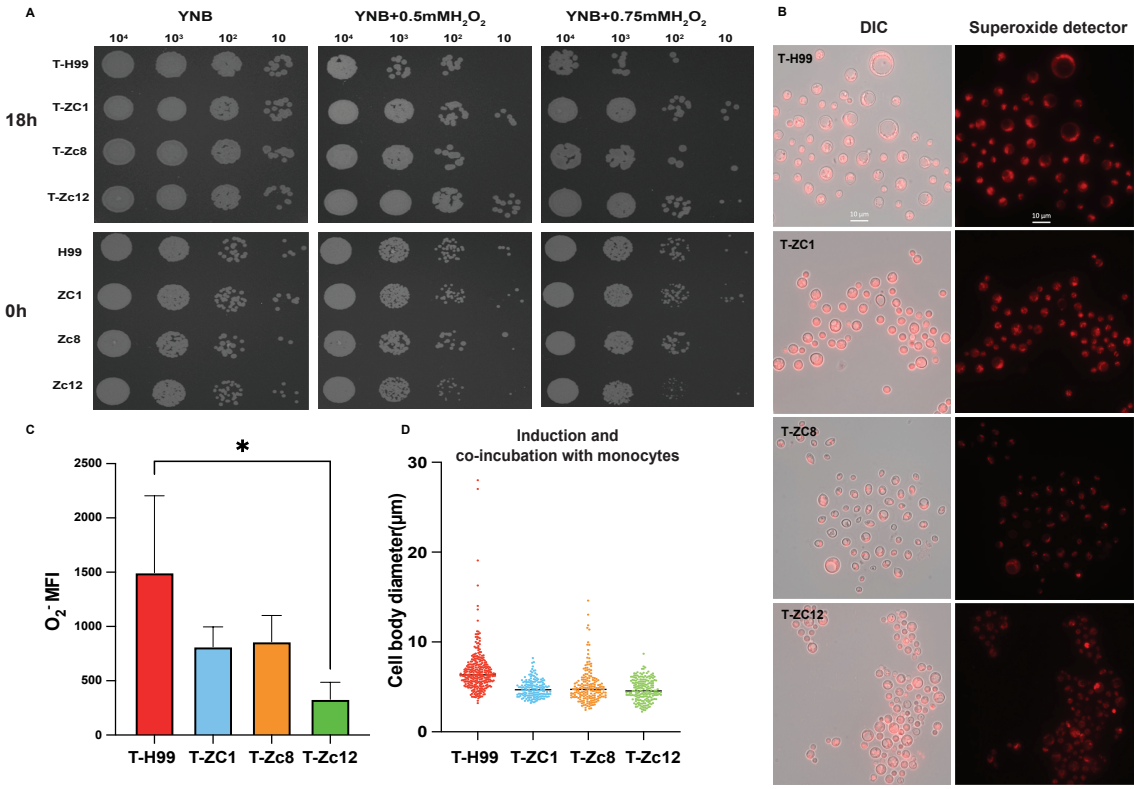


Fig 3.8: Superoxide increase with sizes within clinical isolates after co-incubation with monocytes. (A) Hydrogen peroxide stress spot plates of 3 clinical isolates (Zc1, Zc8, Zc12) with H99 as a control: cells were pre-grown in YNB and directly spotted onto plates (0hr) or titan induced for 18h(18h), and then plated on YNB plates with or without H_2O_2. (B) Micrographs of cells stained with superoxide detector. Scale bar: 20μm. (C) Bar charts of superoxide levels among indicated strains. Cells were stained with a superoxide detector and analysed by flow cytometer. Data represent the mean ± SEM from three independent experiments. Data were assessed for normality by Shapiro-Wilk and analysed by one-way ANOVA, * p=0.0275. (D) Cell sizes of H99 and 3 clinical isolates after *in vitro* induction (24hr) and co-incubation with monocytes: Cell size was assessed for individual cells (cell body diameter, excluding capsule; n>200). Three biological

replicates were performed and a single representative replicate is presented. “T” indicates titanized.

3.8 Endogenous superoxide is required for titan cell formation yet must be detoxified for the generation of large cells

To determine whether superoxide is required for titan cell formation, we treated H99 titan cultures with MnTBAP, a SOD mimetic drug. MnTBAP is readily taken up by live cells and can convert endogenous superoxide into H_2O_2, which is subsequently detoxified by fungal catalases (Cox, Harrison et al. 2003, Narasipura, Ault et al. 2003, Giles, Stajich et al. 2006). Treatment with MnTBAP blocked titan cell formation, with no cell larger than 10μm or with ploidy >8C observed (Fig 3.9A, B). Flow cytometry confirmed that treatment decreased superoxide accumulation (Fig 3.9C). Direct exposure to exogenous H_2O_2 did not affect titanization (Fig 3.5A), suggesting that the MnTBAP-mediated block in titanization is not the result of increased H_2O_2 stress. No defect in growth was observed, and treated cells resembled “typical” yeast cells (<10 μm) in morphology (Fig 3.10 A, B).

These data pose an important biological challenge for the fungal cell: the generation of superoxide is a requirement for titanization, and host factors that increase superoxide also increase fungal cell size, yet excessive endogenous ROS can cause oxidative damage and sensitizes the fungus to exogenous

ROS stress and host cell killing. Balancing this response requires the activity of the oxidative stress response pathway.

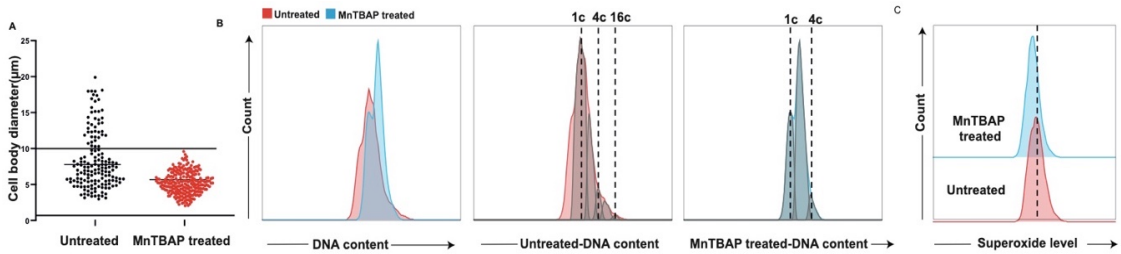


Fig 3.9: Titan cell formation can be inhibited by reducing the accumulation of superoxide. (A) Cell body diameter for *C. neoformans* H99 cells induced to form titans for 24hr in the absence(*red*) or presence(*blue*) of the SOD mimetic drug MnTBAP (1mM). Cell size was assessed for individual cells (cell body diameter, excluding capsule; n>200). (B) DNA content (DAPI) of untreated and MnTBAP treated cells were assessed by flow cytometer. YPD grown yeast cells from matched parent strains and MFI 1C and 2C populations were used to identify 1C and 2C peaks (Fig 3.6B). The dotted lines indicate MFI of different DNA content peaks. (C) Histograms of superoxide levels of titanized cells from untreated and MnTBAP treated cells. Cells were stained with a superoxide detector and analysed by flow cytometer. (B&C) Single cells were identified by FSC-A vs FSC-H to remove doublets. Dotted lines indicate MFI of untreated cells. Three biological replicates were performed and a single representative replicate is presented.

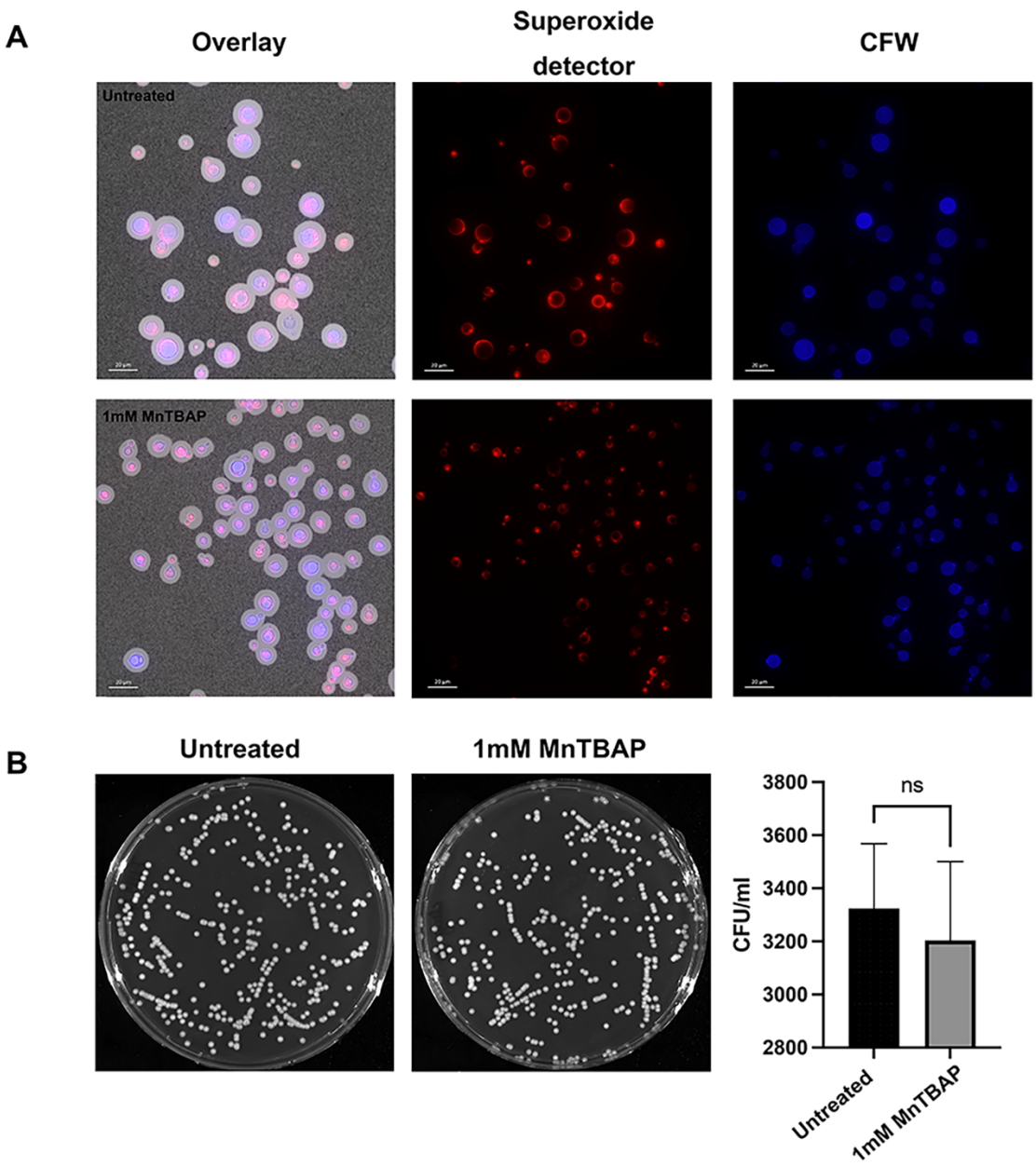


Fig 3.10: Microscopy images of cells treated with MnTBAP during titanization. (A) Cells were stained with India ink and superoxide detector, Top panel: untreated cells, bottom panel: 1mM MnTBAP treated cells, red: superoxide detectors, blue: CFW. Scale bar: 20µm. (B) MnTBAP treatment did not affect growth as assessed by CFU. (left) Untreated and 1mM MnTBAP treated cells (24hrs) were plated on YPD and imaged after 48 hrs. Plates representative of triplicate experiments. Data represent the mean ± SEM from three independent experiments.

The AP-1-like transcription factor Yap1 is a stress response protein induced by oxidative stress in *C. neoformans,* and loss of *YAP1* sensitizes cells to a wide variety of oxidative stress compounds (H_2O_2, t-BOOH (H_2O_2), diamide (O_2^-)) (Paul, Doering et al. 2015, So, Maeng et al. 2019). Consistent with a defect in ROS detoxification, examination of *yap1Δ* titan-induced cultures revealed two key changes (Fig 3.11A, B, C): 1) we did not detect highly polyploid cells in the *yap1Δ* mutant (>16C) and 2) there was a reduction in the percentage of titanides, which were described in detail in chapter2 (Zhou, Zafar et al. 2020). We hypothesized that this might be due to failure of *yap1Δ* cells to detoxify high endogenous superoxide levels observed over the course of titanization (Fig 3.7A). Under basal conditions (YPD, 30°C), Yap1 regulates oxidative resistance genes such as *SOD1* and *SOD2,* which detoxify superoxide to H_2O_2, which is then converted to O_2 and H_2O by catalases (*CAT*1-4) (Reverberi, Zjalic et al. 2008, Paul, Doering et al. 2015, So, Maeng et al. 2019). However, data are lacking about the role of Yap1 during titanization. We asked whether *SOD* regulation is altered after being exposed to titan induction. Since titan culture is highly heterogeneous, we decided to size purify this mixture population into three sub-populations: titans (>10μm), yeasts (>5μm and<10μm), and titanides (<5um). Then we determined the expression of these two genes in H99 and *yap1Δ* from these three titan sub-populations relative to H99 basal yeast phase via RT-PCR. As

shown in Fig 3.11D, in both wild-type H99 and *yap1Δ*, upon titan inducing conditions, *SOD1* is highly induced relative to basal H99 yeast phase, especially in H99 titans and *yap1Δ* yeasts with more than 12-fold increases, (Fig 3.11D). In comparison to H99, both *yap1Δ* titans and titanides showed reduced *SOD1* expression, while *yap1Δ* yeasts showed the opposite trend with increased expression levels (Fig 3.11D). In contrast to *SOD1, SOD2* overall expression is down-regulated, but with an exception of *yap1Δ* yeasts which however showed an about 2-fold increase (Fig 3.11D). Taken together, we believe the reason for reduced polyploid cells and titanides in *yap1Δ* is mainly because Yap1-regulated *SOD1* expression is depressed in these two sub-populations. Meanwhile, for the miss-regulation of these two genes in *yap1Δ* yeasts sub-population, we think this possibly is because the cells from this size threshold have totally different oxidative regulation mechanism from the rest of titan culture.

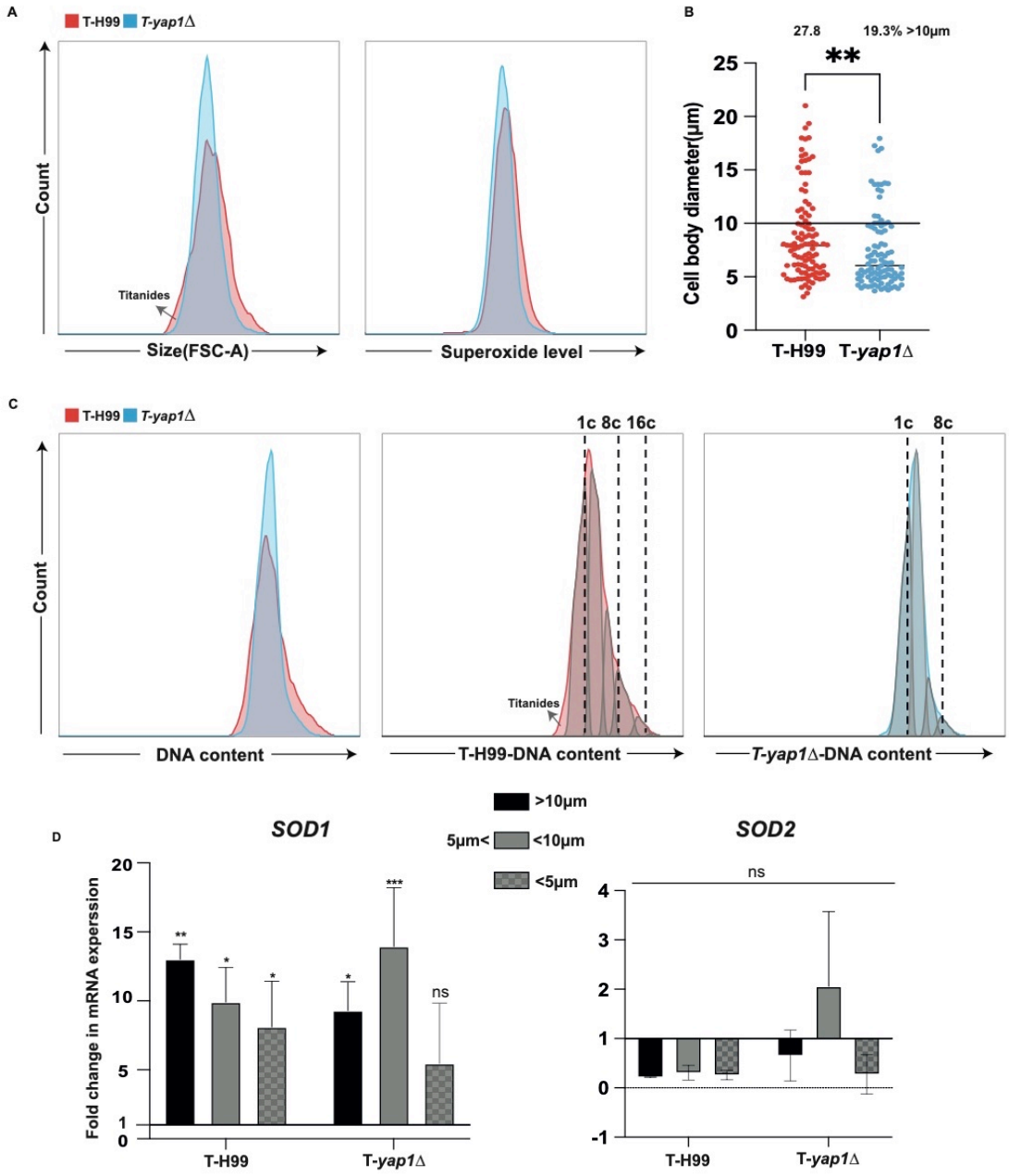


Fig 3.11: Yap1 regulates ROS detoxification and the degree of titan cell formation. (A) Histograms of cell size and superoxide levels of T-H99 (*red*) and T-*yap1Δ* (*blue*) after 24hr titan induction. Cells were stained with a superoxide detector and analysed by flow cytometer. (B) Cell body diameter for *C. neoformans* H99 and *yap1Δ* titan induced cells. Cell size was assessed for individual cells (cell body diameter, excluding capsule; n>100). (C) DNA content of titan induced H99 and

yap1Δ cells (24hr). YPD-grown yeast cells from matched parent strains and MFI 1C and 2C populations were used to identify 1C and 2C peaks. The dotted lines indicate MFI of different DNA content peaks. (A&C) Grey arrows indicate titanide cells. Single cells were identified by FSC-A vs FSC-H to remove doublets. Three biological replicates were performed and a single representative replicate is presented. (D) Relative mRNA expression levels of *SOD1* and *SOD2* in H99 and *yap1Δ* three titan sub-populations: titans>10μm, 5μm<yeasts<10μm, and titanides<5μm. Expression levels were normalized to *ACT1* and *SOD1* and *SOD2* in H99 basal yeast cells (control). Data represent the mean ± SEM from three independent experiments. Data were assessed for normality by Shapiro-Wilk and analysed by One-Way ANOVA to *SOD1* and *SOD2* in control for significant difference. *SOD1*: T-H99 titans ***p*=0.0011, T-H99 yeast ***p*=0.0119; T-H99 titanides **p*=0.0482, T-*yap1Δ* titans **p*=0.0027, T-*yap1Δ* yeast ****p*=0.006. No significant difference was detected for *SOD2.* "T" indicates titanized.

3.9 SOD2 is required for the initial detoxification of superoxide

To directly test the hypothesis that ROS detoxification influences titanization, we examined the requirement for components of this pathway including superoxide dismutase (*SOD1, SOD2*) and catalase (*CAT1, CAT2, CAT3, CAT4*). Deletion mutants were assessed for cell size and endogenous superoxide levels after exposure to inducing conditions for 24 hr. As shown in Fig 3.12A, 3.13A neither *sod1Δ, cat1Δ, cat2Δ, cat3Δ, cat4Δ* single mutants,

nor the *cat1/2/3/4Δ* quadruple mutant, showed any change in titanization capacity or endogenous superoxide accumulation relative to wild type. However, *sod2Δ* exhibited defects in the accumulation of superoxide (Fig 3.12B: right) and reduced formation of large cells (Fig 3.12B: left, 3.12C). *SOD2* encodes Mn-Sod2, the major superoxide dismutase in the mitochondrion, where it converts superoxide to H_2O_2 and is required for resistance to oxidative stress (Giles, Batinic-Haberle et al. 2005). *SOD2* has been previously show to be required for growth at 37°C(Giles, Batinic-Haberle et al. 2005). Examination of the cultures showed that *sod2Δ* mutant cells proliferate as yeast under titan inducing conditions (37°C, 5%CO_2) (Fig 3.12D). While temperature has been identified as one of the conditions influencing robust titan cell induction *in vitro,* titanization can still be observed at 30°C, albeit at reduced levels (Dambuza, Drake et al. 2018, Zhou and Ballou 2018). We therefore compared cell size in *SOD2* and *sod2Δ* cells at 30°C, 5%CO2, in titan-inducing medium (Fig 3.12E). There was no difference in growth between *SOD2* and *sod2Δ* cells at 30°C (Fig 3.12E, 3.13B). Treatment with DPTA NoNoate increased the proportion of large, high ploidy cells for *SOD2* and there was a further increase for the *sod2Δ* mutant (Fig 3.12E, 3.13B). Together, this suggests that detoxification of mitochondrial superoxide by Sod2 is required to enable the yeast-to-titan switch under physiological conditions (37°C, 5%CO_2).

We hypothesized that, in titanizing cells at 37°C, the *sod2Δ* mutant accumulates high levels of superoxide in the mitochondria at the initial stage, resulting in failure to survive the yeast-to-titan transition, and the extremely slow growth rate afterwards is the possible reason of overall low-production of superoxide. The dynamic nature of superoxide during titanization (Fig 3.7A) might indicate different requirements for superoxide detoxification over the course of induction. To test this, *sod2Δ* cells were placed under inducing conditions (37°C, 5%CO_2) and treated with MnTBAP (0.5mM) for the initial 4hr or 8hr only, and then washed and returned to inducing conditions, or maintained in MnTBAP for 18hr. Our data showed that 0.5mM of MnTBAP isn't sufficient lower the overall superoxide level to the extent of stop formation of titan cells (data not show). As shown in Fig 3.12E, MnTBAP treatment of 4 hrs was sufficient to reduce *sod2Δ* superoxide levels comparable with untreated *SOD2* titanized cells (Fig 3.12E). Treatment of *sod2Δ* cells for a further 8 or 18hr increased the overall proportion of large cells, yielding a population similar to *SOD2* titanized cells (Fig 3.12E). These data reveal that *SOD2* is required for initial detoxification for superoxide during titanization, as initial recovery of superoxide dismutase function is sufficient for *sod2Δ* to recover titanization defects.

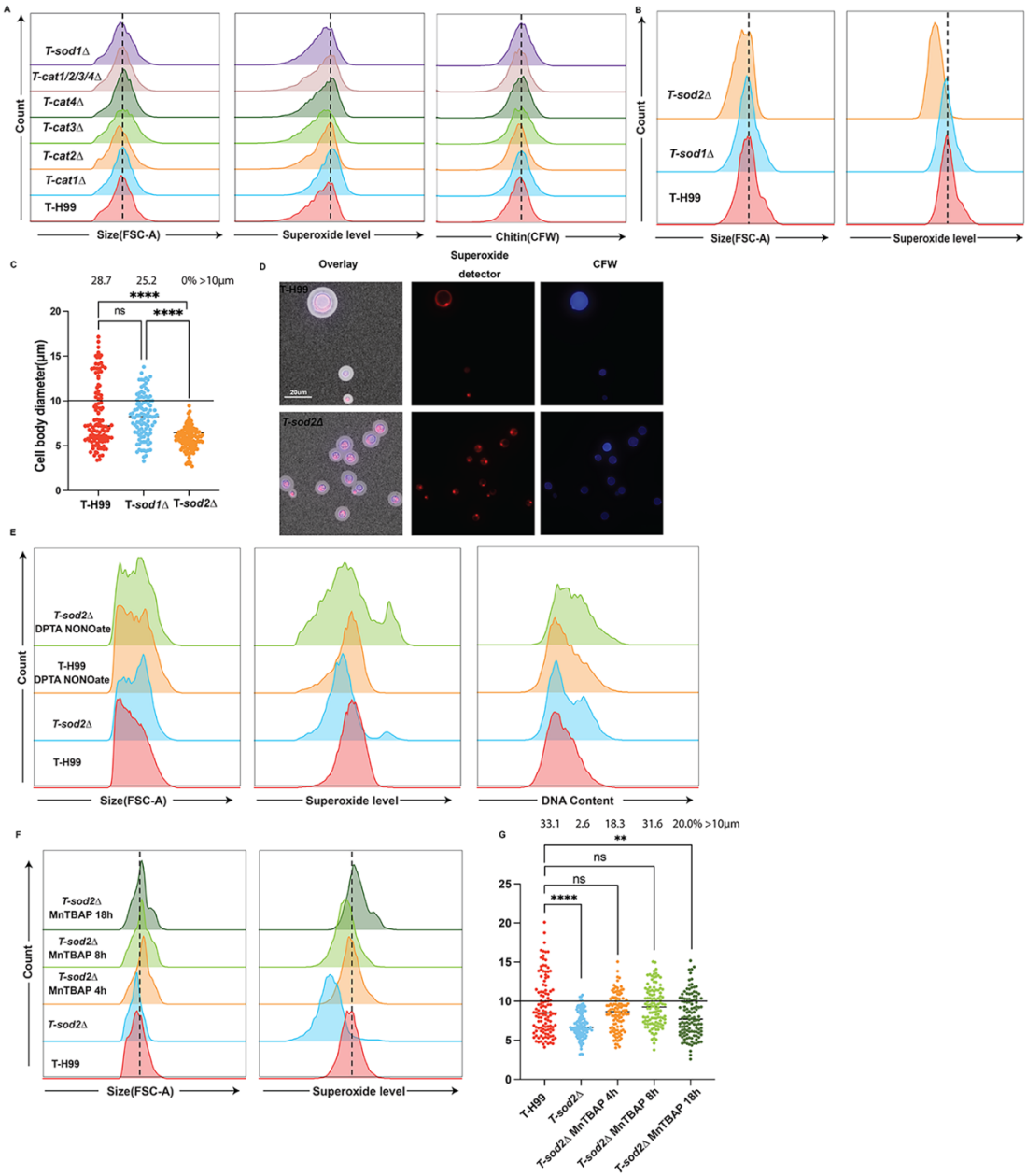


Fig 3.12: Superoxide Dismutase (Sod) but not Catalase (Cat) activity is required for titan cell formation. (A) Histograms of cell size and superoxide levels of different mutants: *sod1Δ, cat1Δ, cat2Δ, cat3Δ, cat4Δ* single mutants, and the cat1/2/3/4Δ quadruple mutant. All mutants and H99 were titan induced for 24hr and stained with superoxide detector, then analysed by flow cytometer for size (FSC-A) (*left*), and superoxide level (*right*). (B) Histograms of superoxide levels and cell size of *SOD*

mutants: *sod1Δ* and *sod2Δ* with H99 as the control. All mutants and H99 were titan induced for 24hr and stained with superoxide detector, then analysed by flow cytometer for size (FSC-A) (*left*), and superoxide level (*right*). (C) Cell body diameter for *C. neoformans* H99, *sod1Δ* and *sod2Δ* titan induced cells. (D)Microscopy images of *sod2Δ* growth after titan induction compared to H99. Cells were stained with superoxide detector (*red*), calcofluor white (CFW) for cell wall (*blue*), and India ink for the capsule. Scale bar: 20μm. (E) Histograms of cell size, superoxide levels, and DNA Content of *SOD2* and *sod2Δ* titan induced cells at 30°C with or without DPTA NONOate (0.3μM) treatment. H99 incubated under similar conditions serves as the control. (F) Histograms of cell size and superoxide levels of *sod2Δ,* and *sod2Δ* treated with 0.5mM MnTBAP for the initial 4h or 8h of titan induction and then washed away or for the entire 18hr titan induction period. (G) Cell body diameter for cells from (F). All cells were stained with superoxide detector and then analysed by flow cytometer for size (FSC-A) (*left*), and superoxide level (*right*). (A&B&E&F) Single cells were identified by FSC-A vs FSC-H to remove doublets. Dotted lines indicate MFI of H99 titanized cells. (C&G) Cell size was assessed for individual cells (cell body diameter, excluding capsule; n>100). Data were assessed for normality by Shapiro-Wilk and analysed by one-way ANOVA. Three biological replicates were performed and a single representative replicate is presented. “T” indicates titanized

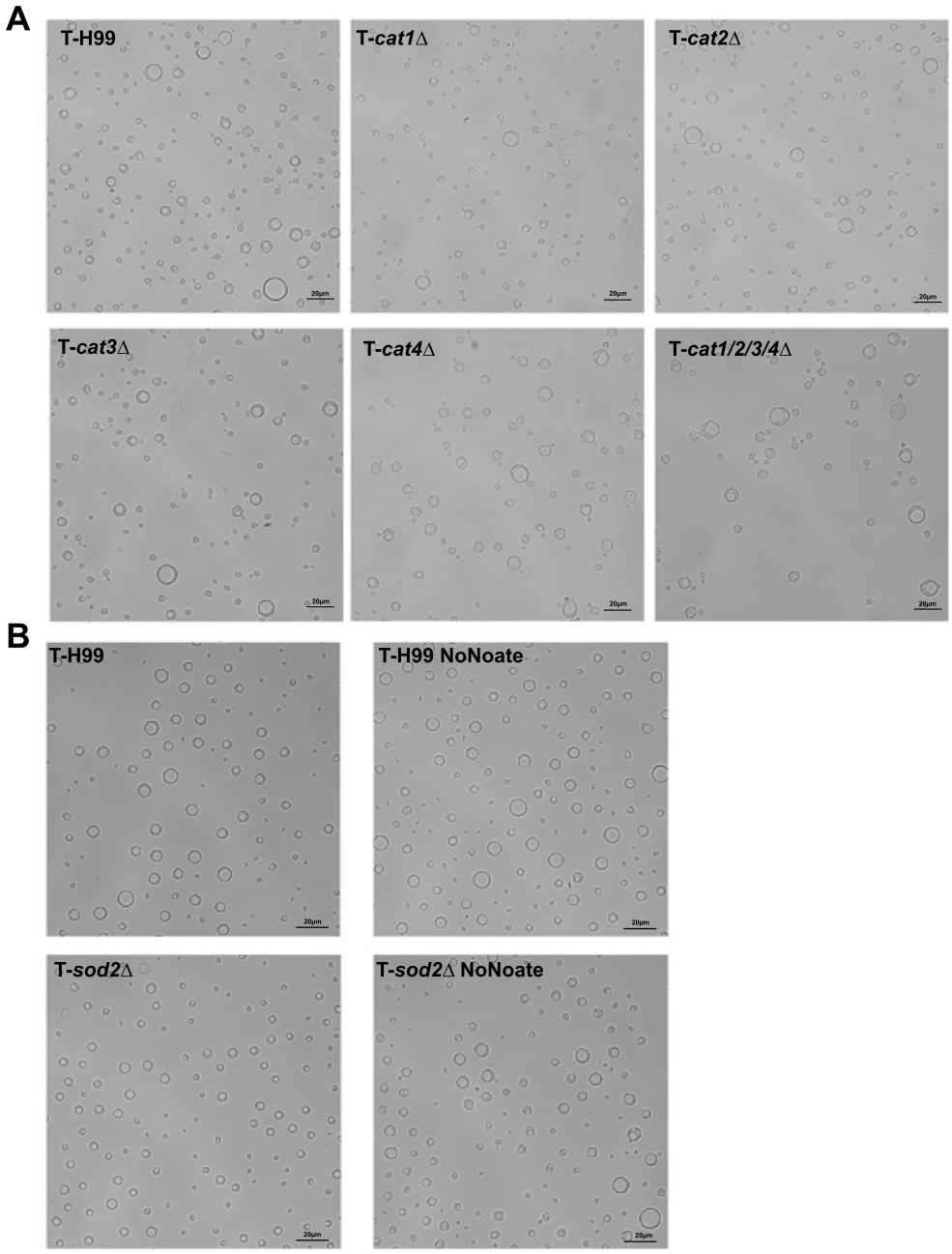


Fig 3.13: (A)Microscopy images of catalases mutants after titanization: *cat1Δ, cat2Δ, cat3Δ, cat4Δ* single mutants, and *cat1/2/3/4Δ* quadruple mutant with H99 as a control. (B) Microscopy images of *SOD2* and *sod2Δ* titan induced cells at 30°C with or without DPTA NONOate (0.3μM) treatment). Three biological replicates were performed and a single representative replicate is presented, T" indicates titanized.

3.10 Titanized cells exhibit high nuclear superoxide and increased DNA damage

Microscopy of titanizing cells revealed that, during the later stages of titanization, superoxide becomes localised to the nucleus (Fig 3.14A). Zhao et al. recently showed that genotoxic stress leads to cryptococcal cell polyploidization (Zhao, Wang et al. 2020). We therefore hypothesize that this excessive endogenous superoxide within the nucleus is a source of genotoxic stress, and predicted that the accumulation of superoxide leads to DNA double-strand breaks (DSBs). To contend with this, cells must undergo DSBs repair through homologous recombination or non-homologous end joining (Yu, Jacobs et al. 2001). We therefore measured the accumulation of Rad51, a member of the RecA-family that is a marker of DSBs (Chen, Nastasi et al. 1997, Yu, Jacobs et al. 2001, Sung, Krejci et al. 2003), in titan and yeast-phase cultures. We used an anti-Rad51 antibody against whole cell lysates from titan-induced and yeast-phase cells, compared to UV-treated yeast cells as a positive control. In H99 titanized (T-H99) cultures, we detected a strong signal for Rad51, comparable with UV-treated cells, while only limited Rad51 was detected in yeast-phase cultures (Fig 3.14B). These data suggest that, in addition to high overall endogenous superoxide levels and mitochondrial polarization, superoxide in the nucleus may trigger the accumulation of DNA DSBs during titanization.

3.11 Sod1 is localised to the nucleus after titan induction

Our observation of nuclear accumulation of superoxide in titanized cells (Fig 3.14A) raised the question of how *C. neoformans* copes with oxidative stress. *C. neoformans* Cn/Zn-Sod1 is predicted to be mitochondrial and cytoplasmic, yet *S. cerevisiae* Cn/Zn-Sod1 has been shown to translocate into the nucleus upon exposure to high oxidative stress (Tsang, Liu et al. 2014). Therefore, we determined the subcellular localization of CnSod1 via N-terminal tagging with GFP under its native promoter. During yeast-phase growth (in YNB), GFP-Sod1 localises to the cytoplasm (Fig 3.14C). However, upon titan-induction, GFP-Sod1 was additionally observed in the nucleus, co-localised with superoxide (Fig 3.14C). This subcellular localization suggests that CnSod1 is important for regulating endogenous ROS levels in the nucleus during titanization. Despite this, loss of *SOD1* had no apparent impact on the capacity of yeast to convert into titan cells (Fig. 3.12A, B).

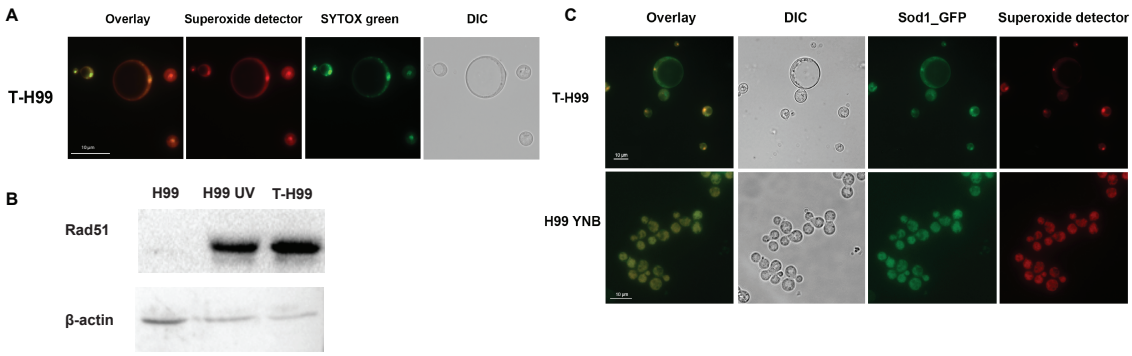


Fig 3.14: Sod1 and superoxide localise to the nucleus of yeast and titan cells under titan inducing conditions. (A) Superoxide co-localizes with nuclei in titanized cells. Fluorescent microscopy images of H99 titanized cells following staining with

superoxide detector dye (*red*) and SYBR green for the nuclei (*green*). Scale bar:10μm. (B) Western blot for Rad51 protein levels in YPD-grown yeast-phase cells (H99), UV treated yeast cells (H99 UV) and titanized cells (T-H99, 24hr) with actin loading control. (C) CnSod1 subcellular localization at the start of titanization (H99 YNB) and 24hr post-induction (T-H99). Green: Sod1-GFP, Red: superoxide detector. Scale bar: 10μm, three biological replicates were performed and a single representative replicate is presented, "T" indicates titanized.

3.12 SOD1 regulates genomic integrity of titan daughters

Given that genotoxic stress can cause chromosomal rearrangement, and that titan cells often produce aneuploid daughters, we predict that the altered regulation of ROS in the nucleus after the deletion of *SOD1* might promote genomic instability in titan daughters (Zhao, Wang et al. , Gerstein, Fu et al. 2015, Zhao, Wang et al. 2020). To test this, we first induced titan cells in either *sod1Δ* or *SOD1* isolates for 48hr and then separated out daughter cells via passage through 4μm filters. This excludes the majority of yeast phase cells and enriches for titan daughter cells (2-3 μm). Daughter cells were plated on YPD at low concentration to isolate single cells. After 48 hr incubation at 30°C, for H99*,* all colonies were uniform in size. However, for *sod1Δ* two different colony sizes were observed: approximately 50% of *sod1Δ* derived colonies were smaller, indicating slower growth rate (Fig 3.16). Because aneuploidy is often correlated with growth defects, we compared the DNA

content of cells from typical sized and small colonies of *sod1Δ* with H99-derived colonies as a control (Torres, Sokolsky et al. 2007). As shown in Fig 3.15A, *sod1Δ* titan daughters showed more variation in base DNA content compared with H99. In addition, slow growing *sod1Δ*-derived colonies exhibited a higher frequency of increased DNA content (aneuploidy) compared with either H99-derived or large *sod1Δ*-derived colonies (Fig 3.15A right panel). In order to validate the presence of aneuploidy, we also re-cultured these slow grown daughters in liquid YPD for 24hr and determined DNA content. As shown in Fig 3.15B, the increased DNA content for slow growing *sod1Δ* titan daughters was stable after re-culture. In summary, these data demonstrate that CnSod1 regulation of ROS in the nucleus is important for genome integrity during titanization and the production of euploid offspring.

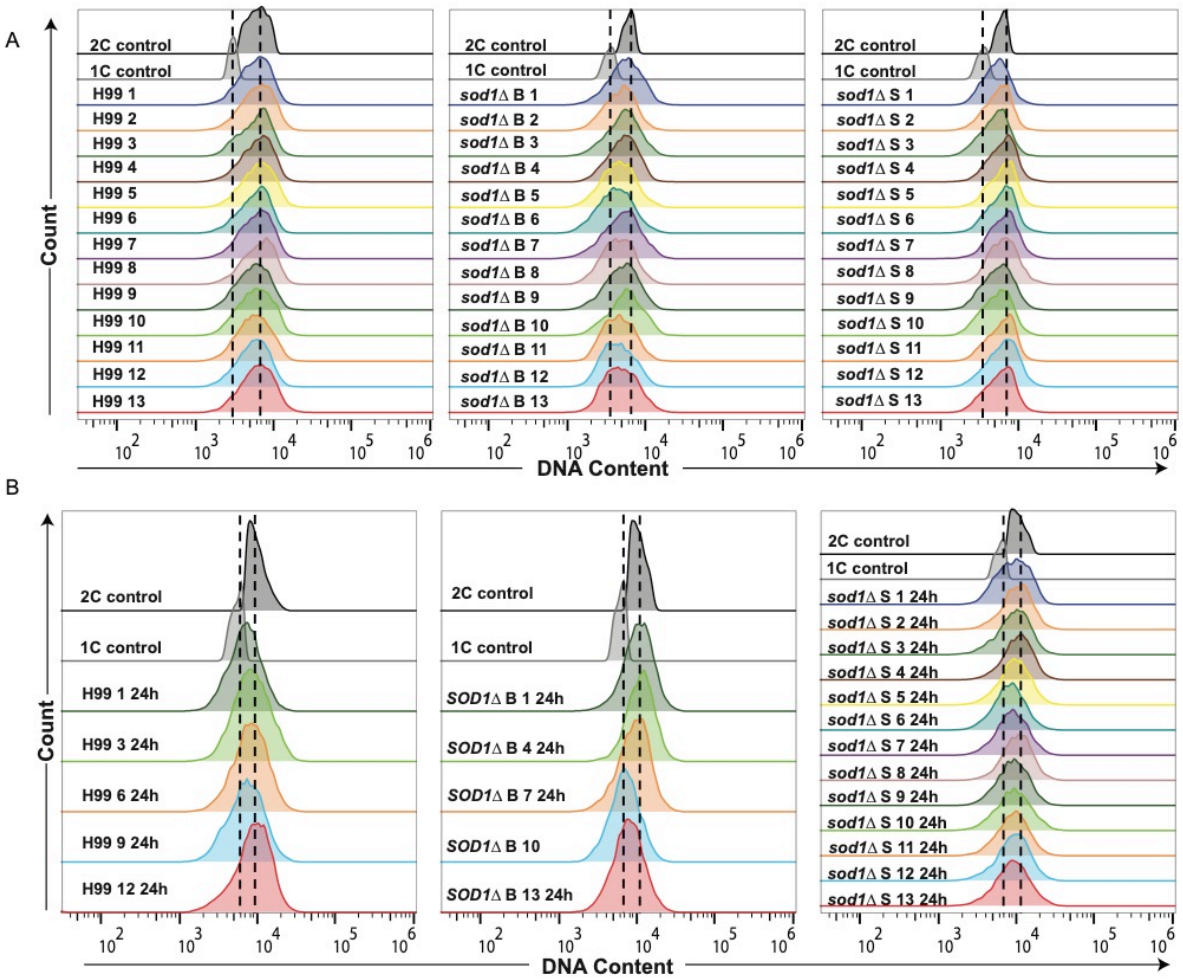


Fig 3.15: Loss of *SOD1* impacts titan daughter ploidy. H99 and *sod1Δ* cultures induced to form titan cells were filtered to enrich for cells <4 μm (titanides) and plated onto YPD plates. DNA content (DAPI) was analysed for colonies (A) after 48 hr directly from YPD plates and (B) after 24 hr overnight YPD culture. (A&B) Histograms of DNA content, left): H99 colonies, middle): *sod1Δ* big colonies, right): *sod1Δ* small colonies. YPD grown yeast cells from matched parent strains and MFI 1C and 2C populations were used for 1C and 2C peaks. Dotted lines indicate the MFI of 1C and 2C peaks. *sod1Δ* B*: sod1Δ* -derived big colonies, *sod1Δ* S: *sod1Δ* -derived small colonies. Three biological replicates were performed and a single representative replicate is presented, T" indicates titanized.

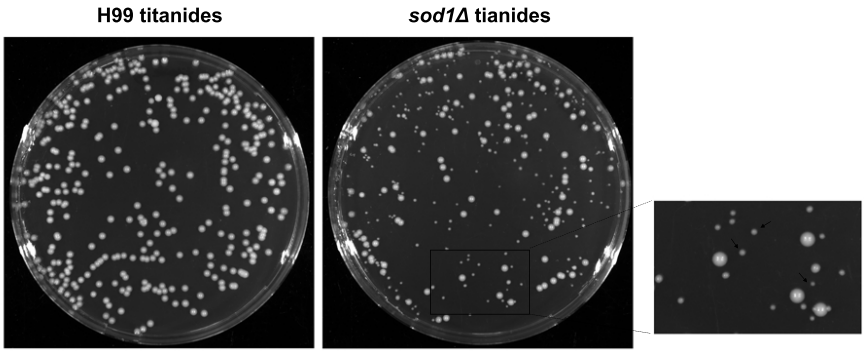


Fig 3.16: H99 and *sod1Δ* titan daughters re-culture plates. *sod1Δ* titan daughters (centre and right) showed two different colony sizes on re-culture plates. Black arrows point to small colonies. Three biological replicates were performed and a single representative replicate is presented.

Discussion

In the host lung, the human fungal pathogen *Cryptococcus neoformans* undergoes a morphological switch from small haploid yeast to large polyploid titan cell, contributing to *C. neoformans* virulence. Titan cells are less readily phagocytosed and can survive host nitrosative and oxidative stresses. We and others previously showed that titanization is triggered by host-relevant signals including CO_2 and lung-resident bacteria, and addition of these factors is sufficient to induce titan cells *in vitro*. Here we investigate the molecular mechanisms that drive this transition and demonstrate that host-derived immune signals can increase the degree and frequency of titanization. Specifically, host-relevant reactive nitrogen species increase the accumulation of endogenous superoxide within cryptococcal cells, particularly within nuclei, where it can cause genotoxic stress. Consistent with this, we observe the accumulation of Rad51 protein, a marker of the double-strand break repair pathway, in titanizing cultures. Blocking superoxide accumulation inhibits titanization, yet titanization also requires superoxide detoxification through superoxide dismutase (SOD) activity. Loss of mitochondrial Sod2 activity locks cells in the yeast phase, while Sod1 influences the production of viable titan daughter cells. We hypothesize that the redox responsive transcription factor Yap1 in part mediates this response by regulating *SOD2/SOD1*. In addition, we show that Sod1 translocates to the nucleus, where it is likely

involved in the detoxification of genotoxic superoxide. Together, these findings reveal a major new regulatory mechanism for the yeast-to-titan transition.

During infection, titan cells impair the host response directly and indirectly by blocking phagocytosis of small cells, resisting host stress, and influencing drug resistance (Okagaki, Wang et al. 2011, Crabtree, Okagaki et al. 2012, Okagaki and Nielsen 2012, Gerstein, Fu et al. 2015). Here, we demonstrate that the host immune response also influences and contributes to titanization. Titan cells form in response to the host lung environment and can be generated via host-relevant stimuli *in vitro* (Okagaki, Strain et al. 2010, Zaragoza, Garcia-Rivera et al. 2010, Dambuza, Drake et al. 2018, Hommel B, Mukaremera L et al. 2018, Trevijano-Contador, de Oliveira et al. 2018). Yet, despite strong evidence that *in vitro* stimuli are sufficient to induce titan cells, *in vitro*-generated titan cells are generally smaller than their *in vivo*-derived counterparts and produce diploid, rather than haploid or aneuploid, daughter cells (Gerstein, Fu et al. 2015, Dambuza, Drake et al. 2018, Hommel B, Mukaremera L et al. 2018, Trevijano-Contador, de Oliveira et al. 2018, Zhou and Ballou 2018). Here, we observed *in vitro* that when titanized cells were engulfed by macrophages, a proportion continued to undergo further cell enlargement within the phagolysosome. This phenomenon raised the hypothesis that host immune cell factors also contribute to titanization. By

testing this hypothesis, we now are able to present a molecular model showing a role for endogenous superoxide in regulating the yeast-to-titan transition and also show how the host influences this process (Fig 3.17).

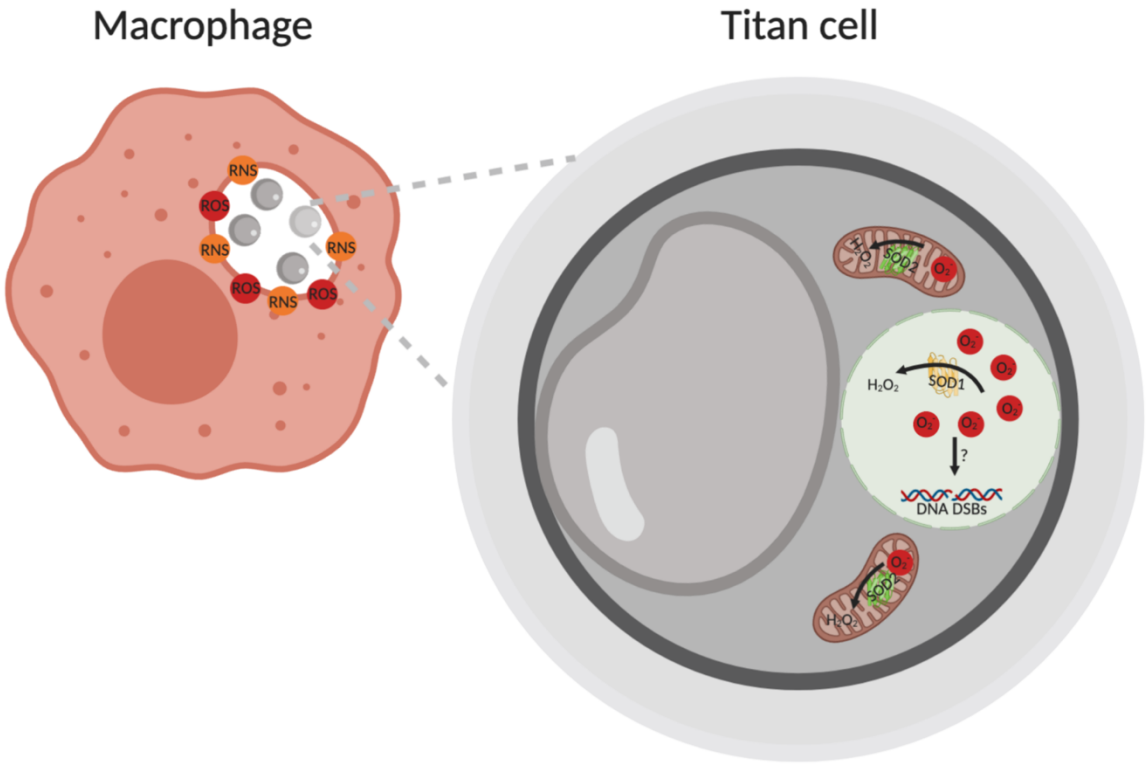


Fig 3.17: Summary of interaction between macrophages and *C. neoformans* titan cells. Macrophages bind and internalize cryptococcal cells through the formation of a phagosome, where they are exposed to antimicrobial effectors including ROS/RNS. However, for titan cells, these host-derived oxidative and nitrosative stresses can lead to increases both in endogenous superoxide and cell size. This endogenous superoxide production is required for titan cell formation and is detoxified by superoxide dismutases Cu/Fe-Sod1 and Mn-Sod2. Mn-Sod2 is a mitochondrial dismutase required for the initial detoxification of superoxide during titanization. Cn/Fe-Sod1 translocates to the nucleus after titan induction, where it

detoxifies genotoxic superoxide in the nucleus. Finally, this genotoxic superoxide is associated with DNA double-strand breaks (DSBs), and loss of detoxification increases progeny aneuploidy.

First, by comparing cells exposed to either LPS+IFN-γ or IL-4 activated phagocytes, we found a positive correlation between increased titanization (cell size and ploidy) and M1 immune cell activation. We further demonstrated that host RNS, more than host ROS, contributes to the accumulation of endogenously generated superoxide within the fungal cell. By exploring the mechanism underlying these changes in endogenous ROS levels, we found that the fungal mitochondrion is highly activated by exogenous RNS, triggering increased production of superoxide, which is required for titanization. Blocking superoxide accumulation through the addition of a Sod mimetic drug blocks titanization, while addition of H_2O_2 or loss of catalase activity that leads to H_2O_2 accumulation has no impact on titanization. Together, these data indicate that superoxide, but not H_2O_2, mediates the yeast-to-titan transition (Fig 3.17).

Second, we show that even in the absence of external RNS, cryptococcal cells in titan inducing conditions exhibit increased endogenous superoxide, which has both mitochondrial and nuclear localization and is dynamic over time and across the population. Free ROS can damage macromolecules and membranes; however, they also represent crucial signalling molecules

involved in fungal growth, differentiation and infection (Heller and Tudzynski 2011, Tudzynski, Heller et al. 2012). The spatiotemporal regulation of ROS production is necessary for sexual development in *A. nidulans*, perithecia formation in both *Neurospra crassa* and *Podospora anseria,* and differentiation of virulence-relevant appressoria and penetration hyphae in *Magnaporthe oryzae* (Lara-Ortiz, Riveros-Rosas et al. 2003, Malagnac, Lalucque et al. 2004, Egan, Wang et al. 2007, Cano-Dominguez, Alvarez-Delfin et al. 2008). Analogous to these other systems, we propose that, in *C. neoformans,* the spike in superoxide production controls the formation of titan cells that are crucial for both fungal survival and pathogenesis.

In *C. neoformans,* two superoxide dismutase (SOD) enzymes neutralize superoxide: Sod1 and Sod2. Both enzyme activities are required for resistance to oxidative stress, however they have different roles in pathogenesis (Cox, Harrison et al. 2003, Giles, Batinic-Haberle et al. 2005). *SOD2* is required for high-temperature growth and targets superoxide generated by mitochondrial Complex III (Cox, Harrison et al. 2003, Giles, Batinic-Haberle et al. 2005). During titanization, detoxification of mitochondrial superoxide by Sod2 is required for fungal cell growth and the initial switch to titan cells. Loss of *SOD2* reduces growth under titan inducing conditions and prevents cells from making the switch to titan morphology, suggesting that factors that perturb *SOD2* activity or otherwise influence mitochondrial ROS

will also perturb titanization. Consistent with this, Trevijano-Contador et al. demonstrated that addition of the mitochondrial inhibitor sodium azide increased the size and frequency of titan-like cells in their *in vitro* assay (Trevijano-Contador, de Oliveira et al. 2018).

Interestingly, previous work showed that deletion of *SOD1* in C*. neoformans* results in reduced virulence and increased sensitivity to iNOS-mediated macrophage killing (Cox, Harrison et al. 2003, Giles, Batinic-Haberle et al. 2005). In addition, the *yap1Δ* mutant exhibits reduced dissemination to the brain and slightly reduced overall virulence (So, Maeng et al. 2019). We demonstrate that the *yap1Δ* mutant fails to produce high ploidy titan cells and has a defect in titanide production, and that loss of *YAP1* impairs regulation of *SOD1.* Although *SOD1* is not required for titan cell formation, detoxification of nuclear superoxide by Sod1 is required for the generation of haploid progeny in the face activation of DNA Double Strand Break repair (Fig 3.14 and 3.15). Specifically, we demonstrate that Sod1 subcellular localization changes over time, translocating to nuclei in induced cells. This localization pattern suggests that Sod1 is involved in the regulation of ROS accumulation in the nucleus, and analysis of the *sod1Δ* mutant suggests that altered regulation may affect genome integrity of titan offspring, leading to the generation of aneuploid progeny.

Finally, we detected a strong signal for the DSB repair protein Rad51 in induced cells, indicating that there is high DNA damage accumulated during the yeast-to-titan switch. A recent paper reported that cryptococcal polyploidization during infection is induced by unknown genotoxic stresses causing DSB (Zhao, Wang et al. 2020). Combined with this, we predict high DNA damage is caused by the accumulation of endogenous superoxide in the nucleus. In the future, the relationship between DSBs and titanization and the source of the nuclear superoxide should be further investigated. After titan induction, both Sod1 and superoxide showed the nuclear location, we, therefore, hypothesize there is a NOX enzyme that translocates into nuclei and works together with Sod1 to regulate the ROS signalling. Despite the fact that until now no NADPH oxidase has been characterized in *C. neoformans*, which however is believed to be another major source for superoxide production in the fungal system (Nauseef 2008, Rossi, Gleason et al. 2017). In *C. albicans*, it is reported that ferric reductase (Fre8), a member of NOX family, can produce superoxide at the growing tip of the polarized cell and Sod5 is co-induced with Fre8 acting as a partner for Fre8 (Rossi, Gleason et al. 2017). Based on our preliminary data, we screened a few possible NADPH oxidases that produce superoxide outside of mitochondria and can potentially translocate into nuclei such as ferric reductase (Fre2, Fre201, and Fre3), and Nox1. However, until now we haven't detected any obvious phenotype for

mutants of these candidates encoding genes on titan cell formation or nuclear superoxide production. Further research will also study the molecular mechanisms by which the superoxide signal is transduced, resulting in titan cell formation.

Together, our data link previous work on the role of major host response molecules to controlling *C. neoformans* proliferation and the morphological switch from yeast-phase growth to titan phase growth, a major mechanism by which *C. neoformans* evades the host. These findings pave the way for future work investigating the underlying regulation of fungal morphogenesis by host-derived and endogenously generated reactive species, including possible chemotherapeutic strategies to block the yeast-to-titan switch.

Chapter 4

Mini introduction

DNA damage contributes to titan cell formation in *Cryptococcus neoformans* by affecting cell cycle transition

4.1 ROS can cause damage to DNA, proteins, and lipids

Reactive oxygen species (ROS), for example superoxide anion(O_2^-), hydrogen peroxide(H_2O_2), and hydroxyl radical (•OH), are highly reactive chemical molecules, produced as by-products of varied cellular processes. These molecules can interact with DNA, proteins, lipids, and other macromolecules leading to oxidative modification, or cause damage to them posing a more serious threat to cell integrity (Cooke, Evans et al. 2003, Salmon, Evert et al. 2004, Pizzimenti, Toaldo et al. 2010). ROS-induced DNA damage can lead to DNA exhibiting chemical base changes, Single- and Double- breaks, structural alterations, and cross-linkage(Cooke, Evans et al. 2003, Salmon, Evert et al. 2004, Halliwell 2006). ROS reactions with lipids normally happen at the cell membrane, where ROS target fatty acid side chains resulting in lipid peroxidation (Halliwell 2006, Pizzimenti, Toaldo et al. 2010, Dantas Ada, Day et al. 2015). For proteins, ROS can cause more diversified modification or damage on proteins such as oxidation of the

peptide backbone and the amino acid side chains, and formation of cross-links between proteins(Halliwell 2006, Dantas Ada, Day et al. 2015). Despite this, there is increasingly more evidence supporting that ROS can be beneficial for a variety of biological processes regulating signal transduction, which includes cellular proliferation and differentiation, even programmed cell death (Pizzimenti, Toaldo et al. 2010, Mittler 2017).

As discussed previously, for human fungal pathogens, there are two major sources of ROS: one is from the exogenous environment which is derived from host immune cell phagosome and another one is from endogenous production generated by fungal mitochondria and/or cytosolic enzyme systems like the NADPH oxidase complex(da Silva Dantas, Patterson et al. 2010, Warris and Ballou 2019). ROS produced by host immune phagocytes is part of the antimicrobial defense response to block infection by fungal pathogens by creating a toxic environment and inducing fungal intracellular oxidative stress(Brown, Haynes et al. 2009, Dantas Ada, Day et al. 2015). In contrast, fungal endogenous ROS production is more recognized for its role in regulating different biological and physiological processes(Lara-Ortiz, Riveros-Rosas et al. 2003, Takemoto, Tanaka et al. 2007, Semighini and Harris 2008, Tudzynski, Heller et al. 2012, Schieber and Chandel 2014, Rossi, Gleason et al. 2017, Warris and Ballou 2018)

4.2 Fungal DNA damage response pathway

As a direct consequence of oxidative DNA damage, genetic changes can result in severe diseases, cancer, and premature aging in humans (Slupphaug, Kavli et al. 2003). Therefore, in order to survive under oxidative stress and maintain genome integrity and stability, cells have evolved a highly organized DNA damage response (DDR) (Shiloh 2001, Maréchal and Zou 2013). From yeasts to humans, DDR pathways are highly conserved composing of protein kinases, mediator proteins, and transcription factors (TFs), and these TFs directly regulate DNA repair and replication, and cell cycling (Fig 4.1) (Shiloh 2001, Maréchal and Zou 2013).

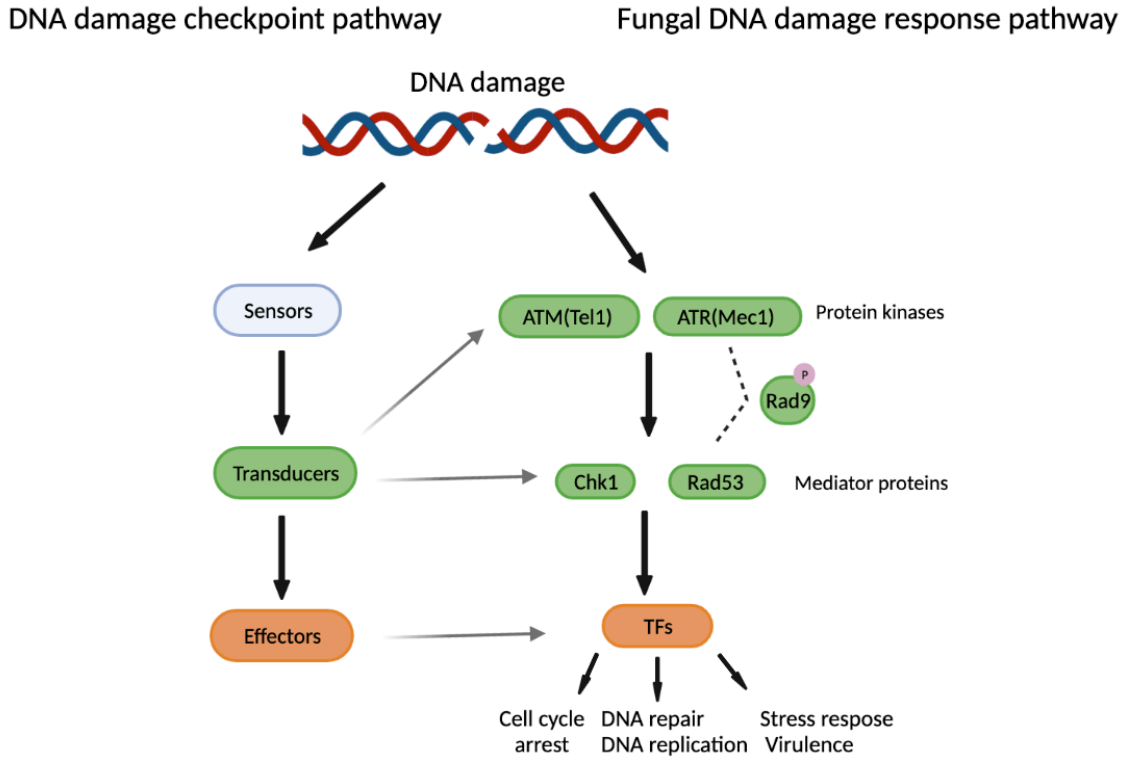


Fig 4.1: The models of DNA damage checkpoint and response pathways. The sensors of the checkpoint pathway can recognize DNA damage, and pass the signals to transducers which continue in processing and amplifying these signals.

Transducers include protein kinases (Mec1 and Tel1) and mediator proteins (Chk1 and Rad53) from the DDR pathway. These protein kinases can further regulate the downstream effectors which transcriptionally control cell cycle arrest, DNA repair and replication, stress response, and virulence.

In both *S. cerevisiae* and *C. neoformans*, DDR pathways are regulated by ataxia-telangiectasia mutated (ATM) and ATM- and Rad3-related (ATR) protein kinases, which are Tel1 and Mec1 respectively. These two kinases belong to the phosphatidylinositide-3-kinase(PI3K) family, and upon DNA damage they can activate their downstream effector kinases Chk1 (human Chk1 homolog) and Rad53 (human Chk2 homolog) via phosphorylating their Ser/Thr (SQ/TQ) sites (Shiloh 2001, Gobbini, Cesena et al. 2013, Maréchal and Zou 2013, Jung, Lee et al. 2019). The activation of Rad53 requires phosphorylation at Ser/Thr sites of adaptor protein Rad9 by Mec1, which then recruits and binds to Rad53 via its forkhead-associated (FHA) domain, and this interaction with Rad9 allows Rad53 to be recognized as substrate for Mec1 (Sun, Hsiao et al. 1998, Schwartz, Duong et al. 2002). The activated Rad53 further phosphorylates its downstream Dun1 kinase, which induces a global transcriptional network that regulates a variety of stress response genes(Jaehnig, Kuo et al. 2013).In humans, Chk1 and Chk2 are primarily activated by ATR (Mec1) and ATM(Tel1) respectively, whereas in yeasts Mec1 can active both Rad53 and Chk1(Shiloh 2001, Gobbini, Cesena et al.

2013, Maréchal and Zou 2013, Jung, Lee et al. 2019). It is also shown that compared to ATM kinase responding only to DSBs, ATR kinase can counteract a wide range of DNA damage including DSBs and DNA lesions that perturb replication (Maréchal and Zou 2013). In addition, in *C. neoformans* Jung et al recently reported that DNA damage response is also involved in fungal pathogenicity as both Rad53 and Chk1 kinases contribute to *Cryptococcus* virulence and mediate antifungal drug resistance (Jung, Lee et al. 2019).

4.3 Cell cycle of *C. neoformans*

Like the model organism *S. cerevisiae*, *C. neoformans* has four main stages in its cell cycle, starting with growth phase 1 (G1). After G1 is the synthesis phase (S), where cells start budding, synthesising DNA, and replicating the spindle-pole-body. After S phase is growth phase 2 (G2), where cells prepare for the final division via nuclear migration, spindle formation, and chromosome segregation. Finally, in mitosis phase (M), duplicated DNA is segregated into mother and daughter cells followed by full cell separation known as cytokinesis. However, in *C. neoformans* there is no clear gap between G1/S/G2 phases, as the initiation of budding occurs almost the same time as DNA synthesis when cells are still undergoing rapid growth (a characteristic of G1). Furthermore, *C. neoformans* can enter into stationary growth as unbudded G1 or G2 cells, unlike *S. cerevisiae* where only

unbudded G1 cells are seen in this phase (Ohkusu, Hata et al. 2001, Ohkusu, Raclavsky et al. 2004).

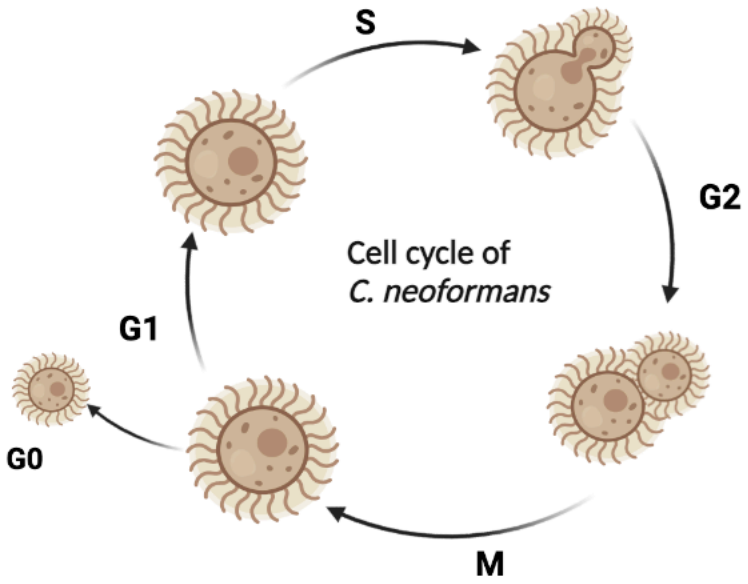


Fig 4.2: Cell cycle of *C. neoformans*. There are mainly 4 phases of this cell cycle: G1, S, G2, and M phases. G1 is the cell growth stage, and when it comes to S phase cell starts to bud and replicate DNA. Cell at G2 phase prepares for the final division which happens at M phase resulting in two daughter cells with equal DNA. *C. neoformans* also has a special stage where cell is quiescent with small cell size and less DNA content as discussed in chapter2.

4.4 DNA damage checkpoints control cell cycle arrest

In *Escherichia coli*, it was first reported that DNA damage induced genetic changes can control cell cycle transition (Painter and Young 1980). Painter et al in 1980 found that ataxia-telangiectasia (AT) cells which are defective in ATM gens and DNA damage response showed a shorter division delay from

G_2 phase into mitosis while this delay allows cells to repair their DNA damage (Painter and Young 1980). Later, similar regulations were observed in yeasts, after that DNA damage checkpoints were initially defined as growth non-essential regulatory pathways which control the cell cycle arrest (Weinert and Hartwell 1988, Rhind and Russell 1998, Zhou and Elledge 2000). More recent evidence showed that these checkpoints also control other important cellular processes such as activation of DNA repair pathways, recruitment of DNA repair proteins to damage sites, and induction of programmed cell death by apoptosis (Zhou and Elledge 2000).

Three main groups of proteins are recognized as DNA damage checkpoints, and they function as DNA damage sensors, signal transducers, and the downstream effectors (Fig 4.1) (Nyberg, Michelson et al. 2002). In this thesis, I am mainly focusing on transducers which include ATM and ATR protein kinases, and their downstream kinases Chk1 and Rad53 in yeasts (Gobbini, Cesena et al. 2013, Jaehnig, Kuo et al. 2013). These checkpoint kinases are activated by the DNA damage signal passed by sensors, which then process and amplify the signal to directly cause cell cycle arrest (Nyberg, Michelson et al. 2002). In *S. cerevisiae*, Mec1 (ATR) and its downstream Rad53 are reported to be essential for DNA lesion repairing and replication, cell cycle progression via transcriptionally regulating their target genes, and

they are also required for cell growth as their inhibition leads to cell death (Zhao, Chabes et al. 2001).

In the previous report, I uncovered that high endogenous superoxide production is required for titan cell formation, and titanized cells exhibit high DNA damage. However, it remains unclear whether there is a direct correlation between titanization and DNA damage and ROS production (Zhou, Desanti et al. 2021). In this chapter, I first determined the relationship between high superoxide production and DNA damage accumulation during titanization. We found that DNA damage upon titan induction is a direct consequence of oxidative stress, and accumulation of DNA damage is also shown to increase the capability for titanizaiton. Besides that, I also explored the possible mechanism underlying this increase. I found that *mec1Δ* mutant exhibited a delayed release from G_2/M phase, and cells arrested at this phase are proven to have a higher potential for titanization.

Results

4.5 Exogenous oxidative stress failed to promote Sod1 nuclear translocation

According to our previous finding, Cn/Zn-Sod1 has been shown to translocate into the nucleus upon *in vitro* titan induction regulating the endogenous ROS levels in the nucleus (Zhou, Desanti et al. 2021). Sod-mediated regulation of superoxide stress is also shown to be very important for the genome integrity of titanides (Zhou, Desanti et al. 2021). Similar relocations of Sod1 were reported in both yeast and mammalian cells, and according to these two reports Sod1 nuclear location can be simply induced by treating with exogenous oxidative stress like H_2O_2(Tsang, Liu et al. 2014, Li, Qiu et al. 2019). In order to further determine the role of oxidative stress in regulating nuclear Sod1 activity, we treated YPD-grown yeast cells with exogenous H_2O_2 for 5h. After increasing the treatment time from 20min to 5h, even to 24h, we found that 5h-treated cells showed the best signal for GFP-Sod1. As shown in Fig 4.3A, GFP-Sod1 failed to show nuclear translocation as what is observed during titanization (Fig 3.14). In addition, we also treated these yeast cells with glucose oxidases (H_2O_2) and DPTA NONOate (NO^-) which were found to be able to enhance oxidative stress in *C. neoformans* (Zhou, Desanti et al. 2021). However, again Sod1 remains within cytoplasm unlike what was reported in other systems. These data indicate that Sod1

translocation that happens during titanization is probably not simply induced by oxidative stress, instead of relying on multiple environmental signals in combination.

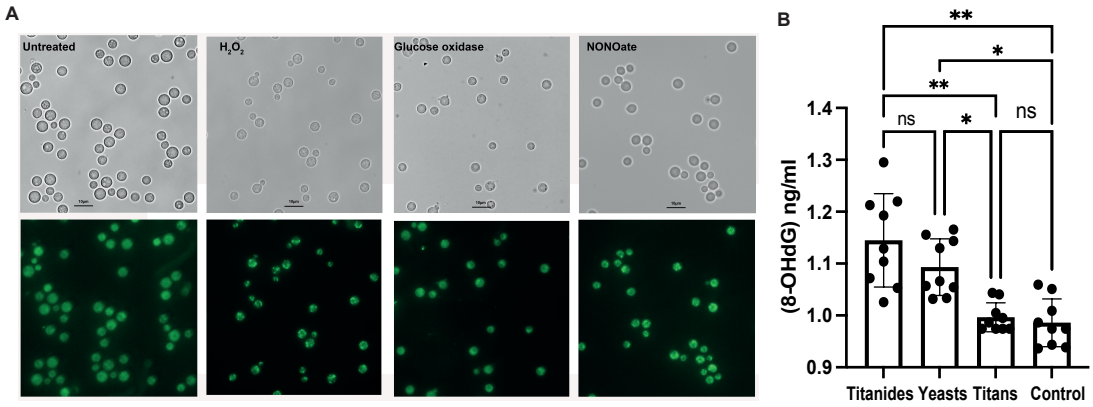


Fig 4.3: (A) Sod1-GFP failed to translocate into the nucleus under different oxidative and nitrosative stresses. Fluorescent microscopy images of Sod1-GFP treated with 1.5mM H_2O_2, 1mU glucose oxidase, or 0.3μM NONOate for 5hr. Green: Sod1-GFP. Scale bar:10μm. Three biological replicates were performed and a single representative replicate is presented. (B) Oxidative stress induced DNA damage in titans, yeasts, and titanides with YPD-yeast cells as a control. 8-OHdG was detected by competitive enzyme-linked immunosorbent assay (ELISA). Three biological replicates are presented(n=3). Data were assessed for normality by Shapiro-Wilk and analysed by One-Way ANOVA. Titanides vs control **p=0.0010; *p=0.0123, Titans vs titans **p=0.0027; *p=0.0274.

4.6 Accumulation of DNA damage is caused by nuclear oxidative stress

In our previous work, we detected both higher nuclear superoxide and increased DNA damage levels from titan induced-cells relative to yeast-phase

cells(Zhou, Desanti et al. 2021). We further predicted that nuclear superoxide-derived oxidative stress has a direct consequence for DNA damage and genome instability (Zhou, Desanti et al. 2021). It is reported that in both human and yeast cells, exposure to oxidative stress can lead to oxidative base damage in the form of 8-hydroxy-2′-deoxyguanosine (8-OHdG)(Valavanidis, Vlachogianni et al. 2009, Litwin, Bocer et al. 2013, Xu, Wu et al. 2020). Therefore, we applied a more direct method to determine whether DNA damage accumulated during titanization is caused by oxidative stress using 8-OHdG as a biomarker. Here, to further differentiate DNA damage levels among various size cells, we decided to separate the mixed titan induced population into three sub-groups based on size: titans (>10μm), yeast (>5μm and<10μm), and titanides (<5μm). As shown in Fig 4.3B, we found that overall titanized cells show higher levels of 8-OHdG in comparison to YPD grown yeast-phase cells, supporting that high DNA damage suggested by Rad51 expression levels (Fig 3. 14) happens during titanization as a result of nuclear oxidative stress. However, the more dramatic increases of 8-OHdG accumulation were observed for titanide and yeast sub-populations instead of titan cells, which exhibited similar DNA damage levels as YPD grown yeast cells (Fig 4.3B). In contrast to our prediction that titan cells would have increased 8-OHdG accumulation as they showed higher endogenous superoxide levels than yeast and titanide cells. Taken together,

we think that during titanization nuclear superoxide-derived oxidative stress is directly causing DNA damage, while the possible reason that only non-titans cells exhibited high oxidative DNA damage is that titan cells rapidly activate DNA damage repair pathway.

4.7 DNA damage response genes control titan cell formation

In *C. neoformans,* DDR pathway kinases CnMec1 and CnTel1 were found to play redundant roles in response to DNA damage, while CnMec1 is the major contributor to both CnRad53- and CnChk1-dependent DNA damage response (Jaehnig, Kuo et al. 2013, Jung, Lee et al. 2019). To directly test the relationship between DNA damage accumulation and titan cell formation, we decided to determine the titanization capabilities of mutants in which either *MEC1*, *RAD53,* or *CHK1* was removed. We compared these three gene deletion mutants with wild-type strain in terms of cell size, superoxide levels, and DNA content 24h post-titanization. As shown in Fig 4.4A, both *mec1Δ* and *rad53Δ* showed increases in titanization (cell size and DNA content) and superoxide accumulation, while *chk1Δ* was comparable to WT cells. In particular, *mec1Δ* showed a significant increase in the proportion of cells that are larger than 10μm (Fig 4.4B). These data indicate that DDR pathway is a negative regulator for titanization, as the loss of *MEC1* and *RAD53* are contributing to titan cell formation at different levels. This regulation is consistent with the previous finding that Mec1 and Rad53 are major

contributors to genotoxic stress and DNA damage response while Chk1 only plays a minor role(Jung, Lee et al. 2019).

This suggests that under titan conditions, where all cells experience nuclear oxidative stress and DNA damage, the two different possible fates (yeast vs titan) for cells are regulated by Mec1 and Rad53. One possible explanation is that Mec1 and Rad53 act prior to or during DNA synthesis by arresting replication in response to DNA lesions, a well-established role for these proteins (G1/S arrest). In cells that are unable to arrest (*MEC1* or *RAD53* mutants, or cells that have already passed checkpoints at the time of damage accumulation), cells replicate their DNA (S-phase) and increase in size (G2) but fail to progress to mitosis, and instead re-enter into G1 to become titan cells. We, therefore, set out to test this model through closer examination of the role of *C. neoformans* cell cycle in affecting titanization.

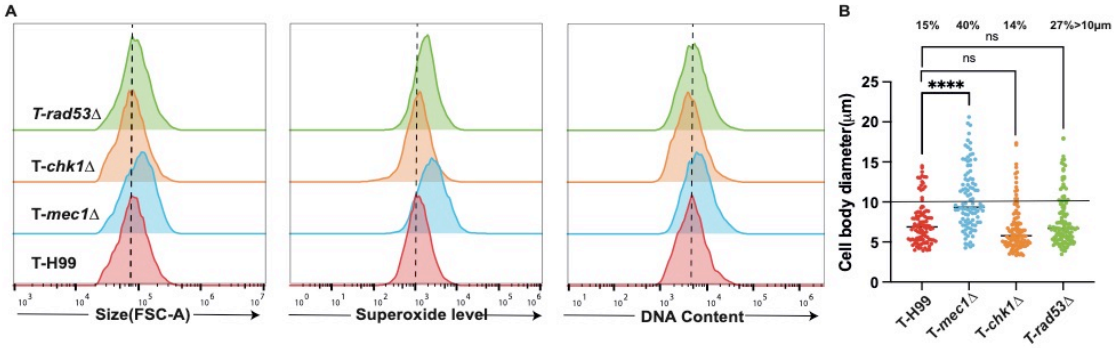


Fig 4.4: DDR pathway mutants exhibit increased titan cell formation. (A) Histogram of cell size, superoxide level, and DNA content of *mec1Δ, chk1Δ*, and *rad53Δ* mutants. All mutants and H99 were titan induced for 24hr and stained with superoxide detector and DAPI, then analysed by flow cytometer for size (FSC-A)

(*left*), superoxide level(*middle*), and DNA content(*right*). The dotted lines indicate MFI of H99. Single cells were identified by FSC-A vs FSC-H to remove doublets. (B) Cell body diameter of *mec1Δ, chk1Δ*, and *rad53Δ* mutants and H99. Cell size was assessed for individual cells (cell body diameter, excluding capsule; n>100). Data were assessed for normality by Shapiro-Wilk and analysed by one-way ANOVA, ****$p<0.0001$. Three biological replicates were performed and a single representative replicate is presented.

4.8 Cells arrested at G2/M phase are more likely to become titan cells

First, we decided to determine whether there is a correlation between cell cycle phases and titanization capability. Here, we applied two drugs: rapamycin and benomyl: rapamycin is an inhibitor of TOR pathway that can induce G1/S arrest prior to DNA synthesis while benomyl is a microtubule inhibitor that can induce G2/M arrest(Hoyt, Totis et al. 1991, Zinzalla, Graziola et al. 2007, Garcia-Rodas, Cordero et al. 2014). YNB cultures were treated with either of these two drugs to induce G1/S or G2/M arrest at the yeast stage, and then these cells were washed and exposed to titan induction. After 24h induction, as shown in Fig 4.5A, B, rapamycin(1μg/ml) pre-treatment totally blocks titan cell formation, as neither cell larger than 10μm nor polyploidy cells were detected (Fig 4.5A, B). In contrast, benomyl (70μg/ml) pre-treated cells showed a significant increase in titan cell formation including cell size, DNA content, and endogenous superoxide level. Besides that,

benomyl pre-treated cells also exhibit a significant increase in the proportion of titan cells(>10μm) with about 28% of the total population. This demonstrates that in response to titan induction, cells in G1/S grow as yeast and are blocked from titan cell formation, while cells in G2/M are able to re-enter the cell cycle rather than undergoing mitosis and become titans.

In addition, we also exposed rapamycin and benomyl pre-treated (10% Sabouraud) cells to an alternative titan induction protocol adopted from Trevijano-Contador et al(Trevijano-Contador, de Oliveira et al. 2018). Similar results were observed: pre-treatment with rapamycin inhibits titan cell formation, while benomyl increases titan cell formation in terms of cell size, superoxide level, and DNA content. (Fig 5C).

To show that the increase of titan cell formation is not due to unintended effects of benomyl, a different method to arrest the cell cycle at G2/M was used. We applied the low oxygen method to synchronize *C. neoformans* cells at G2 in YPD, and then put these cells into titan induction with un-synchronized YPD cells as a control (Ohkusu, Raclavsky et al. 2004). 24h post-induction, we found similar to benomyl treatment, G2 synchrony leads to a higher percentage (28%) of titan cells (>10μm), and slight increases in cell sizes, superoxide levels (Fig 5D, E), and DNA content. In summary, these data suggest that G2/M arrest cells are more likely to become titans while

G1/S arrest cells are blocked from titanization. This may also indicate that DNA synthesis is a major checkpoint for titan cell formation.

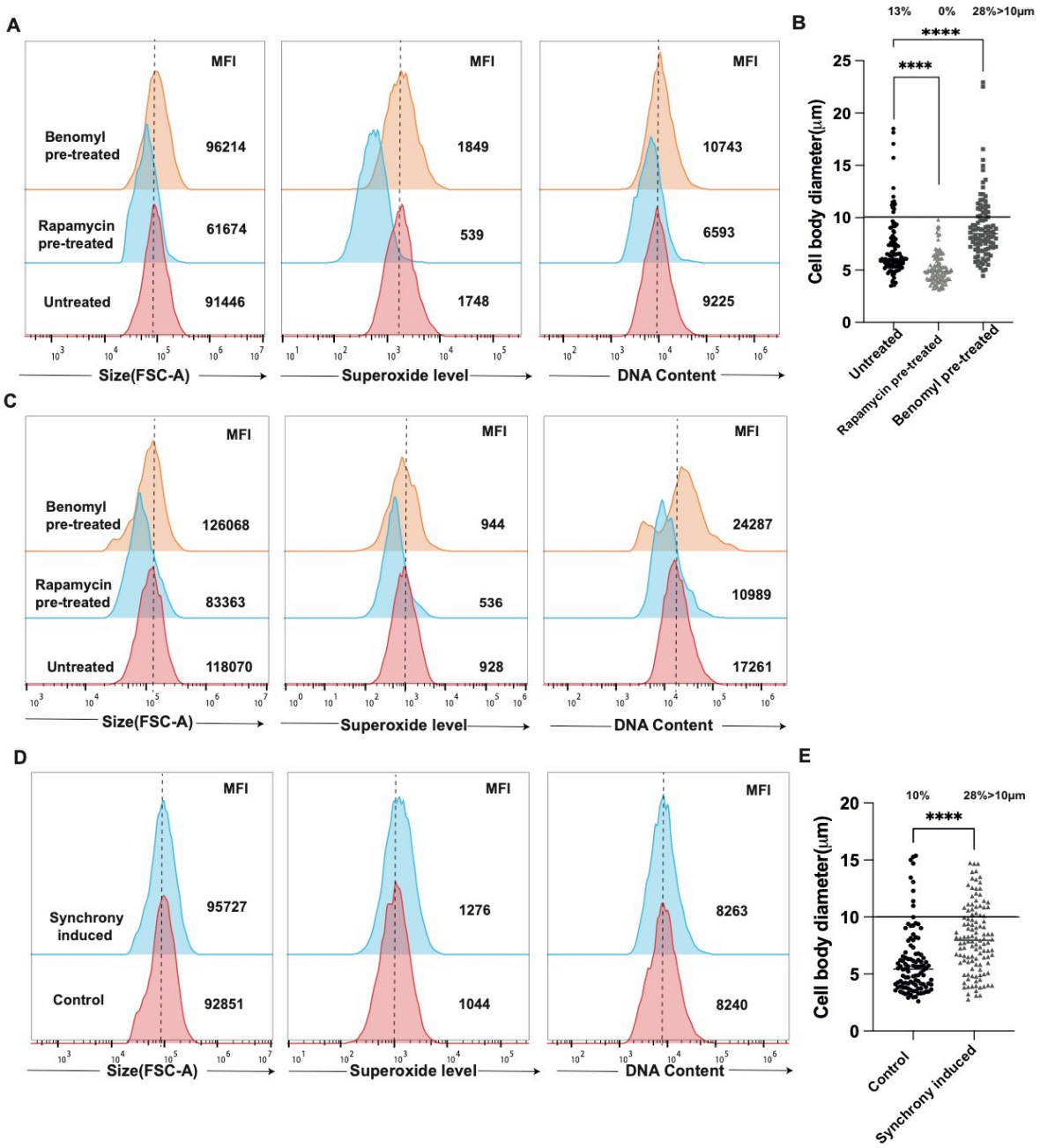


Fig 4.5: Cells arrest at G2/M phase are more likely to become titan cells. (A) Histograms of size (FSC-A) and superoxide levels of titanized cells from untreated, rapamycin(*middle*), and benomyl pre-treated(*top*). Dotted lines indicate median fluorescence intensity (MFI) of untreated cells. (B) *C. neoformans* titanized cell size

from conditions in (A). Cell size was assessed for individual cells (diameter) for the cell body (capsule excluded; n>100). Data were assessed for normality by Shapiro-Wilk and analysed by one-way ANOVA, ****p<0.0001. (C) Histograms of size (FSC-A) and superoxide levels of titanized cells from an alternative induction assay which includes untreated, rapamycin(*middle*), and benomyl pre-treated(*top*). Dotted lines indicate median fluorescence intensity (MFI) of untreated cells. (D) Histograms of size (FSC-A) and superoxide levels of titanized cells from synchrony induced and control (YPD). Dotted lines indicate median fluorescence intensity (MFI) of control cells. (E) *C. neoformans* titanized cell size from conditions in (D). Cell size was assessed for individual cells (diameter) for the cell body (capsule excluded; n>100). Data were assessed for normality by Shapiro-Wilk and analysed by one-way ANOVA, ****p<0.0001. Three biological replicates were performed and a single representative replicate is presented.

4.9 DNA damage accumulation contributes to titanization by affecting cell cycle transitions

Next, we investigated whether DNA repair impacts cell cycle progression. Loss of CnMec1 has the most significant impact on cryptococcal titan cell formation (Fig 4.4). In budding yeast, Mec1 acts as a master regulator for DNA damage response and cell cycle checkpoint.(Zhao, Chabes et al. 2001). To better understand how the attenuation of DDR can contribute to titanization, we started by checking if the loss of *MEC1* can affect the cell

cycle transition. We first synchronized both H99 and *mec1Δ* cells into G2 phase by growing them at high density with low oxygen, then releasing G_2-arrested cells into fresh culture(YPD) and monitoring the cell cycle transition via measuring DNA content by flow cytometry (Ohkusu, Raclavsky et al. 2004). As shown in Fig 4.6A, it seems that *mec1Δ* failed to enter into the M phase from G2 and cells arrest at this phase, as no clear 1C peak was detected over the entire process. Unlike H99 which showed clear 1C and 2C peaks 80 minutes after being released into fresh culture (Fig 4.6A). These indicate that the loss of *MEC1* can lead to an abnormal cell cycle leading to G2/M arrest.

However, growing in YPD rich medium, cells are only experiencing low superoxide levels and DNA damage (Fig 4.3 B), and therefore, we decided to check the effect of deleting *MEC1* when exposing to high superoxide levels and DNA damage experienced during titan induction. We observed the morphology of cells grown in YNB (pre-titanization) in which cells were found to produce very high endogenous superoxide (Fig 3.7), instead of monitoring DNA content, because YNB grown cells tend to form clumps (Fig 3.14), precluding analysis by flow cytometry. As shown in Fig 4.6B, *mec1Δ* exhibits morphology changes at YNB-grown phase showing titan-like and G2 phase morphology including both increased cell sizes and large vacuoles (Fig 4.6B). These observations raise a hypothesis that the increased titanization of

mec1Δ is caused by G2/M phase arrest when cells experience high oxidative stress while DNA repair mechanism is attenuated. To test this hypothesis, we pre-treated *mec1Δ* with rapamycin or benomyl as described above, and compared titanization capabilities with untreated *mec1Δ*. As shown in Fig 4.6C, rapamycin still poses inhibition on titanization on *mec1Δ* as titan cells proportion decreased from around 39% of untreated to 10% of rapamycin pre-treatment, similar as rapamycin can totally block titan cell formation on H99. In contrast, benomyl treatment has no impact on titan cell formation when *MEC1* is deleted. This suggests that rapamycin treatment can rescue *mec1Δ* YNB cells from G2/M arrest, while benomyl-induced G2/M does not have an additive effect in the absence of *MEC1.* In summary, these results revealed that the loss of *MEC1* can lead to G2/M phase arrest without any assistance, and this altered cell cycle can further contribute to titanization.

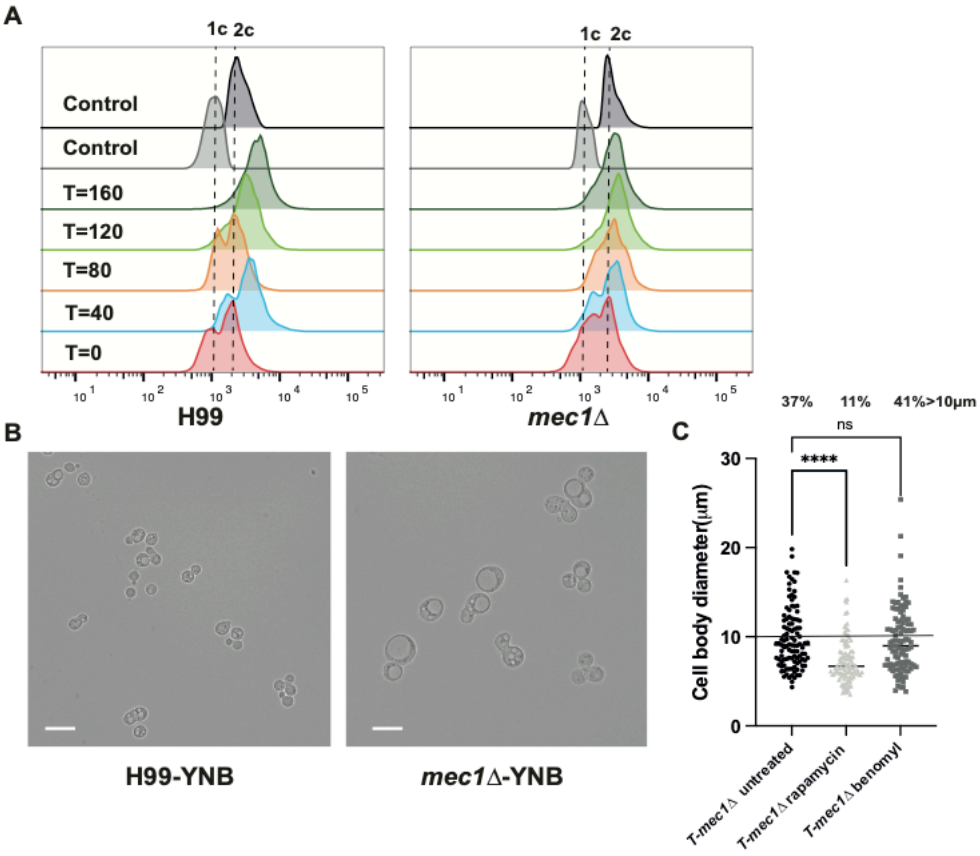


Fig 4.6: *mec1Δ* showed an abnormal cell cycle which further contributes to titanization. (A)Histograms of DNA content of H99 and *mec1Δ* cells after being released from G2 synchrony for 0(T=0), 40(T=40), 80(T=80), 120(T=120), and 160(T=160) minutes. YPD grown yeast cells from matched parent strains and MFI 1C and 2C populations were used to identify 1C and 2C peaks which are indicated by dotted lines. (B) Microscopy images of H99 and *mec1Δ* YNB grown yeast cells. Scale bar: 10μm. (C) Cell body diameter for *mec1Δ*(untreated), *mec1Δ* (rapamycin pre-treated), and *mec1Δ* (benomyl pre-treated) induced to form titans for 24hr. Cell size was assessed for individual cells (cell body diameter, excluding capsule; n>100). Data were assessed for normality by Shapiro-Wilk and analysed by one-way

ANOVA, ****p<0.0001. Three biological replicates were performed and a single representative replicate is presented.

4.10 G2/M phase cells have high mitochondrial potential and endogenous superoxide levels

We found that high endogenous superoxide production is required for yeast-to-titan transition, and mitochondrial potential is positively correlated with titanization (Zhou, Desanti et al. 2021). In the mammalian system, it is reported that compared to other phases of the cell cycle, G2/M phase arrest usually results in cells with increased mitochondrial content and potential, and higher ROS production (Yamamori, Yasui et al. 2012). Therefore, we checked whether G2/M or G1/S arrest cells (yeast stage) also exhibit differences in mitochondrial potential and ROS production in *C. neoformans* cells. We used the fluorescent probe JC-1 again to indicate mitochondrial membrane potential and as shown in Fig 4.7A, benomyl induced G2/M arrest cells exhibited higher mitochondrial potential relative to rapamycin-treated, which is indicated by the increase in the percentage of JC-1 aggregates. This increase of mitochondrial potential is shown to be correlated with ROS production, as we noticed that G2/M arrest cells exhibit higher superoxide levels (Fig 4.7B). In addition, we found that cells became more susceptible to external oxidative stress (H_2O_2) after rapamycin treatment, while benomyl has no effect on oxidative stress detoxification. This suggests that for cryptococcal cells, G2/M

phase cells have more active mitochondria and higher endogenous superoxide production than cells at G1 or S phase, and this is probably the reason why these cells are more likely to become titan cells.

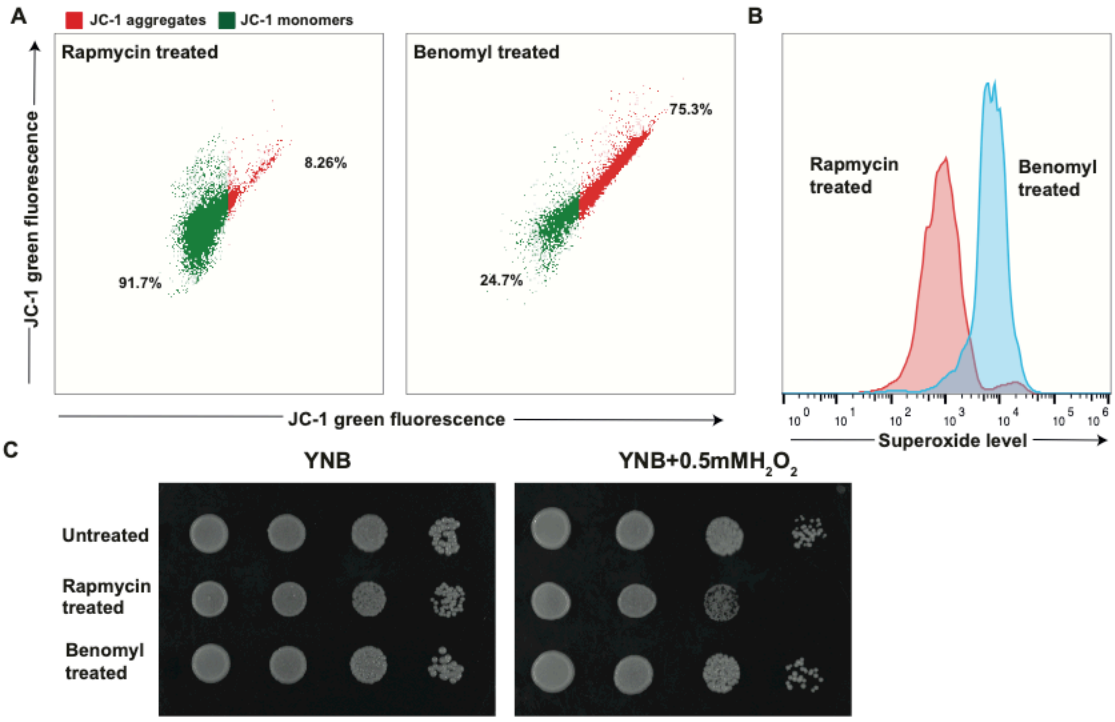


Fig 4.7: G2/M arrest cells showed more active mitochondria and higher endogenous superoxide production. (A) JC-1 green vs red fluorescence scatter plots of rapamycin treated and benomyl treated cells. Red and green dots indicate the JC-1 aggregates and monomers respectively. JC-1 aggregates are gated by red and green (mito tracker) single staining. (B) Histograms of superoxide levels of cells rapamycin treated*(red)* and benomyl treated*(blue)* cells. (C) Oxidative stress spot plates of rapamycin treated and benomyl treated with untreated cells as a control. After treatment, cells were plated onto YNB with or without 0.5mM H_2O_2. Three

biological replicates were performed and a single representative replicate is presented.

Discussion

In our previous research, we revealed the importance of endogenous superoxide production in regulating titan cell formation, and both superoxide and Cn/Zn-Sod1 showed subcellular localization in the nucleus of titanized cells (Zhou, Desanti et al. 2021). Therefore, titanization derived superoxide production was predicted to trigger Cn/Zn-Sod1 nuclear translocation. Here, to validate this prediction we treated Sod1-GFP yeast cells with different exogenous ROS or RNS stress generating reagents. However, what we found is that unlike what was reported in other systems, during cryptococcal titanization CnSod1 translocation cannot be induced by oxidative stress alone (Tsang, Liu et al. 2014, Li, Qiu et al. 2019). In other systems, it is also shown that after Sod1 translocation into the nucleus, it can act as a transcription factor regulating the expression of genes that control oxidative stress, DNA replication, and DNA repair, etc (Tsang, Liu et al. 2014, Li, Qiu et al. 2019). Combined with the finding that CnSod1 is required for genome integrity of titanides, we hypothesise that nuclear CnSod1 may also bind to promoters and regulate the expression of those genes to help with detoxification of oxidative stress and DNA damage.

Next, we decided to look for evidence of oxidative damage in DNA, which would be consistent with our hypothesis that genome instability during cryptococcal polyploidization is caused by oxidative stress (Zhao, Wang et al.

2020). By directly measuring oxidative modifications in DNA, we showed that DNA damage accumulated during titanizaiton is caused by oxidative stress, and among different sub-populations, titanides and yeasts are the cells that undergo the most damage. We predicted that there might be a positive correlation between accumulation of superoxide and oxidative DNA damage in the nucleus. In other words, cells that have high superoxide levels would also exhibit high DNA damage signals. However, titans which have the highest superoxide production showed the lowest levels of oxidative DNA damage relative to the other two sub-populations. One possible reason for this observation is that tian cells are more active on DNA repairing however this requires further works. Future studies will compare the expression levels of genes that directly control DNA repair.

After revealing the relationship between oxidative stress and DNA damage, we then tested the correlation between DNA damage accumulation and titan cell formation. Through analysis of titanization capabilities of mutants including *mec1Δ, chk1Δ, and rad53Δ*, we showed that missing DDR pathway components contribute to titan cell formation. Despite this increase in titan cells, a recent report demonstrated that both *rad53Δ* and *chk1Δ* are attenuated in pathogenicity for unclear reasons, and the perturbation of these two genes can reduce drug resistance (amphotericin B) in YPD rich medium (Jung, Lee et al. 2019). Mutant phenotypes suggest that a certain amount of

DNA damage accumulation is beneficial for the cryptococcal cells to form titans through unknown mechanisms. Since Mec1 is a well-known as cell cycle checkpoint, and the loss of *MEC1* can cause cell cycle arrest, we hypothesize that the DNA damage signal is regulating titan cells via affecting cell cycle transition (Zhao, Chabes et al. 2001, Nyberg, Michelson et al. 2002). To test this idea, we chemically induced G1/S and G2/M phase arrested yeast cells and compared the titan capabilities of these cells when exposed to two different titan induction conditions. Under all conditions, more titan cells were detected from G2/M pre-induced cells, while G1/S arrest cells totally failed to produce titan cells. Besides that, we also noticed *CnMEC1* is required for cells successfully entering into M phase when experiencing high oxidative DNA damage. Taken together, we believe that superoxide generated upon titan induction causes DNA damage to accumulate, which in turn contributes to titan cells via delaying cell cycle progression. These results are consistent with earlier reports about cell cycle transcriptionally regulating virulence factors like capsule and melanization expression in *C. neoformans* (Garcia-Rodas, Trevijano-Contador et al. 2015, Kelliher, Leman et al. 2016).

Finally, to better understand the reasons why cells from G2/M phase are more likely to become titan cells, we checked whether there is a variation in mitochondrial activity and ROS production of cells from different phases. Our results showed G2/M arrest can result in a higher mitochondrial potential and

increased superoxide production, both of which were demonstrated to be positively correlated with titanization. We then conclude that these are possible reasons for the increased titanizaiton capabilities. This thesis showed the link between titanizaiton and DNA damage and cell cycle for the first time, which provides a new insight into the understanding of the mechanisms underlying titan cell formation.

Final discussion and future work

This thesis addresses a few key questions regarding understanding the mechanism that drives titan cell formation and how different titan sub-populations affect the interaction with the host. Chapter 2 demonstrates that in response to the host environment signals both non-titanizing and titanizing isolates generate heterogeneous populations with two/three sub-populations that maintain distinct cell sizes and DNA contents. We additionally observed changes in capsule and IgM binding upon titan induction relative to other capsule-inducing protocols. While both population heterogeneity and changes on capsule structure will have implications for drug resistance and host cell interactions. Future studies will investigate the impact of different sub-populations (manually separated) on long-term immune responses including investigation of T cell polarization mediated by the different clinical isolates.

In chapter 3, host-relevant reactive nitrogen species was found to increase the accumulation of endogenous superoxide within cryptococcal cells and this endogenous superoxide production is also found to be required for yeast-to-titan transition. Moreover, fungal endogenous superoxide exhibits subcellular localization to nuclei where it can cause genotoxic stress and can further lead to DNA damage accumulation. Future work will further understand how superoxide regulates titan cell formation and uncover the major source for nuclear superoxide production.

Finally, in chapter 4, we reveal that there is a positive correlation between superoxide production, DNA damage, and titan cell formation. DNA damage

accumulated during titanization is a direct consequence of sustained superoxide activity and delayed DNA repair and this accumulation can further cause cell cycle arrest. Additionally, cells arrested at G2/M phase are more likely to become titan cells with higher mitochondrial potential and increased superoxide production. Taken together, we believe that superoxide generated upon titan induction causes DNA damage to accumulate, which in turn contributes to titan cells via delaying cell cycle progression. Future work will further determine the reason that cells at G2/M phase have higher potential on becoming titan cells and explore the role of nuclear CnSod1 in regulating the detoxification of oxidative stress.

Materials and methods

Strains, media and growth conditions *C. neoformans* H99 was kindly provided by Andrew Alspaugh, Duke University, NC, USA. Zc1, Zc8 and Zc12 clinical isolated were collected from ACTA Lusaka Trial in Lusaka, Zambia (Vanhove, Beale et al. 2016, Molloy, Kanyama et al. 2018) and kindly provided by Tihana Bicanic and Matthew Fisher. Strains were cultured routinely on YPD (1% yeast extract, 2% bacto-peptone, 2% glucose, 2% bacto-agar) plates stored at 4°C. Titan cell *in vitro* induction was performed as described in (Dambuza, Drake et al. 2018).Cells were pre-cultured at 37°C, 150rpm, in 10ml YNB without amino acids (Sigma-Aldrich) in which 2% of glucose was added according to manufacturer's protocol. After 24 hrs, cells were normalized to OD_{600}=0.001 in 1×PBS (phosphate-buffered saline) with 10% of Heat inactivated Fetal Bovine Serum (HI-FBS) (Sigma-Aldrich F9665) and incubated at 37°C, 5%CO_2 for 24 hrs unless otherwise indicated.

Table 1: Strain list

Strains	Genotype	Parent	Source
H99	Clinical isolate VNI		North Carolina
Zc1	Clinical isolate VNI		Zambia
Zc8	Clinical isolate VNI		Zambia
Zc12	Clinical isolate VNI		Zambia

sod1Δ	*SOD1::URA5*	H99	(Cox, Harrison et al. 2003)
sod2Δ	*SOD2::NAT*	KN99	Madhani 2015, FGSC
cat1Δ	*MATαCAT1::URA5*	H99	(Giles, Stajich et al. 2006)
cat2Δ	*MATαCAT2::NAT*	H99	(Giles, Stajich et al. 2006)
cat3Δ	*MATαCAT3::URA5*	H99	(Giles, Stajich et al. 2006)
cat4Δ	*MATαCAT4::URA5*	H99	(Giles, Stajich et al. 2006)
cat1/2/3/4Δ	*MATαCAT1::URA5 CAT2::NAT CAT3::URA5 CAT4::NEO ura5*	H99	(Giles, Stajich et al. 2006)
yap1Δ	*MATαYAP1::NAT*	H99	(Jung, Yang et al. 2015)
ERB454	*pSOD1 –GFP-SOD1-NAT*	H99	This study

mec1Δ	*MATαMEC1::NAT*	H99	(Jung, Yang et al. 2015, Lee, So et al. 2016)
chk1Δ	*MATαCHK1::NAT*	H99	(Jung, Yang et al. 2015, Lee, So et al. 2016)
rad531Δ	*MATαRAD53::NAT*	H99	(Jung, Yang et al. 2015, Lee, So et al. 2016)

J774.1 cell culture: For most *in vitro* infection assays, we used the J774.1 murine macrophage cell line. Cells were routinely passaged in Dulbecco's modifies Eagle medium (DMEM+) culture media with serum (DMEM, low glucose, from Sigma-Aldrich; 10% HI-FBS; 1% penicillin-streptomycin solution from Sigma-Aldrich; 1% 200mM L-glutamine from Sigma-Aldrich) and 100ng/ml LPS (Sigma) and 1000U/ml IFN-γ (R&D Systems) were added as indicated overnight. All assays were performed with cells in passages 4 to 10. 24h before infection, 1×10^5 macrophages J774.1 were seeded into 12-well plastic plates in 1ml DMEM culture media with serum (DMEM+) and activated with 10U/ml IFN- γ.

Murine infection model (chapter2): Female C57BL/6 mice were used at 8-10 weeks of age and were maintained in individually-ventilated cages under specific pathogen-free conditions at the Biomedical Research facility at the University of Birmingham (Birmingham, UK). Animals were provided with food and water *ad libitum.* All experimentation conformed to the terms and conditions of United Kingdom Home Office license for research on animals (PPL/PBE275C33) and the University of Birmingham ethical committee.

Cryptococcosis Infection Model (chapter2): Yeast was grown in SabDex broth (Sigma-Aldrich), grown at 30°C with shaking for 18-24 hours. Yeast cells were washed in PBS, counted, and delivered to mice intranasally while under isofluorane anaesthesia. Animals were infected with $2x10^5$ CFU. For analysis of lung and brain fungal burdens, animals were euthanized and organs weighed, homogenized in PBS, and serially diluted before plating onto YPD agar supplemented with Penicillin/Streptomycin (Invitrogen). Colonies were counted after incubation at 30°C for 48 hours.

Human primary monocytes isolation and culture: All human tissue work was performed as approved by the University of Birmingham Ethics Committee under reference ERN_15-0804b. On day of draw, 25-30 ml of blood was withdrawn from anonymized healthy volunteers by venepuncture and was directly used for monocytes isolation with double layer percoll. Before adding the blood, two of different densities of percoll were layered in

the universal tubes with 6 ml of 1.079 on the top and 6 ml of 1.089 at the bottom. After 6 ml of whole blood was layered over dual gradient, the universal tubes were centrifuged at 150g for 8mins, followed by 10mins at 129g without acceleration or breaks. The white disc of peripheral blood mononuclear cells (PBMCs) was removed from the top and mixed with red blood cell lysis buffer to clear away red blood cells. After centrifuge for 6 mins at 400g, PBMCs were washed twice in cold 1×PBS (centrifuged at 1000 g for 6 mins in between), resuspended in warm RPMI 1640 with 5% HI-AB serum, counted, and then plate onto 12 well plate at 1×10^6 cells per well. The covered plate was incubated at 37°C, 5%CO_2 overnight, after which non-adhere cells were removed by washing with fresh RPMI.

***In vitro* phagocytosis assays:** The intracellular proliferation assay was performed as previously described (Smith, Dixon et al. 2015). 24h before infection, 1×10^5macrophages J774 were seeded into 12-well plastic plates (Narra, Maeda et al.) in 1 ml DMEM culture media with serum (DMEM+) and activated with 10 U/ml IFN-γ. Before infection, *C. neoformans* cells were collected from titanization culture and washed three times with sterile 1×PBS. After normalising to 1×10^6 cells/ml in 300 µl DMEM+, cells were opsonized with 10µg/ml anticapsular 18B7 antibody by incubating at 37°C for 30min (Casadevall, Cleare et al. 1998). Then opsonized *C. neoformans* cells were added into activated J774.1 macrophages to give a multiplicity of infection

(MOI) ratio of 10:1. After 2 hrs (time point 0), infected wells were washed at least three time with pre-warm 1×PBS until all un-engulfed *C. neoformans* cells were removed from the wells.

Human monocytes were infected with opsonized cells for 4h without IFN-γ activation, and at this point all supernatants were collected for cytokine qualification. 4h post-infection, monocytes were divided into two groups: with or without IFN-γ (10 U/ml) activation and then infection continued for another 20h. Total 24h later, all supernatants were collected again with LPS (100ng/ml) as a positive control added at the same time as fungal cells and uninfected as negative control.

Macrophage infection rates: At time point 0, attached *C. neoformans* cells and macrophages were stained with Calcoflour white (CFW, 10μg/ml) and Lyso-Tracker Red (ThermoFisher, 1μM) in dark for 10 min and then fixed with 1 ml 4% paraformaldehyde (PFA) in 1×PBS at 37°C for 5min. After washing with 1×PBS, at least 5 frames from each single infected well were randomly selected and imaged with Nikon Ti-E microscope, capturing 500 cells. All images were analysed with FIJI and experiments were repeated 3 times for biological replicates.

Filtered titans phagocytosis assays: After 24h of *in vitro* induction, H99 titanised total population was passed through an 11μm filter (Fisher Scientific, UK) to separate titan (>11μm) and typical cells (<11μm). Then both

populations were washed, normalized and opsonize independently before adding to infection assays. Activation and infection of macrophages with opsonized *C. neoformans* cells followed the same protocol as described above.

Intracellular proliferation and vomocytosis assays. At time point 0 of phagocytosis assays, extracellular cells were removed by washing with warm fresh DMEM+. All samples were maintained at 37°C, 5%CO_2 in the Nikon Ti-E microscope chamber and imaged for 18h via time-lapse. Images were taken every 15 min and compiled into single movie files for analysis using NIS elements or FIJI software. Movies then were scored visually for intracellular proliferation rate, macrophage death and vomocytosis percentage. Vomocytosis scoring followed the guidelines described in Gilbert et al., 2017 (Gilbert, Seoane et al. 2017).

J774.1 macrophages live imaging assay: At time point 0 of phagocytosis assays, extracellular cells were removed by washing with warm fresh DMEM+. All samples were maintained at 37°C, 5%CO_2 in the Nikon Ti-E microscope chamber and imaged for 18h via time-lapse. Images were taken every 15 min and compiled into single movie files for analysis using NIS elements or FIJI software. Movies then were monitored visually for cell size changes over time.

Murine bone marrow derived macrophages (chapter3): For each experiment, rear legs from one mouse were disinfected for 1 minute in 70% ethanol. The muscles were removed and both extremities of the femurs and tibias were cut to flush the bone marrow out with complete medium (RPMI 1640 with L-glutamin, 0.1 mg/mL Penicilin/Streptomycin mix, 10% Heat-Inactivated Fetal Bovine Serum) into a 6 well plate using a small needle associated to a syringe. The bone marrows were put in suspension in 8mL complete media solution by gentle up and down with a p1000 pipette. These cell suspensions were filtered on a 100µm mesh, transferred in a 50mL tube and the well rinsed with 2mL of complete media that were added to the cell suspension while rinsing the mesh. After a 3 minutes centrifugation at 400g, the cell pellets were resuspended in 10mL of complete media. Small aliquots of these cell suspensions were diluted at 1/10 before proceeding to leucocyte counting on a Neubauer Chamber under the microscope. Further to that count, the cells were centrifuged and resuspended in complete media containing 20ng/mL of mouse recombinant murine M-CSF in order to dispense $5x10^5$ cells per well of a 24 well plate in a final volume of 500uL ("day 0"). At day 3, 500uL of M-CSF complete media were added to the wells. At day 6 or 7, 500uL of culture media was removed and 500uL of new M-CSF complete media were added to the wells. The following day the wells were gently washed two to three time with warm complete medium in order to

remove non-adherent cells and were incubated with complete medium supplemented or not with 10 ng/mL of recombinant murine IL-4 (Peprotech) or a mixture of 100 ng/ml LPS (Sigma) and 1000 U/ml IFN-γ (R&D Systems). The presence of adherent macrophages was confirmed by observation under microscope.

In some cases, bone marrow was frozen for future use. Following filtration through 100µm mesh, bone marrow cells were centrifuged, resuspended in 1mL of freezing media (L-glutamin supplemented RPMI 1640 containing 0.05 mg/mL Penicilin/Streptomycin, 45% Heat-Inactivated Fetal Bovine Serum, 10% DMSO), and transferred in a micro-vial to be frozen in a Mr Frosty cell container at -70°C over-night before being transferred in liquid nitrogen. Cells were recovered by bringing the micro-vial to 37°C in a water bath and slowly diluting with 9 mL warm complete media. After centrifugation, cells were resuspended in 10 mL complete media, small aliquots were diluted at 1/10 in a 0.2% trypan blue solution to identify dead cells, and live leucocytes were counted on a Neubauer Chamber under the microscope. Further to this count, the cells were cultured as described above.

Mice for bone marrow (chapter3): Male B6.129S-*Cybb*^{tm1Din}/J (*Cybb*$^{-/-}$) or B6.129P2-*Nos2*^{tm1Laul}J (*Nos2*$^{-/-}$) or C57BL/6 mice were used at 10-33 weeks of age and were maintained in individually-ventilated cages under specific pathogen-free conditions at the Biomedical Research facility at the

University of Birmingham (Birmingham, UK). Animals were provided with food and water *ad libitum.* All experimentation conformed to the terms and conditions of United Kingdom Home Office license for research on animals (PPL/PBE275C33) and the University of Birmingham ethical committee.

Cell wall staining: Cells from 24 hrs induced titan cultures were collected, washed twice with 1xPBS and resuspended in 500ul McIlvain's buffer (0.2M Na_2HPO_4, 0.1M citric acid PH 6.0). Cells were stained with EosinY (5µg/ml) in dark for 10mins and repeated for washes with McIlvaine's buffer, then resuspended in 500ul 1×PBS. CFW (10µg/ml) and ConA (50µg/ml) were added into samples and maintained in the dark for 10 mins. After washing twice with 1×PBS, cells were imaged with a Zeiss Axio Observer and analysed for fluorescent intensities with Attune NxT Flow cytometer.

Flow cytometry for cell ploidy: Cells were fixed and stained according to the protocol of (Dambuza, Drake et al. 2018). Cells were fixed with 50% methanol for 15 mins, washed 3 times with 1×PBS and stained with0.3µg/ml DAPI. Cells were analysed for DNA content using an Attune NxT Flow cytometer with violet laser. All flow cytometry data were analysed with FlowJo. Doublets and clumps were excluded using recommended gating system of FSC-H vs FSC-A, which was determined to be more parsimonious than SSC-H vs SSC-W followed by FSC-H vs. FSC-W. Autofluorescence in the DAPI

channel was excluded by comparison to unstained cells. Gates for 1C and 2C were established with haploid controls cultured in YPD liquid media as described in the text.

Superoxide staining: Cells were collected and washed twice with 1×PBS, then stained with superoxide detection reagent (Enzo Life Sciences) (1:500 dilution) (Marschall and Tudzynski 2016). As designed, this orange reagent is a cell-permeable probe that reacts specifically with superoxide, generating an orange fluorescent product (Enzo Life Sciences). Live stained cells were imaged with Zeiss Axio Observer and analysed for fluorescent intensities with Attune Nxt Flow cytometer YL2 channel.

JC-1 staining: The Abcam JC1-mitochondrial membrane potential assay kit was used according to the manufacturer's instruction. Live stained cells were imaged with Zeiss Axio Observer and 10,000 cells analysed for fluorescent intensities with Attune Nxt Flow cytometer BL1 and BL2 channels. Doublets and clumps were excluded using recommend gating system of SSC-H vs SSC-W followed by FSC-H vs. FSC-W, and auto-fluorescence was excluded using unstained cells.

DPTA NONOate treatment: After culturing in YNB overnight, cells were induced for titanization as described above with adding extra 0.3μM of DPTA NONOate (Enzo Life Sciences) which was resuspended in DMSO (Dimethyl sulfoxide). 48h post-induction, cells were analysed with Attune Nxt Flow

cytometer both for cell sizes and superoxide production with untreated cells as a control.

Flow cytometry for cell size and superoxide level after *in vitro* infection: Following co-culture, macrophages were lysed and both fungi and macrophages were collected, centrifuged, and washed once with 1xPBS. Cells were stained with anti-IgM (Crp127) FITC(BL1-A) and superoxide detector dye (Enzo Life Sciences) (Probert, Zhou et al. 2019). Cells including both fungal and macrophages were analysed for using an Attune NxT Flow cytometer. Doublets and clumps were excluded by gating on FSC-A vs FSC-H, and fungi were identified by positive capsule staining (BL1-A). BL1-A+ cells were then examined for size (FSC-A) and superoxide staining (YL2-A).

Glucose oxidase treatment: After culturing in YNB overnight, cells were induced for titanization as described above with adding extra 1mU of glucose oxidase (generates 1nmoles H_2O_2/min). 24h post-induction, cells were analysed with Attune Nxt Flow cytometer both for cell sizes and superoxide production with untreated cell as a control.

Cell sizes measurement: Cell diameter was measured using FIJI, with frames randomly selected, all cells in a given frame analyzed, and at least 5 images acquired per sample for each of two independent runs. Total cell number of each samples was >200. All statistical analyses were performed using Graphpad Prism.

MnTBAP treatment: After culturing in YNB overnight, cells were induced for titanization as described above with adding extra 1mM MnTBAP which was resuspended in PBS plus NaOH (PH=7.0). After 24h incubation in dark, cells were analysed with Attune Nxt Flow cytometer both for cell sizes and superoxide production with untreated cell as a control. For *sod2Δ* treatment, 500μM MnTBAP was added into for initial 4h or 8h, then drug was washed away with PBS and cells were resuspended with 1×PBS with 10% of HI-FBS (titan-induction buffer).

Rapamycin and benomyl treatment: After growing in YNB with rapamycin at 1μg/ml or benomyl at 70μg/ml overnight, *C. neoformans* cells were then induced for titanization as described above for 24hr. Cell viability was checked with oxidative stress plates.

Oxidative stress plating: *C. neoformans* cells were collected from YNB overnight (0hr) and 18hrs post titan induction cultures, then plated in 10-fold serial dilutions from 1×10^6 cells/ml onto YNB or YNB plus 0.5mM H_2O_2. Plates were incubated at 30°C for 2 days and imaged.

Generation of Sod1-GFP:*C. neoformans* strain ERB454 expressing GFP-Sod1 via the native *SOD1* promoter with Neurceothrycin (NAT) resistance was generated as follows: The eGFP sequence was amplified from pHGNAT plasmid (pCN19, a kind gift from Connie Nichols and Andy Alspaugh) using primers ERB574 and ERB575 (Price, Nichols et al. 2008).

The 600bp promoter of *CAT3* (CNAG_00575) (pCAT3) was amplified using primers ERB524 (ccggaagcttCTCACCTTTCGCATTCCTTT) and ERB525 (TCGCCCTTGCTCACCATAGTGCGTCATAATTACCGTGG) to introduce HinDIII and BamHI flanking restriction sites and an internal NdeI restriction site. Primer ERB525 additionally enabled overlap PCR with the eGFP fragment. The pHGNAT plasmid was modified to excise the *HIS3* promoter sequence and eGFP sequences via HinDIII and BamHI restriction digest. The linearized plasmid backbone was ligated with the p*CAT3*-GFP PCR construct, resulting in plasmid pCAT3GNAT (pEB048) enabling excision of the *CAT3* promoter. The *SOD1* promoter and 5'UTR (CNAG_01019) were amplified using primers ERB532 (ccggaagcttCACACTCGGCACTATCGG) and ERB533 (ggcatatgAGGAAGATATGGATGAGAGGT) (225bp product) The p*CAT3* insert in pEB048 was excised by HinDIII/NdeI digest and replaced with the SOD1 promoter upstream of eGFP to produce plasmid pSOD1GFP-NAT (pEB060). A 1.1kb region encoding the *SOD1* ORF (CNAG_01019) was amplified using primers ERB585 (ggatccATGGTCAAGGTACGTACAGTA) and ERB586 (cctgaggATGCAATGTTGGAATGTACT) to incorporate BamHI and SauI restriction sites in frame. The resulting construct was cloned via BamHI and SauI into the plasmid pEB060 in-frame with eGFP to produce plasmid pEB061 (pSOD1-GFP-SOD1-NAT). Genomic integration into H99

was performed using the biolistic transformation method as previously described(Toffaletti, Rude et al. 1993, Davidson, Cruz et al. 2000).

RT-PCR: *C. neoformans* cells were titan induced for 48 hrs, after filtering to separate different sub-populations, centrifuged, snapped frozen in liquid nitrogen. Total RNA was isolated using the RNeasy Plus mini kit (Qiagen) and 100ng of total RNA was used for reverse transcription using SuperScript IV reverse transcriptase (Thermo fisher scientific) according to the manufacture's recommendations. Total 50ng of cDNA used for RT-PCR (Applied Biosystems PowerUp SYBR Green Master Mix, Thermo fisher scientific) using the following primers *ACT1*-F: ATGGACGGTGAAGAAGTTGC, *ACT1*-R: GGAGCTTCGGTCAACAAAAC, *SOD1*-F: TATGCTTCACCCAGGAGTCG, *SOD1*-R: ATTACCGAGGTCACCAACGT, *SOD2*-F: GTACCGCTCTTCCTCGAG, *SOD2*-R: TGGTGTGATGGAGGTTCATA. *SOD1* and *SOD2* expression was normalised to *ACT1* and then normalised to *SOD1* and *SOD2* of H99 basal stage yeast cells according to the Delta-Delta C(t) method.

Western blotting: *C. neoformans* cells were grown in titan induction condition for 48-72h and YPD overnight. For overnight YPD cells, they were divided into two groups: 1) YPD-grown cells used as a negative control and 2) cells were treated with UV 100 J/m^2 for 1h used for a positive control. Cells were collected by centrifugation and washed two times with cold PBS, and

cell pellets were flash frozen with liquid nitrogen (store at -80°C). Cell pellets were suspended with 2ml lysing buffer (50 mM Tris-HCl [pH 7.0], 150mM NaCl, 50mM Tris, 5mM EDTA and 1% Triton X-100) and 0.5ml of o.5-mm glass beads (Millipore Sigma) on ice. After that, the cells were broken using a bead beater for 5 cycles of 2x30 s at the maximum speed with 1 min cooling on ice. Broken cells were centrifuged at maximum speed at 4°C for 10min, then supernatant was transferred into a sterile Eppendorf tube. Total protein was diluted with 1xPBS and the concentration was determined using a Bradford reagent (Sigma-Aldrich). Samples of 50 µg of protein were separated on a 10% SDS PAGE gel, then transferred to a nitrocellulose membrane. The blot was blocked in 10% BSA in 1×PBS with 0.1% Tween 20. Both Rad51-specific and anti-actin antibodies were used at a 1:2,000 dilution, and the blot was incubated overnight at 4°C. HRP-conjugated anti-rabbit IgG secondary antibody was used at a 1:4,000 dilution, and the blot was incubated for 2 h at 25°C(RT). Finally, the blot was incubated with Clarity Western ECL substrate (Bio-Rad) according to the manufacture's instruction, and the image was acquired through a ChemiDoc Touch Imaging system (Bio-Rad).

8-OHdG ELISA assays: a competitive 8-OHdG ELISA kit (Abcam, UK) was used to detect the concentration of 8-OHdG according to the manufacturer's instructions. The DNA samples were purified from cell lysates, and 1µg DNA per sample was used. DNA samples were digested with

nuclease P1(New England BioLabs, UK) at 37°C for 30min and then treated with TSAP thermosensitive alkaline phosphatase (Promega) at 37°C for 15min followed by a 10min boiling at 75°C to deactivate enzymes. After cooling down on ice, DNA samples are ready to use otherwise can be stored at -20°C.

Statistic: All data analysed in this thesis were assessed for normality by Shapiro-Wilk and found as not normal distribution. Therefore, we applied the one-way ANOVA to compare the means between different groups and determine whether any of these means are statistically significantly different from each other.

Reference

1. Aguirre, J., W. Hansberg and R. Navarro (2006). "Fungal responses to reactive oxygen species." Medical Mycology **44**(Supplement_1): S101-S107.
2. Aguirre, K. M. and G. W. Gibson (2000). "Differing requirement for inducible nitric oxide synthase activity in clearance of primary and secondary Cryptococcus neoformans infection." Medical Mycology **38**: 343-353.
3. Alanio, A., F. Vernel-Pauillac, A. Sturny-Leclere and F. Dromer (2015). "Cryptococcus neoformans host adaptation: toward biological evidence of dormancy." mBio **6**(2).
4. Alspaugh, J. A. and D. L. Granger (1991). "Inhibition of Cryptococcus neoformans replication by nitrogen oxides supports the role of these molecules as effectors of macrophage-mediated cytostasis." Infection and Immunity **59**(7): 2291-2296.
5. Alspaugh, J. A., J. R. Perfect and J. Heitman (1997). "Cryptococcus neoformans mating and virulence are regulated by the G-protein alpha subunit GPA1 and cAMP." Genes and Development **11**(23): 3206-3217.
6. Alspaugh, J. A., R. Pukkila-Worley, T. Harashima, L. M. Cavallo, D. Funnell, G. M. Cox, J. R. Perfect, J. W. Kronstad and J. Heitman (2002). "Adenylyl cyclase functions downstream of the Galpha protein Gpa1 and controls mating and pathogenicity of Cryptococcus neoformans." Eukaryotic Cell **1**(1): 75-84.
7. Andrews, D. L., J. D. Egan, M. E. Mayorga and S. E. Gold (2000). "The Ustilago maydis ubc4 and ubc5 genes encode members of a MAP kinase cascade required for filamentous growth." Mol Plant Microbe Interact **13**(7): 781-786.
8. Anthony, R. M., J. F. Urban, F. Alem, H. A. Hamed, C. T. Rozo, J.-L. Boucher, N. Van Rooijen and W. C. Gause (2006). "Memory TH2 cells induce alternatively activated macrophages to mediate protection against nematode parasites." Nature Medicine **12**(8): 955-960.
9. Arora, S., M. A. Olszewski, T. M. Tsang, R. A. McDonald, G. B. Toews and G. B. Huffnagle (2011). "Effect of cytokine interplay on macrophage polarization during chronic pulmonary infection with Cryptococcus neoformans." Infect Immun **79**(5): 1915-1926.
10. Ashton, P. M., L. T. Thanh, P. H. Trieu, D. Van Anh, N. M. Trinh, J. Beardsley, F. Kibengo, W. Chierakul, D. A. B. Dance, S. Rattanavong, V. Davong, L. Q. Hung, N. V. V. Chau, N. L. N. Tung, A. K. Chan, G. E. Thwaites, D. G. Lalloo, C. Anscombe, L. T. H. Nhat, J. Perfect, G. Dougan, S. Baker, S. Harris and J. N. Day (2019). "Three phylogenetic groups have driven the recent population expansion of Cryptococcus neoformans." Nat Commun **10**(1): 2035.
11. Aslanyan, L., V. V. Ekhar, C. M. DeLeon-Rodriguez and L. R. Martinez (2017). "Capsular specific IgM enhances complement-mediated phagocytosis and killing

of Cryptococcus neoformans by methamphetamine-treated J774.16 macrophage-like cells." International immunopharmacology **49**: 77-84.
12. Baba, T. (1988). "Electron microscopic cytochemical analysis of hepatic granuloma induced by Cryptococcus neoformans." Mycopathologia **104**(1): 37-46.
13. Bahn, Y.-S. and K.-W. Jung (2013). "Stress signaling pathways for the pathogenicity of Cryptococcus." Eukaryotic cell **12**(12): 1564-1577.
14. Beltrán, B., A. Mathur, M. R. Duchen, J. D. Erusalimsky and S. Moncada (2000). "The effect of nitric oxide on cell respiration: A key to understanding its role in cell survival or death." Proceedings of the National Academy of Sciences **97**(26): 14602.
15. Bicanic, T., C. Bottomley, A. Loyse, A. E. Brouwer, C. Muzoora, K. Taseera, A. Jackson, J. Phulusa, M. C. Hosseinipour, C. van der Horst, D. Limmathurotsakul, N. J. White, D. Wilson, R. Wood, G. Meintjes, T. S. Harrison and J. N. Jarvis (2015). "Toxicity of Amphotericin B Deoxycholate-Based Induction Therapy in Patients with HIV-Associated Cryptococcal Meningitis." Antimicrob Agents Chemother **59**(12): 7224-7231.
16. Bockmuhl, D. P. and J. F. Ernst (2001). "A potential phosphorylation site for an A-type kinase in the Efg1 regulator protein contributes to hyphal morphogenesis of Candida albicans." Genetics **157**(4): 1523-1530.
17. Bose, I., A. J. Reese, J. J. Ory, G. Janbon and T. L. Doering (2003). "A yeast under cover: the capsule of Cryptococcus neoformans." Eukaryotic Cell **2**(4): 655-663.
18. Brown, A. J., S. Budge, D. Kaloriti, A. Tillmann, M. D. Jacobsen, Z. Yin, I. V. Ene, I. Bohovych, D. Sandai, S. Kastora, J. Potrykus, E. R. Ballou, D. S. Childers, S. Shahana and M. D. Leach (2014). "Stress adaptation in a pathogenic fungus." J Exp Biol **217**(Pt 1): 144-155.
19. Brown, A. J., K. Haynes and J. Quinn (2009). "Nitrosative and oxidative stress responses in fungal pathogenicity." Curr Opin Microbiol **12**(4): 384-391.
20. Cadet, J. and J. R. Wagner (2013). "DNA base damage by reactive oxygen species, oxidizing agents, and UV radiation." Cold Spring Harb Perspect Biol **5**(2).
21. Cano-Dominguez, N., K. Alvarez-Delfin, W. Hansberg and J. Aguirre (2008). "NADPH oxidases NOX-1 and NOX-2 require the regulatory subunit NOR-1 to control cell differentiation and growth in Neurospora crassa." Eukaryot Cell **7**(8): 1352-1361.
22. Casadevall, A., W. Cleare, M. Feldmesser, A. Glatman-Freedman, D. L. Goldman, T. R. Kozel, N. Lendvai, J. Mukherjee, L. A. Pirofski, J. Rivera, A. L. Rosas, M. D. Scharff, P. Valadon, K. Westin and Z. Zhong (1998). "Characterization of a murine monoclonal antibody to Cryptococcus neoformans polysaccharide that is a candidate for human therapeutic studies." Antimicrob Agents Chemother **42**(6): 1437-1446.

23. Chen, F., A. Nastasi, Z. Shen, M. Brenneman, H. Crissman and D. J. Chen (1997). "Cell cycle-dependent protein expression of mammalian homologs of yeast DNA double-strand break repair genes Rad51 and Rad52." Mutation Research/DNA Repair **384**(3): 205-211.
24. Chen, Y., A. P. Litvintseva, A. E. Frazzitta, M. R. Haverkamp, L. Wang, C. Fang, C. Muthoga, T. G. Mitchell and J. R. Perfect (2015). "Comparative analyses of clinical and environmental populations of Cryptococcus neoformans in Botswana." Mol Ecol **24**(14): 3559-3571.
25. Chrisman, C. J., P. Albuquerque, A. J. Guimaraes, E. Nieves and A. Casadevall (2011). "Phospholipids trigger Cryptococcus neoformans capsular enlargement during interactions with amoebae and macrophages." PLoS Pathog **7**(5): e1002047.
26. Coelho, C., A. L. Bocca and A. Casadevall (2014). "The intracellular life of Cryptococcus neoformans." Annual review of pathology **9**: 219-238.
27. Cooke, M. S., M. D. Evans, M. Dizdaroglu and J. Lunec (2003). "Oxidative DNA damage: mechanisms, mutation, and disease." The FASEB Journal **17**(10): 1195-1214.
28. Cox, G. M., T. S. Harrison, H. McDade, C. Taborda, G. Heinrich, A. Casadevall and J. R. Perfect (2003). "Superoxide Dismutase Influences the Virulence of Cryptococcus
29. neoformans by Affecting Growth within Macrophages." Infection and Immunity **71**(1): 173-180.
30. Cox, G. M., T. S. Harrison, H. C. McDade, C. P. Taborda, G. Heinrich, A. Casadevall and J. R. Perfect (2003). "Superoxide dismutase influences the virulence of Cryptococcus neoformans by affecting growth within macrophages." Infection and Immunity **71**(1): 173-180.
31. Crabtree, J. N., L. H. Okagaki, D. L. Wiesner, A. K. Strain, J. N. Nielsen and K. Nielsen (2012). "Titan cell production enhances the virulence of Cryptococcus neoformans." Infect Immun **80**(11): 3776-3785.
32. Cruickshank, J. G., R. Cavill and M. Jelbert (1973). "Cryptococcus neoformans of unusual morphology." Appl Microbiol **25**(2): 309-312.
33. D'Souza, C. A., J. A. Alspaugh, C. Yue, T. Harashima, G. M. Cox, J. R. Perfect and J. Heitman (2001). "Cyclic AMP-dependent protein kinase controls virulence of the fungal pathogen Cryptococcus neoformans." Molecular and Cellular Biology **21**(9): 3179-3191.
34. da Silva Dantas, A., M. J. Patterson, D. A. Smith, D. M. Maccallum, L. P. Erwig, B. A. Morgan and J. Quinn (2010). "Thioredoxin regulates multiple hydrogen peroxide-induced signaling pathways in Candida albicans." Mol Cell Biol **30**(19): 4550-4563.
35. Dambuza, I. M., T. Drake, A. Chapuis, X. Zhou, J. Correia, L. Taylor-Smith, N. LeGrave, T. Rasmussen, M. C. Fisher, T. Bicanic, T. S. Harrison, M. Jaspars, R. C. May, G. D. Brown, R. Yuecel, D. M. MacCallum and E. R. Ballou (2018).

"The Cryptococcus neoformans Titan cell is an inducible and regulated morphotype underlying pathogenesis." PLoS Pathogens **14**(5): e1006978.
36. Dambuza, I. M., T. Drake, A. Chapuis, X. Zhou, J. Correia, L. Taylor-Smith, N. LeGrave, T. Rasmussen, M. C. Fisher, T. Bicanic, T. S. Harrison, M. Jaspars, R. C. May, G. D. Brown, R. Yuecel, D. M. MacCallum and E. R. Ballou (2018). "The Cryptococcus neoformans Titan cell is an inducible and regulated morphotype underlying pathogenesis." PLoS Pathog **14**(5): e1006978.
37. Dantas Ada, S., A. Day, M. Ikeh, I. Kos, B. Achan and J. Quinn (2015). "Oxidative stress responses in the human fungal pathogen, Candida albicans." Biomolecules **5**(1): 142-165.
38. Dantas, A. d. S., A. Day, M. Ikeh, I. Kos, B. Achan and J. Quinn (2015). "Oxidative stress responses in the human fungal pathogen, Candida albicans." Biomolecules **5**(1): 142-165.
39. Davidson, R. C., M. C. Cruz, R. A. Sia, B. Allen, J. A. Alspaugh and J. Heitman (2000). "Gene disruption by biolistic transformation in serotype D strains of Cryptococcus neoformans." Fungal genetics and biology : FG B **29**(1): 38-48.
40. Davis, D. (2003). "Adaptation to environmental pH in Candida albicans and its relation to pathogenesis." Current Genetics **44**(1): 1-7.
41. Davis, D. A. (2009). "How human pathogenic fungi sense and adapt to pH: the link to virulence." Current Opinion in Microbiology **12**(4): 365-370.
42. Davis, M. J., T. M. Tsang, Y. Qiu, J. K. Dayrit, J. B. Freij, G. B. Huffnagle and M. A. Olszewski (2013). "Macrophage M1/M2 polarization dynamically adapts to changes in cytokine microenvironments in Cryptococcus neoformans infection." mBio **4**(3): e00264.
43. Davis, M. J., T. M. Tsang, Y. Qiu, J. K. Dayrit, J. B. Freij, G. B. Huffnagle and M. A. Olszewski (2013). "Macrophage M1/M2 polarization dynamically adapts to changes in cytokine microenvironments in Cryptococcus neoformans infection." mBio **4**(3): e00264-00213.
44. Day, J. N., T. N. Hoang, A. V. Duong, C. T. Hong, P. T. Diep, J. I. Campbell, T. P. Sieu, T. T. Hien, T. Bui, M. F. Boni, D. G. Lalloo, D. Carter, S. Baker and J. J. Farrar (2011). "Most cases of cryptococcal meningitis in HIV-uninfected patients in Vietnam are due to a distinct amplified fragment length polymorphism-defined cluster of Cryptococcus neoformans var. grubii VN1." J Clin Microbiol **49**(2): 658-664.
45. Day, J. N., S. Qihui, L. T. Thanh, P. H. Trieu, A. D. Van, N. H. Thu, T. T. H. Chau, N. P. H. Lan, N. V. V. Chau, P. M. Ashton, G. E. Thwaites, M. F. Boni, M. Wolbers, N. Nagarajan, P. B. O. Tan and S. Baker (2017). "Comparative genomics of Cryptococcus neoformans var. grubii associated with meningitis in HIV infected and uninfected patients in Vietnam." PLoS Negl Trop Dis **11**(6): e0005628.

46. de Jesus Berrios, M., L. Liu, J. C. Nussbaum, G. M. Cox, J. S. Stamler and J. Heitman (2003). "Enzymes that counteract nitrosative stress promote fungal virulence." Current biology : CB **13**(22): 1963-1968.
47. Del Poeta, M. (2004). "Role of phagocytosis in the virulence of Cryptococcus neoformans." Eukaryot Cell **3**(5): 1067-1075.
48. Delobel, P. and C. Tesniere (2014). "A simple FCM method to avoid misinterpretation in Saccharomyces cerevisiae cell cycle assessment between G0 and sub-G1." PLoS One **9**(1): e84645.
49. Denham, S. T. and J. C. S. Brown (2018). "Mechanisms of Pulmonary Escape and Dissemination by Cryptococcus neoformans." J Fungi (Basel) **4**(1).
50. Denham, S. T., S. Verma, R. C. Reynolds, C. L. Worne, J. M. Daugherty, T. E. Lane and J. C. S. Brown (2018). "Regulated Release of Cryptococcal Polysaccharide Drives Virulence and Suppresses Immune Cell Infiltration into the Central Nervous System." Infect Immun **86**(3).
51. Egan, M. J., Z.-Y. Wang, M. A. Jones, N. Smirnoff and N. J. Talbot (2007). "Generation of reactive oxygen species by fungal NADPH oxidases is required for rice blast disease." Proceedings of the National Academy of Sciences of the United States of America **104**(28): 11772-11777.
52. Erwig, L. P. and N. A. Gow (2016). "Interactions of fungal pathogens with phagocytes." Nat Rev Microbiol **14**(3): 163-176.
53. Evans, R. J., Z. Li, W. S. Hughes, J. T. Djordjevic, K. Nielsen and R. C. May (2015). "Cryptococcal phospholipase B1 is required for intracellular proliferation and control of titan cell morphology during macrophage infection." Infect Immun **83**(4): 1296-1304.
54. Feldmesser, M., Y. Kress and A. Casadevall (2001). "Dynamic changes in the morphology of Cryptococcus neoformans during murine pulmonary infection." Microbiology **147**(8): 2355-2365.
55. Fernandes, K. E., A. Brockway, M. Haverkamp, C. A. Cuomo, F. van Ogtrop, J. R. Perfect and D. A. Carter (2018). "Phenotypic Variability Correlates with Clinical Outcome in Cryptococcus Isolates Obtained from Botswanan HIV/AIDS Patients." MBio **9**(5).
56. Fernandes, K. E., C. Dwyer, L. T. Campbell and D. A. Carter (2016). "Species in the Cryptococcus gattii Complex Differ in Capsule and Cell Size following Growth under Capsule-Inducing Conditions." mSphere **1**(6).
57. Forche, A., D. Abbey, T. Pisithkul, M. A. Weinzierl, T. Ringstrom, D. Bruck, K. Petersen and J. Berman (2011). "Stress alters rates and types of loss of heterozygosity in Candida albicans." mBio **2**(4).
58. Forche, A., G. Cromie, A. C. Gerstein, N. V. Solis, T. Pisithkul, W. Srifa, E. Jeffery, D. Abbey, S. G. Filler, A. M. Dudley and J. Berman (2018). "Rapid Phenotypic and Genotypic Diversification After Exposure to the Oral Host Niche in Candida albicans." Genetics **209**(3): 725-741.

59. Garcia-Barbazan, I., N. Trevijano-Contador, C. Rueda, B. de Andres, R. Perez-Tavarez, I. Herrero-Fernandez, M. L. Gaspar and O. Zaragoza (2016). "The formation of titan cells in Cryptococcus neoformans depends on the mouse strain and correlates with induction of Th2-type responses." Cell Microbiol **18**(1): 111-124.
60. Garcia-Rodas, R., R. J. Cordero, N. Trevijano-Contador, G. Janbon, F. Moyrand, A. Casadevall and O. Zaragoza (2014). "Capsule growth in Cryptococcus neoformans is coordinated with cell cycle progression." MBio **5**(3): e00945-00914.
61. Garcia-Rodas, R., N. Trevijano-Contador, E. Roman, G. Janbon, F. Moyrand, J. Pla, A. Casadevall and O. Zaragoza (2015). "Role of Cln1 during melanization of Cryptococcus neoformans." Front Microbiol **6**: 798.
62. Gerstein, A. C., M. S. Fu, L. Mukaremera, Z. Li, K. L. Ormerod, J. A. Fraser, J. Berman and K. Nielsen (2015). "Polyploid titan cells produce haploid and aneuploid progeny to promote stress adaptation." MBio **6**(5): e01340-01315.
63. Giacometti, R., F. Kronberg, R. M. Biondi and S. Passeron (2009). "Catalytic isoforms Tpk1 and Tpk2 of Candida albicans PKA have non-redundant roles in stress response and glycogen storage." Yeast **26**(5): 273-285.
64. Gilbert, A. S., P. I. Seoane, P. Sephton-Clark, A. Bojarczuk, R. Hotham, E. Giurisato, A. R. Sarhan, A. Hillen, G. V. Velde, N. S. Gray, D. R. Alessi, D. L. Cunningham, C. Tournier, S. A. Johnston and R. C. May (2017). "Vomocytosis of live pathogens from macrophages is regulated by the atypical MAP kinase ERK5." Sci Adv **3**(8): e1700898.
65. Giles, S., I. Batinic-Haberle, J. Perfect and G. Cox (2005). "*Cryptococcus neoformans* Mitochondrial Superoxide Dismutase: an Essential Link between Antioxidant Function and High-Temperature Growth." Eukaryotic Cell **4**(1): 46-54.
66. Giles, S. S., I. Batinic-Haberle, J. R. Perfect and G. M. Cox (2005). "Cryptococcus neoformans Mitochondrial Superoxide Dismutase: an Essential Link between Antioxidant Function and High-Temperature Growth." Eukaryotic Cell **4**(1): 46-54.
67. Giles, S. S., T. R. T. Dagenais, M. R. Botts, N. P. Keller and C. M. Hull (2009). "Elucidating the pathogenesis of spores from the human fungal pathogen Cryptococcus neoformans." Infection and Immunity **77**(8): 3491-3500.
68. Giles, S. S., J. E. Stajich, C. Nichols, Q. D. Gerrald, J. A. Alspaugh, F. Dietrich and J. R. Perfect (2006). "The Cryptococcus neoformans catalase gene family and its role in antioxidant defense." Eukaryotic Cell **5**(9): 1447-1459.
69. Gish, S. R., E. J. Maier, B. C. Haynes, F. H. Santiago-Tirado, D. L. Srikanta, C. Z. Ma, L. X. Li, M. Williams, E. C. Crouch, S. A. Khader, M. R. Brent and T. L. Doering (2016). "Computational Analysis Reveals a Key Regulator of Cryptococcal Virulence and Determinant of Host Response." MBio **7**(2): e00313-00316.

70. Gobbini, E., D. Cesena, A. Galbiati, A. Lockhart and M. P. Longhese (2013). "Interplays between ATM/Tel1 and ATR/Mec1 in sensing and signaling DNA double-strand breaks." DNA Repair **12**(10): 791-799.
71. Gordon, S. and P. R. Taylor (2005). "Monocyte and macrophage heterogeneity." Nat Rev Immunol **5**(12): 953-964.
72. Gusa, A., J. D. Williams, J. E. Cho, A. F. Averette, S. Sun, E. M. Shouse, J. Heitman, J. A. Alspaugh and S. Jinks-Robertson (2020). "Transposon mobilization in the human fungal pathogen Cryptococcus is mutagenic during infection and promotes drug resistance in vitro." Proc Natl Acad Sci U S A.
73. Halliwell, B. (2006). "Oxidative stress and cancer: have we moved forward?" Biochemical Journal **401**(1): 1-11.
74. Hardison, S. E., S. Ravi, K. L. Wozniak, M. L. Young, M. A. Olszewski and F. L. Wormley (2010). "Pulmonary Infection with an Interferon-γ-Producing Cryptococcus neoformans Strain Results in Classical Macrophage Activation and Protection." The American Journal of Pathology **176**(2): 774-785.
75. He, X., D. M. Lyons, D. L. Toffaletti, F. Wang, Y. Qiu, M. J. Davis, D. L. Meister, J. K. Dayrit, A. Lee, J. J. Osterholzer, J. R. Perfect and M. A. Olszewski (2012). "Virulence factors identified by Cryptococcus neoformans mutant screen differentially modulate lung immune responses and brain dissemination." Am J Pathol **181**(4): 1356-1366.
76. Heller, J. and P. Tudzynski (2011). "Reactive Oxygen Species in Phytopathogenic Fungi: Signaling, Development, and Disease." Annual Review of Phytopathology **49**(1): 369-390.
77. Heung, L. J. and T. M. Hohl (2019). "Inflammatory monocytes are detrimental to the host immune response during acute infection with Cryptococcus neoformans." PLoS Pathog **15**(3): e1007627.
78. Hickman, M. A., G. Zeng, A. Forche, M. P. Hirakawa, D. Abbey, B. D. Harrison, Y. M. Wang, C. H. Su, R. J. Bennett, Y. Wang and J. Berman (2013). "The 'obligate diploid' Candida albicans forms mating-competent haploids." Nature **494**(7435): 55-59.
79. Hohmann, S., M. Krantz and B. Nordlander (2007). Chapter Two - Yeast Osmoregulation. Methods in Enzymology. D. Häussinger and H. Sies, Academic Press. **428:** 29-45.
80. Hommel B, Mukaremera L, Cordero RJB, Desjardins CA, Sturny-Leclere A and e. a. Perfect JR (2018). "Identification of environmental and genetic factors important for Cryptococcus neoformans titan cell formation using new in vitro inducing conditions." PLoS Pathog.
81. Hommel, B., L. Mukaremera, R. J. B. Cordero, C. Coelho, C. A. Desjardins, A. Sturny-Leclere, G. Janbon, J. R. Perfect, J. A. Fraser, A. Casadevall, C. A. Cuomo, F. Dromer, K. Nielsen and A. Alanio (2018). "Titan cells formation in Cryptococcus neoformans is finely tuned by environmental conditions and

modulated by positive and negative genetic regulators." PLoS Pathog **14**(5): e1006982.
82. Hoyt, M. A., L. Totis and B. T. Roberts (1991). "S. cerevisiae genes required for cell cycle arrest in response to loss of microtubule function." Cell **66**(3): 507-517.
83. Hwang, C.-S., G.-e. Rhie, J.-H. Oh, W.-K. Huh, H.-S. Yim and S.-O. Kang (2002). "Copper- and zinc-containing superoxide dismutase (Cu/ZnSOD) is required for the protection of Candida albicans against oxidative stresses and the expression of its full virulence." Microbiology **148**(Pt 11): 3705-3713.
84. Iglesias, D. E., S. S. Bombicino, L. B. Valdez and A. Boveris (2015). "Nitric oxide interacts with mitochondrial complex III producing antimycin-like effects." Free Radic Biol Med **89**: 602-613.
85. Italiani, P. and D. Boraschi (2014). "From Monocytes to M1/M2 Macrophages: Phenotypical vs. Functional Differentiation." Frontiers in Immunology **5**(514).
86. Jaehnig, Eric J., D. Kuo, H. Hombauer, Trey G. Ideker and Richard D. Kolodner (2013). "Checkpoint Kinases Regulate a Global Network of Transcription Factors in Response to DNA Damage." Cell Reports **4**(1): 174-188.
87. Johnston, S. A. and R. C. May (2010). "The human fungal pathogen Cryptococcus neoformans escapes macrophages by a phagosome emptying mechanism that is inhibited by Arp2/3 complex-mediated actin polymerisation." PLoS Pathogens **6**(8).
88. Johnston, S. A. and R. C. May (2013). "Cryptococcus interactions with macrophages: evasion and manipulation of the phagosome by a fungal pathogen." Cell Microbiol **15**(3): 403-411.
89. Jung, K.-W., Y. Lee, E. Y. Huh, S. C. Lee, S. Lim and Y.-S. Bahn (2019). "Rad53- and Chk1-Dependent DNA Damage Response Pathways Cooperatively Promote Fungal Pathogenesis and Modulate Antifungal Drug Susceptibility." mBio **10**(1): e01726-01718.
90. Jung, K. W., D. H. Yang, S. Maeng, K. T. Lee, Y. S. So, J. Hong, J. Choi, H. J. Byun, H. Kim, S. Bang, M. H. Song, J. W. Lee, M. S. Kim, S. Y. Kim, J. H. Ji, G. Park, H. Kwon, S. Cha, G. L. Meyers, L. L. Wang, J. Jang, G. Janbon, G. Adedoyin, T. Kim, A. K. Averette, J. Heitman, E. Cheong, Y. H. Lee, Y. W. Lee and Y. S. Bahn (2015). "Systematic functional profiling of transcription factor networks in Cryptococcus neoformans." Nat Commun **6**: 6757.
91. Kaludercic, N. and V. Giorgio (2016). "The Dual Function of Reactive Oxygen/Nitrogen Species in Bioenergetics and Cell Death: The Role of ATP Synthase." Oxidative medicine and cellular longevity **2016**: 3869610-3869610.
92. Kassim, S. Y., X. Fu, W. C. Liles, S. D. Shapiro, W. C. Parks and J. W. Heinecke (2005). "NADPH Oxidase Restrains the Matrix Metalloproteinase Activity of Macrophages." Journal of Biological Chemistry **280**(34): 30201-30205.

93. Kelliher, C. M., A. R. Leman, C. S. Sierra and S. B. Haase (2016). "Investigating Conservation of the Cell-Cycle-Regulated Transcriptional Program in the Fungal Pathogen, Cryptococcus neoformans." PLoS Genet **12**(12): e1006453.
94. Lambou, K., C. Lamarre, R. Beau, N. Dufour and J.-P. Latgé (2010). "Functional analysis of the superoxide dismutase family in Aspergillus fumigatus." Molecular Microbiology **75**(4): 910-923.
95. Lara-Ortiz, T., H. Riveros-Rosas and J. Aguirre (2003). "Reactive oxygen species generated by microbial NADPH oxidase NoxA regulate sexual development in Aspergillus nidulans." Mol Microbiol **50**(4): 1241-1255.
96. Lauvau, G., P. Loke and T. M. Hohl (2015). "Monocyte-mediated defense against bacteria, fungi, and parasites." Semin Immunol **27**(6): 397-409.
97. Lauvau, G. and S. M. Soudja (2015). "Mechanisms of Memory T Cell Activation and Effective Immunity." Adv Exp Med Biol **850**: 73-80.
98. Lee, K.-T., Y.-S. So, D.-H. Yang, K.-W. Jung, J. Choi, D.-G. Lee, H. Kwon, J. Jang, L. L. Wang, S. Cha, G. L. Meyers, E. Jeong, J.-H. Jin, Y. Lee, J. Hong, S. Bang, J.-H. Ji, G. Park, H.-J. Byun, S. W. Park, Y.-M. Park, G. Adedoyin, T. Kim, A. F. Averette, J.-S. Choi, J. Heitman, E. Cheong, Y.-H. Lee and Y.-S. Bahn (2016). "Systematic functional analysis of kinases in the fungal pathogen Cryptococcus neoformans." Nature Communications **7**(1): 12766.
99. Leipheimer, J., A. L. M. Bloom, C. S. Campomizzi, Y. Salei and J. C. Panepinto (2019). "Translational Regulation Promotes Oxidative Stress Resistance in the Human Fungal Pathogen Cryptococcus neoformans." mBio **10**(6): e02143-02119.
100. Leopold Wager, C. M., C. R. Hole, K. L. Wozniak and F. L. Wormley, Jr. (2016). "Cryptococcus and Phagocytes: Complex Interactions that Influence Disease Outcome." Front Microbiol **7**: 105.
101. Leopold Wager, C. M. and F. L. Wormley, Jr. (2014). "Classical versus alternative macrophage activation: the Ying and the Yang in host defense against pulmonary fungal infections." Mucosal Immunol **7**(5): 1023-1035.
102. Lessing, F., O. Kniemeyer, I. Wozniok, J. Loeffler, O. Kurzai, A. Haertl and A. Brakhage Axel (2007). "The Aspergillus fumigatus Transcriptional Regulator AfYap1 Represents the Major Regulator for Defense against Reactive Oxygen Intermediates but Is Dispensable for Pathogenicity in an Intranasal Mouse Infection Model." Eukaryotic Cell **6**(12): 2290-2302.
103. Li, X., S. Qiu, J. Shi, S. Wang, M. Wang, Y. Xu, Z. Nie, C. Liu and C. Liu (2019). "A new function of copper zinc superoxide dismutase: as a regulatory DNA-binding protein in gene expression in response to intracellular hydrogen peroxide." Nucleic Acids Research **47**(10): 5074-5085.
104. Li, Z. and K. Nielsen (2017). "Morphology Changes in Human Fungal Pathogens upon Interaction with the Host." J Fungi (Basel) **3**(4).

105. Litvack, M. L., M. Post and N. Palaniyar (2011). "IgM Promotes the Clearance of Small Particles and Apoptotic Microparticles by Macrophages." PLOS ONE **6**(3): e17223.
106. Litvintseva, A. P., L. Kestenbaum, R. Vilgalys and T. G. Mitchell (2005). "Comparative analysis of environmental and clinical populations of Cryptococcus neoformans." J Clin Microbiol **43**(2): 556-564.
107. Litwin, I., T. Bocer, D. Dziadkowiec and R. Wysocki (2013). "Oxidative stress and replication-independent DNA breakage induced by arsenic in Saccharomyces cerevisiae." PLoS genetics **9**(7): e1003640-e1003640.
108. Liu, O. W., C. D. Chun, E. D. Chow, C. Chen, H. D. Madhani and S. M. Noble (2008). "Systematic genetic analysis of virulence in the human fungal pathogen Cryptococcus neoformans." Cell **135**(1): 174-188.
109. Love, G. L., G. D. Boyd and D. L. Greer (1985). "Large Cryptococcus neoformans isolated from brain abscess." J Clin Microbiol **22**(6): 1068-1070.
110. Ma, H., F. Hagen, D. J. Stekel, S. A. Johnston, E. Sionov, R. Falk, I. Polacheck, T. Boekhout and R. C. May (2009). "The fatal fungal outbreak on Vancouver Island is characterized by enhanced intracellular parasitism driven by mitochondrial regulation." Proc Natl Acad Sci U S A **106**(31): 12980-12985.
111. Malagnac, F., H. Lalucque, G. Lepère and P. Silar (2004). "Two NADPH oxidase isoforms are required for sexual reproduction and ascospore germination in the filamentous fungus Podospora anserina." Fungal genetics and biology : FG & B **41**(11): 982-997.
112. Maréchal, A. and L. Zou (2013). "DNA damage sensing by the ATM and ATR kinases." Cold Spring Harbor perspectives in biology **5**(9): a012716.
113. Maresca, B. and G. S. Kobayashi (2000). "Dimorphism in Histoplasma capsulatum and Blastomyces dermatitidis." Contributions to microbiology **5**: 201-216.
114. Marschall, R. and P. Tudzynski (2016). "Reactive oxygen species in development and infection processes." Seminars in Cell & Developmental Biology **57**: 138-146.
115. May, R. C., N. R. Stone, D. L. Wiesner, T. Bicanic and K. Nielsen (2016). "Cryptococcus: from environmental saprophyte to global pathogen." Nat Rev Microbiol **14**(2): 106-117.
116. Mendoza-Martínez, A. E., N. Cano-Domínguez and J. Aguirre (2020). "Yap1 homologs mediate more than the redox regulation of the antioxidant response in filamentous fungi." Fungal Biology **124**(5): 253-262.
117. Mendoza-Martínez, A. E., F. Lara-Rojas, O. Sánchez and J. Aguirre (2017). "NapA Mediates a Redox Regulation of the Antioxidant Response, Carbon Utilization and Development in Aspergillus nidulans." Frontiers in Microbiology **8**(516).

118. Mills, C. D., K. Kincaid, J. M. Alt, M. J. Heilman and A. M. Hill (2000). "M-1/M-2 Macrophages and the Th1/Th2 Paradigm." The Journal of Immunology **164**: 6166-6173.
119. Missal, T., M. Pusateri, M. Donlin, K. Chambers, J. Corbett and J. K. Lodge (2006). "Posttranslational, Translational, and Transcriptional Responses to Nitric Oxide Stress in Cryptococcus neoformans: Implications for Virulence." Eukaryotic Cell **5**(3): 518-529.
120. Missall, T. A. and J. K. Lodge (2005). "Function of the thioredoxin proteins in Cryptococcus neoformans during stress or virulence and regulation by putative transcriptional modulators." Mol Microbiol **57**(3): 847-858.
121. Mittler, R. (2017). "ROS Are Good." Trends in Plant Science **22**(1): 11-19.
122. Molloy, S. F., C. Kanyama, R. S. Heyderman, A. Loyse, C. Kouanfack, D. Chanda, S. Mfinanga, E. Temfack, S. Lakhi, S. Lesikari, A. K. Chan, N. Stone, N. Kalata, N. Karunaharan, K. Gaskell, M. Peirse, J. Ellis, C. Chawinga, S. Lontsi, J. G. Ndong, P. Bright, D. Lupiya, T. Chen, J. Bradley, J. Adams, C. van der Horst, J. J. van Oosterhout, V. Sini, Y. N. Mapoure, P. Mwaba, T. Bicanic, D. G. Lalloo, D. Wang, M. C. Hosseinipour, O. Lortholary, S. Jaffar, T. S. Harrison and A. T. S. Team (2018). "Antifungal Combinations for Treatment of Cryptococcal Meningitis in Africa." N Engl J Med **378**(11): 1004-1017.
123. Morrow, C. A., I. R. Lee, E. W. Chow, K. L. Ormerod, A. Goldinger, E. J. Byrnes, 3rd, K. Nielsen, J. Heitman, H. J. Schirra and J. A. Fraser (2012). "A unique chromosomal rearrangement in the Cryptococcus neoformans var. grubii type strain enhances key phenotypes associated with virulence." mBio **3**(2).
124. Mukaremera, L., K. K. Lee, J. Wagener, D. L. Wiesner, N. A. R. Gow and K. Nielsen (2018). "Titan cell production in Cryptococcus neoformans reshapes the cell wall and capsule composition during infection." The Cell Surface **1**(1): 15-24.
125. Mukaremera, L., T. R. McDonald, J. N. Nielsen, C. J. Molenaar, A. Akampurira, C. Schutz, K. Taseera, C. Muzoora, G. Meintjes, D. B. Meya, D. R. Boulware and K. Nielsen (2019). "The Mouse Inhalation Model of Cryptococcus neoformans Infection Recapitulates Strain Virulence in Humans and Shows that Closely Related Strains Can Possess Differential Virulence." Infection and Immunity **87**.
126. Narasipura, S. D., J. G. Ault, M. J. Behr, V. Chaturvedi and S. Chaturvedi (2003). "Characterization of Cu,Zn superoxide dismutase (SOD1) gene knock-out mutant of Cryptococcus neoformans var. gattii: role in biology and virulence." Molecular Microbiology **47**(6): 1681-1694.
127. Narra, R., J. M. Maeda, H. Temba, J. Mghamba, A. Nyanga, A. L. Greiner, M. Bakari, K. D. Beer, S. R. Chae, K. G. Curran, R. B. Eidex, J. J. Gibson, T. Handzel, S. J. Kiberiti, R. S. Kishimba, H. Lukupulo, T. Malibiche, K. Massa, A. E. Massay, L. S. McCrickard, G. J. McHau, V. Mmbaga, A. A. Mohamed, E. R. Mwakapeje, E. Nestory, A. E. Newton, E. Oyugi, A. Rajasingham, M. E.

Roland, N. Rusibamayila, S. Sembuche, L. J. Urio, T. A. Walker, A. Wang and R. E. Quick (2017). "Notes from the Field: Ongoing Cholera Epidemic - Tanzania, 2015-2016." MMWR Morb Mortal Wkly Rep **66**(6): 177-178.
128. Nauseef, W. M. (2008). "Biological Roles for the NOX Family NADPH Oxidases." Journal of Biological Chemistry **283**(25): 16961-16965.
129. Nikolaou, E., I. Agrafioti, M. Stumpf, J. Quinn, I. Stansfield and A. J. P. Brown (2009). "Phylogenetic diversity of stress signalling pathways in fungi." BMC Evolutionary Biology **9**(1): 44.
130. Noble, S. M., B. A. Gianetti and J. N. Witchley (2017). "Candida albicans cell-type switching and functional plasticity in the mammalian host." Nat Rev Microbiol **15**(2): 96-108.
131. Nyberg, K. A., R. J. Michelson, C. W. Putnam and T. A. Weinert (2002). "Toward Maintaining the Genome: DNA Damage and Replication Checkpoints." Annual Review of Genetics **36**(1): 617-656.
132. O'Meara, T. R., S. M. Holmer, K. Selvig, F. Dietrich and J. A. Alspaugh (2013). "Cryptococcus neoformans Rim101 is associated with cell wall remodeling and evasion of the host immune responses." MBio **4**(1).
133. O'Meara, T. R., D. Norton, M. S. Price, C. Hay, M. F. Clements, C. B. Nichols and J. A. Alspaugh (2010). "Interaction of Cryptococcus neoformans Rim101 and protein kinase A regulates capsule." PLoS Pathogens **6**(2): e1000776.
134. O'Rourke, S. M., I. Herskowitz and E. K. O'Shea (2002). "Yeast go the whole HOG for the hyperosmotic response." Trends in Genetics **18**(8): 405-412.
135. Ohkusu, M., K. Hata and K. Takeo (2001). "Bud emergence is gradually delayed from S to G2 with progression of growth phase." FEMS microbiology letters **194**: 251-255.
136. Ohkusu, M., V. Raclavsky and K. Takeo (2004). "Induced synchrony in Cryptococcus neoformans after release from G2-arrest." Antonie van Leeuwenhoek **85**(1): 37-44.
137. Okagaki, L. H. and K. Nielsen (2012). "Titan cells confer protection from phagocytosis in Cryptococcus neoformans infections." Eukaryot Cell **11**(6): 820-826.
138. Okagaki, L. H., A. K. Strain, J. N. Nielsen, C. Charlier, N. J. Baltes, F. Chrétien, J. Heitman, F. Dromer and K. Nielsen (2010). "Cryptococcal cell morphology affects host cell interactions and pathogenicity." PLoS Pathogens **6**(6): e1000953.
139. Okagaki, L. H., Y. Wang, E. R. Ballou, T. R. O'Meara, Y.-S. Bahn, J. A. Alspaugh, C. Xue and K. Nielsen (2011). "Cryptococcal titan cell formation is regulated by G-protein signaling in response to multiple stimuli." Eukaryotic Cell **10**(10): 1306-1316.
140. Osterholzer, J. J., R. Surana, J. E. Milam, G. T. Montano, G.-H. Chen, J. Sonstein, J. L. Curtis, G. B. Huffnagle, G. B. Toews and M. A. Olszewski

(2009). "Cryptococcal Urease Promotes the Accumulation of Immature Dendritic Cells and a Non-Protective T2 Immune Response within the Lung." The American Journal of Pathology **174**(3): 932-943.

141. Painter, R. B. and B. R. Young (1980). "Radiosensitivity in ataxia-telangiectasia: a new explanation." Proceedings of the National Academy of Sciences of the United States of America **77**(12): 7315-7317.
142. Park, B. J., K. A. Wannemuehler, B. J. Marston, N. Govender, P. G. Pappas and T. M. Chiller (2009). "Estimation of the current global burden of cryptococcal meningitis among persons living with HIV/AIDS." AIDS (London, England) **23**(4): 525-530.
143. Paul, S., T. L. Doering and W. S. Moye-Rowley (2015). "Cryptococcus neoformans Yap1 is required for normal fluconazole and oxidative stress resistance." Fungal genetics and biology : FG & B **74**: 1-9.
144. Pizzimenti, S., C. Toaldo, P. Pettazzoni, M. U. Dianzani and G. Barrera (2010). "The "two-faced" effects of reactive oxygen species and the lipid peroxidation product 4-hydroxynonenal in the hallmarks of cancer." Cancers **2**(2): 338-363.
145. Poderoso, J. J., M. C. Carreras, C. Lisdero, N. Riobó, F. Schöpfer and A. Boveris (1996). "Nitric oxide inhibits electron transfer and increases superoxide radical production in rat heart mitochondria and submitochondrial particles." Archives of biochemistry and biophysics **328**(1): 85-92.
146. Poderoso, J. J., C. Lisdero, F. Schöpfer, N. Riobó, M. C. Carreras, E. Cadenas and A. Boveris (1999). "The regulation of mitochondrial oxygen uptake by redox reactions involving nitric oxide and ubiquinol." The Journal of biological chemistry **274**(53): 37709-37716.
147. Pollock, J. D., D. A. Williams, M. A. C. Gifford, L. L. Li, X. Du, J. Fisherman, S. H. Orkin, C. M. Doerschuk and M. C. Dinauer (1995). "Mouse model of X–linked chronic granulomatous disease, an inherited defect in phagocyte superoxide production." Nature Genetics **9**(2): 202-209.
148. Price, M. S., C. B. Nichols and J. A. Alspaugh (2008). "The Cryptococcus neoformans Rho-GDP dissociation inhibitor mediates intracellular survival and virulence." Infection and Immunity **76**(12): 5729-5737.
149. Probert, M., X. Zhou, M. Goodall, S. A. Johnston, E. Bielska, E. R. Ballou and R. C. May (2019). "A Glucuronoxylomannan Epitope Exhibits Serotype-Specific Accessibility and Redistributes towards the Capsule Surface during Titanization of the Fungal Pathogen Cryptococcus neoformans." Infection and Immunity **87**.
150. Probert, M., X. Zhou, M. Goodall, S. A. Johnston, E. Bielska, E. R. Ballou and R. C. May (2019). "A Glucuronoxylomannan Epitope Exhibits Serotype-Specific Accessibility and Redistributes towards the Capsule Surface during Titanization of the Fungal Pathogen Cryptococcus neoformans." Infect Immun **87**(4).

151. Rajasingham, R., R. M. Smith, B. J. Park, J. N. Jarvis, N. P. Govender, T. M. Chiller, D. W. Denning, A. Loyse and D. R. Boulware (2017). "Global burden of disease of HIV-associated cryptococcal meningitis: an updated analysis." Lancet Infect Dis **17**(8): 873-881.
152. Ramachandran, A., D. R. Moellering, E. Ceaser, S. Shiva, J. Xu and V. Darley-Usmar (2002). "Inhibition of mitochondrial protein synthesis results in increased endothelial cell susceptibility to nitric oxide-induced apoptosis." Proceedings of the National Academy of Sciences **99**: 6643-6648.
153. Reverberi, M., S. Zjalic, A. Ricelli, F. Punelli, E. Camera, C. Fabbri, M. Picardo, C. Fanelli and A. Fabbri Anna (2008). "Modulation of Antioxidant Defense in Aspergillus parasiticus Is Involved in Aflatoxin Biosynthesis: a Role for the ApyapA Gene." Eukaryotic Cell **7**(6): 988-1000.
154. Rhind, N. and P. Russell (1998). "Mitotic DNA damage and replication checkpoints in yeast." Current opinion in cell biology **10**(6): 749-758.
155. Robertson, E. J., G. Najjuka, M. A. Rolfes, A. Akampurira, N. Jain, J. Anantharanjit, M. von Hohenberg, M. Tassieri, A. Carlsson, D. B. Meya, T. S. Harrison, B. C. Fries, D. R. Boulware and T. Bicanic (2014). "Cryptococcus neoformans ex vivo capsule size is associated with intracranial pressure and host immune response in HIV-associated cryptococcal meningitis." J Infect Dis **209**(1): 74-82.
156. Rohatgi, S. and L.-A. Pirofski (2015). "Host immunity to Cryptococcus neoformans." Future microbiology **10**(4): 565-581.
157. Rossi, D. C. P., J. E. Gleason, H. Sanchez, S. S. Schatzman, E. M. Culbertson, C. J. Johnson, C. A. McNees, C. Coelho, J. E. Nett, D. R. Andes, B. P. Cormack and V. C. Culotta (2017). "Candida albicans FRE8 encodes a member of the NADPH oxidase family that produces a burst of ROS during fungal morphogenesis." PLoS Pathog **13**(12): e1006763.
158. Saito, H. and K. Tatebayashi (2004). "Regulation of the Osmoregulatory HOG MAPK Cascade in Yeast." The Journal of Biochemistry **136**(3): 267-272.
159. Salmon, T. B., B. A. Evert, B. Song and P. W. Doetsch (2004). "Biological consequences of oxidative stress-induced DNA damage in Saccharomyces cerevisiae." Nucleic acids research **32**(12): 3712-3723.
160. Schieber, M. and N. S. Chandel (2014). "ROS function in redox signaling and oxidative stress." Current biology : CB **24**(10): R453-R462.
161. Schwartz, M. F., J. K. Duong, Z. Sun, J. S. Morrow, D. Pradhan and D. F. Stern (2002). "Rad9 Phosphorylation Sites Couple Rad53 to the Saccharomyces cerevisiae DNA Damage Checkpoint." Molecular Cell **9**(5): 1055-1065.
162. Selvig, K. and J. A. Alspaugh (2011). "pH Response Pathways in Fungi: Adapting to Host-derived and Environmental Signals." Mycobiology **39**(4): 249-256.
163. Semighini, C. P., A. F. Averette, J. R. Perfect and J. Heitman (2011). "Deletion of Cryptococcus neoformans AIF ortholog promotes chromosome

aneuploidy and fluconazole-resistance in a metacaspase-independent manner." PLoS Pathogens **7**(11): e1002364.

164. Semighini, C. P. and S. D. Harris (2008). "Regulation of apical dominance in Aspergillus nidulans hyphae by reactive oxygen species." Genetics **179**(4): 1919-1932.

165. Serbina, N. V., T. Jia, T. M. Hohl and E. G. Pamer (2008). "Monocyte-mediated defense against microbial pathogens." Annu Rev Immunol **26**: 421-452.

166. Shiloh, Y. (2001). "ATM and ATR: networking cellular responses to DNA damage." Current Opinion in Genetics & Development **11**(1): 71-77.

167. Sionov, E., Y. C. Chang, H. M. Garraffo and K. J. Kwon-Chung (2009). "Heteroresistance to fluconazole in Cryptococcus neoformans is intrinsic and associated with virulence." Antimicrob Agents Chemother **53**(7): 2804-2815.

168. Sionov, E., H. Lee, Y. C. Chang and K. J. Kwon-Chung (2010). "Cryptococcus neoformans overcomes stress of azole drugs by formation of disomy in specific multiple chromosomes." PLoS Pathogens **6**(4): e1000848.

169. Slupphaug, G., B. Kavli and H. E. Krokan (2003). "The interacting pathways for prevention and repair of oxidative DNA damage." Mutation Research/Fundamental and Molecular Mechanisms of Mutagenesis **531**(1): 231-251.

170. Smith, L. M., E. F. Dixon and R. C. May (2015). "The fungal pathogen Cryptococcus neoformans manipulates macrophage phagosome maturation." Cell Microbiol **17**(5): 702-713.

171. So, Y.-S., S. Maeng, D.-H. Yang, H. Kim, K.-T. Lee, S.-R. Yu, J. L. Tenor, V. K. Giri, D. L. Toffaletti, S. Arras, J. A. Fraser, J. R. Perfect and Y.-S. Bahn (2019). "Regulatory Mechanism of the Atypical AP-1-Like Transcription Factor Yap1 in Cryptococcus neoformans." mSphere **4**.

172. Song, M.-H., J.-W. Lee, M. S. Kim, J.-K. Yoon, T. C. White, A. Floyd, J. Heitman, A. K. Strain, J. N. Nielsen, K. Nielsen and Y.-S. Bahn (2012). "A flucytosine-responsive Mbp1/Swi4-like protein, Mbs1, plays pleiotropic roles in antifungal drug resistance, stress response, and virulence of Cryptococcus neoformans." Eukaryotic cell **11**(1): 53-67.

173. Stone, N. R. H., J. Rhodes, M. C. Fisher, S. Mfinanga, S. Kivuyo, J. Rugemalila, E. S. Segal, L. Needleman, S. F. Molloy, J. Kwon-Chung, T. S. Harrison, W. Hope, J. Berman and T. Bicanic (2019). "Dynamic ploidy changes drive fluconazole resistance in human cryptococcal meningitis." The Journal of Clinical Investigation **129**(3): 999-1014.

174. Sun, Z., J. Hsiao, D. S. Fay and D. F. Stern (1998). "Rad53 FHA Domain Associated with Phosphorylated Rad9 in the DNA Damage Checkpoint." Science **281**(5374): 272.

175. Sung, P., L. Krejci, S. Van Komen and M. G. Sehorn (2003). "Rad51 Recombinase and Recombination Mediators." Journal of Biological Chemistry **278**(44): 42729-42732.
176. Takemoto, D., A. Tanaka and B. Scott (2007). "NADPH oxidases in fungi: diverse roles of reactive oxygen species in fungal cellular differentiation." Fungal genetics and biology : FG & B **44**(11): 1065-1076.
177. Taylor, P. R. and S. Gordon (2003). "Monocyte heterogeneity and innate immunity." Immunity **19**(1): 2-4.
178. Todd, R. T., T. D. Wikoff, A. Forche and A. Selmecki (2019). "Genome plasticity in Candida albicans is driven by long repeat sequences." Elife **8**.
179. Toffaletti, D. L., T. H. Rude, S. A. Johnston, D. T. Durack and J. R. Perfect (1993). "Gene transfer in Cryptococcus neoformans by use of biolistic delivery of DNA." Journal of bacteriology **175**(5): 1405-1411.
180. Torres, E. M., T. Sokolsky, C. M. Tucker, L. Y. Chan, M. Boselli, M. J. Dunham and A. Amon (2007). "Effects of Aneuploidy on Cellular Physiology and Cell Division in Haploid Yeast." Science **317**(5840): 916.
181. Trevijano-Contador, N., H. C. de Oliveira, R. García-Rodas, S. A. Rossi, I. Llorente, Á. Zaballos, G. Janbon, J. Ariño and Ó. Zaragoza (2018). "Cryptococcus neoformans can form titan-like cells in vitro in response to multiple signals." PLOS Pathogens **14**(5): e1007007.
182. Trevijano-Contador, N., H. C. de Oliveira, R. García-Rodas, S. A. Rossi, I. Llorente, Á. Zaballos, G. Janbon, J. Ariño and Ó. Zaragoza (2018). "Cryptococcus neoformans can form titan-like cells in vitro in response to multiple signals that require the activation of several transduction pathways." PLoS Pathog **14**(5): e1007007.
183. Trevijano-Contador, N., K. M. Pianalto, C. B. Nichols, O. Zaragoza, J. A. Alspaugh and L.-a. Pirofski (2020). "Human IgM Inhibits the Formation of Titan-Like Cells in Cryptococcus neoformans." Infection and Immunity **88**.
184. Tsang, C. K., Y. Liu, J. Thomas, Y. Zhang and X. F. Zheng (2014). "Superoxide dismutase 1 acts as a nuclear transcription factor to regulate oxidative stress resistance." Nat Commun **5**: 3446.
185. Tsang, C. K., Y. Liu, J. Thomas, Y. Zhang and X. F. S. Zheng (2014). "Superoxide dismutase 1 acts as a nuclear transcription factor to regulate oxidative stress resistance." Nature Communications **5**(1): 3446.
186. Tudzynski, P., J. Heller and U. Siegmund (2012). "Reactive oxygen species generation in fungal development and pathogenesis." Current Opinion in Microbiology **15**(6): 653-659.
187. Upadhya, R., L. T. Campbell, M. J. Donlin, R. Aurora and J. K. Lodge (2013). "Global transcriptome profile of Cryptococcus neoformans during exposure to hydrogen peroxide induced oxidative stress." PLoS One **8**(1): e55110.

188. Valavanidis, A., T. Vlachogianni and C. Fiotakis (2009). "8-hydroxy-2' -deoxyguanosine (8-OHdG): A critical biomarker of oxidative stress and carcinogenesis." J Environ Sci Health C Environ Carcinog Ecotoxicol Rev **27**(2): 120-139.
189. Vanhove, M., M. A. Beale, J. Rhodes, D. Chanda, S. Lakhi, G. Kwenda, S. Molloy, N. Karunaharan, N. Stone, T. S. Harrison, T. Bicanic and M. C. Fisher (2016). "Genomic epidemiology of Cryptococcus yeasts identifies adaptation to environmental niches underpinning infection across an African HIV/AIDS cohort." Mol Ecol.
190. Vanhove, M., M. A. Beale, J. Rhodes, D. Chanda, S. Lakhi, G. Kwenda, S. Molloy, N. Karunaharan, N. Stone, T. S. Harrison, T. Bicanic and M. C. Fisher (2017). "Genomic epidemiology of Cryptococcus yeasts identifies adaptation to environmental niches underpinning infection across an African HIV/AIDS cohort." Mol Ecol **26**(7): 1991-2005.
191. Voelz, K., D. Lammas and R. C. May (2009). "Cytokine signaling regulates the outcome of intracellular macrophage parasitism by Cryptococcus neoformans." Infection and Immunity.
192. Warris, A. and E. R. Ballou (2018). "Oxidative responses and fungal infection biology." Semin Cell Dev Biol.
193. Warris, A. and E. R. Ballou (2019). "Oxidative responses and fungal infection biology." Semin Cell Dev Biol **89**: 34-46.
194. Weinert, T. A. and L. H. Hartwell (1988). "The RAD9 gene controls the cell cycle response to DNA damage in Saccharomyces cerevisiae." Science **241**(4863): 317.
195. Wiesner, D. L., C. A. Specht, C. K. Lee, K. D. Smith, L. Mukaremera, S. T. Lee, C. G. Lee, J. A. Elias, J. N. Nielsen, D. R. Boulware, P. R. Bohjanen, M. K. Jenkins, S. M. Levitz and K. Nielsen (2015). "Chitin recognition via chitotriosidase promotes pathologic type-2 helper T cell responses to cryptococcal infection." PLoS Pathog **11**(3): e1004701.
196. Xu, L., T. Wu, S. Lu, X. Hao, J. Qin, J. Wang, X. Zhang, Q. Liu, B. Kong, Y. Gong, Z. Liu and C. Shao (2020). "Mitochondrial superoxide contributes to oxidative stress exacerbated by DNA damage response in RAD51-depleted ovarian cancer cells." Redox Biology **36**: 101604.
197. Yamamori, T., H. Yasui, M. Yamazumi, Y. Wada, Y. Nakamura, H. Nakamura and O. Inanami (2012). "Ionizing radiation induces mitochondrial reactive oxygen species production accompanied by upregulation of mitochondrial electron transport chain function and mitochondrial content under control of the cell cycle checkpoint." Free Radical Biology and Medicine **53**(2): 260-270.
198. Yu, X., S. A. Jacobs, S. C. West, T. Ogawa and E. H. Egelman (2001). "Domain structure and dynamics in the helical filaments formed by RecA and

Rad51 on DNA." Proceedings of the National Academy of Sciences **98**(15): 8419-8424.
199. Yu, X., S. A. Jacobs, S. C. West, T. Ogawa and E. H. Egelman (2001). "Domain structure and dynamics in the helical filaments formed by RecA and Rad51 on DNA." Proceedings of the National Academy of Sciences **98**: 8419-8424.
200. Zafar, H., S. Altamirano, E. R. Ballou and K. Nielsen (2019). "A titanic drug resistance threat in Cryptococcus neoformans." Curr Opin Microbiol **52**: 158-164.
201. Zaragoza, O. (2011). "Multiple Disguises for the Same Party: The Concepts of Morphogenesis and Phenotypic Variations in Cryptococcus neoformans." Front Microbiol **2**: 181.
202. Zaragoza, O., C. J. Chrisman, M. V. Castelli, S. Frases, M. Cuenca-Estrella, J. L. Rodriguez-Tudela and A. Casadevall (2008). "Capsule enlargement in Cryptococcus neoformans confers resistance to oxidative stress suggesting a mechanism for intracellular survival." Cell Microbiol **10**(10): 2043-2057.
203. Zaragoza, O., J. Garcia-Rivera, J. D. Nosanchuk, M. Cuenca-Estrella, J. Rodriguez-Tudela and A. Casadevall (2010). "Fungal Cell Gigantism during Mammalian Infection." PLoS Pathogens **6**(6): 1-18.
204. Zaragoza, O. and K. Nielsen (2013). "Titan cells in Cryptococcus neoformans: cells with a giant impact." Curr Opin Microbiol **16**(4): 409-413.
205. Zhang, J., K. Martinez-Gomez, E. Heinzle and S. A. Wahl (2019). "Metabolic switches from quiescence to growth in synchronized Saccharomyces cerevisiae." Metabolomics **15**(9): 121.
206. Zhang, Y., F. Wang, K. C. Tompkins, A. McNamara, A. V. Jain, B. B. Moore, G. B. Toews, G. B. Huffnagle and M. A. Olszewski (2009). "Robust Th1 and Th17 Immunity Supports Pulmonary Clearance but Cannot Prevent Systemic Dissemination of Highly Virulent Cryptococcus neoformans H99." The American Journal of Pathology **175**(6): 2489-2500.
207. Zhao, X., A. Chabes, V. Domkin, L. Thelander and R. Rothstein (2001). "The ribonucleotide reductase inhibitor Sml1 is a new target of the Mec1/Rad53 kinase cascade during growth and in response to DNA damage." The EMBO Journal **20**(13): 3544-3553.
208. Zhao, Y., Y. Wang, S. Upadhyay, C. Xue and X. Lin "Activation of Meiotic Genes Mediates Ploidy Reduction during Cryptococcal Infection." Current Biology.
209. Zhao, Y., Y. Wang, S. Upadhyay, C. Xue and X. Lin (2020). "Activation of Meiotic Genes Mediates Ploidy Reduction during Cryptococcal Infection." Current Biology **30**(8): 1387-1396.e1385.
210. Zhou, B.-B. S. and S. J. Elledge (2000). "The DNA damage response: putting checkpoints in perspective." Nature **408**(6811): 433-439.

211. Zhou, X. and E. R. Ballou (2018). "The Cryptococcus neoformans Titan Cell: From In Vivo Phenomenon to In Vitro Model." Current Clinical Microbiology Reports **5**(4): 252-260.
212. Zhou, X., G. E. Desanti, R. C. May, I. M. Dambuza and E. R. Ballou (2021). "Host-derived Reactive Nitrogen Species mediate the Cryptococcus neoformans yeast-to-titan switch via fungal-derived superoxide." bioRxiv: 2021.2003.2001.433276.
213. Zhou, X., H. Zafar, P. Sephton-Clark, S. H. Mohamed, A. Chapuis, M. Makarova, D. M. MacCallum, R. A. Drummond, I. M. Dambuza and E. R. Ballou (2020). "Host environmental conditions induce small fungal cell size and alter population heterogeneity in Cryptococcus neoformans" bioRxiv: 2020.2001.2003.894709.
214. Zinzalla, V., M. Graziola, A. Mastriani, M. Vanoni and L. Alberghina (2007). "Rapamycin-mediated G1 arrest involves regulation of the Cdk inhibitor Sic1 in Saccharomyces cerevisiae." Molecular Microbiology **63**(5): 1482-1494.